School of Industrial and Information Engineering

Master thesis in materials engineering and nanotechnology

POLITECNICO
MILANO 1863

Density Functional Theory simulations of Raman and UV-VIS spectra of carbon atom wires

Supervisor: Prof. Casari Carlo Spartaco
Co-supervisor: Dr. Milani Alberto

Master degree of:
Dalla Via Andrea, matricola 876789

Academic year 2017-2018

List of Figures

1.1 Graphical representation of the sp^3, sp^2 and ideal sp allotropes 17
1.2 Progress on carbon nanostructures development and further studies [1] 18
1.3 Theoretical E(k) dispersion relation for the infinite 'polyyne' (or carbyne- α), in the left, and infinite 'cumulene' (or carbyne - β) in the right [2] 19
1.4 Phonon dispersion relation representing the opening of a gap for the theoretical infinite carbyne 20
1.5 Some of the most important physical fabrication techniques [2] 21
1.6 AFM images of Ph-Py[6],(c) is constant-height CO-tip AFM images of the precursor and (f) is the corresponding Laplace-filtered AFM images with structural ball-and-stick models overlaid as a visual aid done by Pavlicek et al [3] 23
1.7 Several different structures identified by Raman spectroscopy . 24

2.1 B3LYP(left) and CAM-B3LYP (right) α, β parameter dependence on the distance 46
2.2 Flowchart diagram for the DFT procedure 47
2.3 Typical input structure for the DFT Gaussian program 48
2.4 Flowchart diagram for the TDDFT procedure 52
2.5 Typical input structure for TDDFT Gaussian program 52

3.1 All modes present in short chain cumulenes (< 12 carbon atoms in chain) and their node representation 60

4.1 Single triplet minima difference over all the different chain lengths 69
4.2 Molecular orbital configuration for both O-cumu and S-cumu [4] 69
4.3 BLA behaviour as a function of chain length for S-cumu[n] . . 74
4.4 HOMO-LUMO gap as a function of chain length for S-cumu[n] 75

4.5 Variation of the polarizability with respect of the BLA oscillation, from top left (S-cumu[12]) to bottom right (S-cumu[4]) 78
4.6 Normalized Raman spectrum for all type of chains, the number on the top right refer to the number of carbon atom per chain 79
4.7 Raman spectra over a selected frequency range (on the left) and over all the spectrum (on the right) 82
4.8 β^* mode (even chains) 83
4.9 γ mode (even chains) 84
4.10 δ mode (even chains) 85
4.11 α mode (even chains) 86
4.12 ϵ mode (even chains) 87
4.13 ζ mode (even chains) 88
4.14 η mode ($S - C_{11} - S$ and $S - C_{12} - S$ chains) 89
4.15 Raman spectra for odd chains 91
4.16 β^* mode (odd chains) 92
4.17 γ mode (odd chains) 93
4.18 δ mode (odd chains) 94
4.19 ϵ mode (odd chains) 95
4.20 ζ mode (odd chains) 96
4.21 Single triplet minima difference over all the different chain lengths, also the previous values for the S-cumu[n] are reported as a comparison 98
4.22 BLA dependence on the chain length for O-cumu[n] wires . . . 99
4.23 HOMO-LUMO gap as a function of chain length for O-cumu[n] 100
4.24 Variation of the polarizability with respect of the BLA oscillation, from top left (O-cumu[12]) to bottom right (O-cumu[4]) 103
4.25 Normalized Raman spectrum for all type of O-cumu chains, the number on the top right refer to the number of carbon atom per chain 104
4.26 Calculated Raman spectra for O-cumu[2n] 106
4.27 β^* mode (even chains) 107
4.28 γ mode (even chains) 108
4.29 δ mode (even chains) 109
4.30 α mode (even chains) 110
4.31 ϵ mode (even and odd chains) 111
4.32 Raman spectra for odd chains 113
4.33 β^* mode (odd chains) 114
4.34 γ mode (odd chains) 115
4.35 δ mode (odd chains) 116
4.36 Some of the structures compared 117

4.37 ECC mode wavenumber dependence on the bond length alternation, the labels for each point are relative to the number of carbon atoms in chain 118
4.38 HOMO-LUMO gap dependence on the bond length alternation, the labels for each point are relative to the number of carbon atoms in chain 119
4.39 Values for the bond length alternation of bis(diphenyl), diphenyl and hydrogen polyynes compared to the BLA of sulfur, carbon , vinylidene and oxygen cumulenes 121
4.40 BLA behaviour for cumulenes 122
4.41 Values of the gap for different carbon atom wires 123
4.42 Computed values of Raman activity of several different wires: S, O, C, vynilidene terminated cumulenes and H terminated polyynes with 12 carbon atoms in chain 124
4.43 Calculated Raman spectra (normalized) of most relevant modes for each cumulene and polyynes 126
4.44 Calculated Raman spectra for the three polyyne molecules studied for 12 internal carbon atom in the wire 127

5.1 PBE0/cc-pVTZ lorentian fitting for H-Py[n] compared to experimental data obtained in our laboratory. A FWHM of 10 nm was chosen in order to have the best graphical representation 135
5.2 Calculated UV-vis spectra of hydrogen polyynes from H-Py[4] (bottom) to H-Py[16] (top) by PBE0/cc-pVTZ calculations and comparison with experimental data (made by Tabata [5] and in our laboratory [6]) 136
5.3 Analysis of the main peak for H-Py[10] with variation of the n° of γ considered 139
5.4 UV-visible spectra of hydrogen polyynes from H-Py[4] (bottom) to H-Py[16] (top), the high energetic (low wavelength) transitions are magnified in order to see the shift of each peak with chain length 139
5.5 The different transitions for H-Py[6] 141
5.6 HOMO-LUMO π_x and π_y molecular orbitals for H-Py[12] . . . 142
5.7 Experimentally determined position of the forbidden transition peaks for H-Py[4] and H-Py[6] 144
5.8 PBE0/cc-pVTZ determined lorentian fitting for Ph-Py[n] compared with experimental results both of Tabata and made in our laboratory, the FWHM was chosen arbitrarily for the best graphical representation 145

5.9 Ground state configuration (on the left), first excited state configuration, for which a dipole-allowed transition is possible from the ground state, representing the high wavelength transitions on the spectrum (on the right) 146
5.10 PBE0/cc-pVTZ calculated UV-vis spectra for diphenyl polyynes (Ph-Py[n]) 148
5.11 Analysis of a peak for Ph-Py[10] with variation of the n° of γ considered 150
5.12 PBE0/cc-pVTZ calculated vibronic spectra for Ph-Py[n], n=4,6,8,10 compared with the lorentian fitted spectrum 151
5.13 Shape of the HOMO and LUMO levels for a Ph-Py[10] wire . 153
5.14 CAM-B3LYP/cc-pVTZ vibronic spectra after Franck-Condon compared with experimental data made in our laboratory(top) and Tabata's (bottom) 157
5.15 CAM-B3LYP/cc-pVTZ vibronic spectra rigidly shifted by 20 nm compared with experimental data made in our laboratory 158
5.16 HSE06/cc-pVTZ vibronic spectra compared with experimental data made in our laboratory(left) and Tabata's (right) . . . 159
5.17 CAM-B3LYP/cc-pVTZ vibronic spectrum for Ph-Py[10] compared to the previous PBE0/cc-pVTZ calculations 161
5.18 HSE06/cc-pVTZ vibronic spectrum for Ph-Py[10] compared to the previous PBE0/cc-pVTZ calculations 162

List of Tables

4.1 Values calculated for multiplicity analysis of S-cumu wires . . 68
4.2 Computed bond length, BLA and HOMO-LUMO gap values for each of the O-cumu[n] chains with n=4,...,12 76
4.3 Calculated data for the wavenumber and Raman activity of significant peaks for even-carbon chains S-cumu[2n] 81
4.4 Calculated data for the wavenumber and Raman activity of significant peaks for odd-carbon chains S-cumu[2n+1] 90
4.5 Values calculated for multiplicity analysis of O-cumu wires . . 97
4.6 Computed bond length, BLA and HOMO-LUMO gap values for each of the O-cumu[n] chains with n=4,...,12 102
4.7 Calculated data for the wavenumber and Raman activity of significant peaks for even-carbon chains O-cumu[2n] 105
4.8 Calculated data for the wavenumber and Raman activity of significant peaks for odd-carbon chains O-cumu[2n+1] 112

5.1 Important parameters for the construction of lorentian fitted spectrum (PBE0/cc-pVTZ) of H-Py wires 134
5.2 Important parameters for the construction of vibronic spectrum (PBE0/cc-pVTZ) of H-Py wires 137
5.3 γ computational details for H-Py wires 140
5.4 Important parameters for the construction of lorentian fitted spectrum (PBE0/cc-pVTZ) of Ph-Py wires 147
5.5 Important parameters for the construction of vibronic spectrum (PBE0/cc-pVTZ) of Ph-Py wires 149
5.6 γ parameter computational details for Ph-Py wires 152
5.7 Important parameters for the construction of vibronic spectra with B3LYP, HSE06 and CAM-B3LYP exchange-correlation functionals for H-Py wires 155
5.8 Important parameters for the construction of vibronic spectra with CAM-B3LYP and HSE06 exchange-correlation functionals for Ph-Py wires 160

6.1 Important values for Ph-Py[n] chains with n=4,6,8,10,12. ϕ represent the phenyl end group. 168
6.2 Important values for BPh-Py[n] chains with n=4,6,8,10,12. ϕ represent a phenyl endgroup 169
6.3 Important values for Vyn-cumu[n] with n=4,..,12. 170
6.4 Important values for carbon cumulenes for each of the Cn-cumu[n] chains with n=4,5,6,7,8,9,10,11,12 171
6.5 Important values for H-Py[n] with n=4,6,8,10,12. 172

Contents

0.0.1 Estratto - italiano 12
0.0.2 Abstract - english 12
0.0.3 Sommario - italiano 13
0.0.4 Summary - english 15

1 Introduction on carbon atomic wires(CAWs) 17
1.0.1 Carbon nanostructures 17
1.0.2 Properties of polyynic and cumulenic CAWs 19
1.0.3 Production techniques 21
1.0.4 Characterization techniques 22
1.0.5 Potential applications 25

2 Fundamentals of density functional theory 27
2.1 Wave function and Schrödinger equation 28
2.2 Born Oppenheimer approximation 30
2.3 LCAO 31
2.4 Approximations of the Hartree-Fock method 32
2.4.1 Mean field approximation 32
2.4.2 Slater determinant approximation 33
2.5 The Hartree-Fock method 36
2.5.1 The Roothann-Hall equations 37
2.5.2 The construction of the basis set 38
2.5.3 SCF method 39
2.6 Density functional theory 40
2.6.1 The Hohenberg-Kohn theorems 40
2.6.2 Kohn- Sham equation 42
2.6.3 Exchange and correlation functional 44
2.6.4 Hybrid functionals 45
2.7 GAUSSIAN input details for the optimization and Raman analysis 47
2.8 Time dependent DFT 48
2.8.1 Runge-Gross theorem 48

2.8.2 Time-dependent Kohn Sham equations 49
2.8.3 Exchange-correlation functions for TDDFT 50
2.9 GAUSSIAN input details for excited state and vibronic spectra determination 51

3 Fundamentals of Raman and UV-vis spectroscopy 53
3.1 Vibrational dynamics 53
3.2 Raman spectroscopy 57
3.2.1 Effective conjugation coordinate theory 58
3.2.2 Classification of different modes 59
3.3 Basis of quantum transitions and UV-vis spectroscopy 61
3.3.1 Fermi golden rule 61
3.3.2 The dipole operator 62
3.3.3 UV - visible spectroscopy 64
3.3.4 Frank-Condon principle 64

4 Investigation of structural and electronic properties for carbon atom wires 67
4.1 Sulfur cumulenes 67
4.1.1 Electronic configuration of ground state for sulfur cumulenes 68
4.1.2 Modulation of HOMO-LUMO gap and BLA with chain length for S-cumu chains 73
4.1.3 Analysis of Raman intensity parameters for S-cumu[n] chains 77
4.2 Oxygen cumulenes 97
4.2.1 Electronic configuration of ground state for O-cumu chains 97
4.2.2 Modulation of HOMO-LUMO gap and BLA with chain length for O-cumu chains 99
4.2.3 Analysis of Raman intensity parameters for O-cumu[n] chains 103
4.3 Discussion on structural and electronic properties of different CAWs 117
4.3.1 Correlation between structural, electronic and vibrational properties 118
4.3.2 Bond-length alternation (BLA) 121
4.3.3 Energy gap and conjugation 123
4.3.4 Identification of Raman activity between cumulenes and H terminated chains 124

4.3.5 Identification of Raman activity between polyyinic chains (Ph, BPh and H) 126
4.4 Final considerations of the overall structural and electronic values determined 128

5 Prediction of the vibronic spectra for H-Py[n] and Ph-Py[n] 131
5.1 Methodology and calculation details 132
5.2 TDDFT predicted UV-visible spectrum and its comparison with the experimental data 133
5.3 Functional dependence on the spectrum 154
5.4 Discussion on the vibronic transitions and UV-visible spectra determined 163

6 Conclusions 165
6.1 Appendix 167

0.0.1 Estratto - italiano

La tesi è focalizzata sullo studio computazionale Gaussian DFT/TDDFT di catene di carbonio ibridizzate sp, e delle loro proprietà strutturali, elettroniche e spettroscopiche in relazione alla lunghezza della catena e al tipo di terminale. In particolare sarà presentato lo spettro Raman di catene cumuleniche terminate S o O, e lo spettro vibronico di catene poliiniche terminate H o fenile.

0.0.2 Abstract - english

The thesis is focused on Gaussian DFT/TDDFT analysis of sp hybridized carbon wires, the structural and optoelectronic properties will be analyzed in relation of different chain length and endgroups. In particular it will be presented the Raman spectra of cumulenic structures with S, O endgroups, and the vibronic spectra of polyynic chains with H or phenyl endgroups.

0.0.3 Sommario - italiano

Il carbonio è un importante elemento che può generare una vasta varietà di strutture ibridizzate, dalla struttura sp^3 del diamante a quella sp^2 del grafene, per arrivare alla ideale catena ibridizzata sp chiamata carbina.
Nel secolo scorso gli studi sono stati focalizzati soprattutto sulla ricerca della carbina infinita, e sulla caratterizzazione di catene di carbonio che hanno ricevuto interesse nel campo dell'astrofisica e astrochimica.
Invece, negli ultimi anni, l'interesse si è spostato nella produzione e caratterizzazione di carbon atom wires (CAWs) per le loro eccezionali proprietà meccaniche e elettroniche.
Le catene in carbonio non sono solo interessanti per queste proprietà, ma anche per la possibilità di variare queste ultime tramite la modificazione della loro lunghezza o del loro terminale. Tramite applicazione di uno stress assiale è inoltre possibile promuovere il passaggio della catena da isolante a semiconduttiva, modificando inoltre le proprietà strutturali, molto promettente per future applicazioni nel campo dell'elettronica molecolare.
Questa tesi in particolare è focalizzata sullo studio, tramite tecniche computazionali basate sulla DFT (density functional theory) di differenti catene di carbonio e nella analisi delle loro proprietà strutturali, elettroniche e ottiche.
Le catene ibridizzate sp son sistemi policoniugati , caratterizzate da un elevato accoppiamento elettrone-fonone, quindi sarà possibile investigare queste proprietà sulla base di tecniche spettroscopiche quali Raman e UV-vis.
Lo spettro Raman è stato determinato attraverso l'uso del programma Gaussian e dell'utilizzo della teoria DFT (density functional theory), in particolare per strutture come le S-cumu[n] (o $S-C_n-S$) e le O-cumu[n] (o $O-C_n-O$), interessanti per la loro struttura quasi equalizzata (cumulenica).
Lo spettro UV-vis è stato costruito a partire dal programma Gaussian utilizzando la teoria DFT time dependent (TDDFT) per determinare un semplice spettro iniziale costituito puramente dal fitting lorenziano dei dati ricavati. Il conseguente uso del programma UVFC sviluppato nel nostro laboratorio ci ha permesso di determinare lo spettro vibronico rendendo conto anche dei fattori di Franck-Condon, per strutture quali H-Py[n] (o $H-C_n-H$) e Ph-Py[n] (con terminazione fenile). Queste catene sono state scelte perchè erano presenti dati sperimentali rilevati nel nostro laboratorio e esterni, utili alla validazione del lavoro e a eventuali confronti.
L'analisi da noi riportata sottolinea la profonda importanza dei metodi computazionali, sia per un'affidabile interpretazione degli spettri sperimentali, che per l'analisi delle proprietà di sistemi policoniugati. Abbiamo effettuato un'importante passo avanti in questo campo, con l'introduzione dell'analisi

dei fattori di Franck-Condon per lo sviluppo di uno spettro vibronico confrontabile con dati sperimentali.
L'importanza del lavoro non è solo correlata a questo importante sviluppo computazionale e nel campo della ricerca, ma nel contempo vuole essere la base per potenziali applicazioni di questi sistemi sia nel campo tecnologico che industriale.

0.0.4 Summary - english

Carbon is an important element that can generate a wide variety of different structures based on its hybridization states, moving from the sp^3 hybridized structure of diamond to the sp^2 graphene and the ideal sp-carbon allotrope named carbyne
In the last century the studies on *sp*-carbon structures were mainly focused on the search for the infinite *sp* carbyne, and on the characterization of short linear carbon chains interesting in the astrophysics and astrochemistry field. In the recent years the topic has shifted to the production and characterization of carbon atom wires (CAWs) due to their interesting properties and on the potential applications (especially for the molecular electronics field).
CAWs are studied not only for the exceptional mechanical and electronic properties but also for the ability to tune significantly these properties by modifying chain length and end-chain groups [6].
Moreover, It was demonstrated that generating an axial stress on this sp carbon structures can promote an insulator to semiconductor transition and modify also the structural properties [7] (BLA) , which is promising for potential applications.
In the context of this thesis work we will focus on DFT computation of structural, electronic and spectroscopic properties for different finite length *sp* hybridized CAWs.
Sp hybridized carbon chains are polyconjugated systems, characterized by an high electron-phonon coupling, therefore both the electronic and the structural properties of these systems can be investigated through Raman and UV-vis spectroscopy. Their analysis allow to give a detailed interpretation on the molecular phenomena taking place in the material.
It should be noted that some previous works [1, 2, 8, 9] have already underlined the important relation between this properties in detail for similar systems.
Raman spectra will be determined through the use of the Gaussian program and DFT (density functional theory), in detail for sulfur cumulenes ($S - C_n - S$- defined as S-cumu[n]) and oxygen cumulenes ($O - C_n - O$ - defined as O-cumu[n]), these wires are particularly interesting for their quasi equalized (cumulenic) structure.
UV-vis spectra will be computed starting with the Gaussian program and time dependant DFT calculations to determine a simple spectrum based on a lorentian fitting of the ground to excited state parameters found in preliminary TDDFT calculations. The consequent use of the UVFC program will allow us to build the vibronic spectra considering also the Franck-Condon factors. This will be carried out in particular for H-Py[n] and Ph-Py[n]

structures which have been experimentally characterized in our laboratory [6].
These systems represent an ideal test case since UV-visible spectra have been experimentally measured by Tabata et al. [5] (for H-Py[8] to H-Py[16]), in our laboratory [6] for (Ph-Py[2] to Ph-Py[10]) and for (H-Py[6] to H-Py[16]) and these experimental reference are necessary to have a validation of our results and a detailed discussion.
We underlined the importance of computational methods, not only for a correct interpretation of experimental spectroscopic results, but also on the analysis of the properties of polyconjugated systems. In this work an important step was done in this field, with the introduction of Franck-Condon factors analysis to compute a proper vibronic spectra comparable with experimental results.
The importance of this work is not only correlated on the computational results and on the research field, but at the same time is a basis for potential applications of these systems both on the technological and the industrial field.

Chapter 1

Introduction on carbon atomic wires(CAWs)

1.0.1 Carbon nanostructures

The last few decades has seen carbon based nanostructures as a rising matter of interest in both science and technology.
Many people have been honored with the nobel price in relation of important discoveries in these field, the first one awarded to H. Kroto and R. Smalley for the discovery of fullerenes in 1996 [10] and most recently to A. Geim and K. Novoselov for research on graphene in 2010 [11].
Among these carbon nanostructures, the search for the "lacking allotrope", named carbyne (fig. (1.1)), the ideal infinite chain of sp-hybridized carbon atoms, was a matter of interest at the end of the last century.

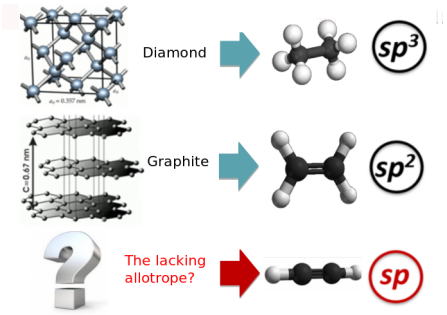

Figure 1.1: Graphical representation of the sp^3, sp^2 and ideal sp allotropes

To this day the longest sp carbon chain discovered was composed by about 6000 carbon atoms and was found inside a double-wall carbon nanotube [12]. In isolated form only a structure consisting of 44 carbon atoms has been

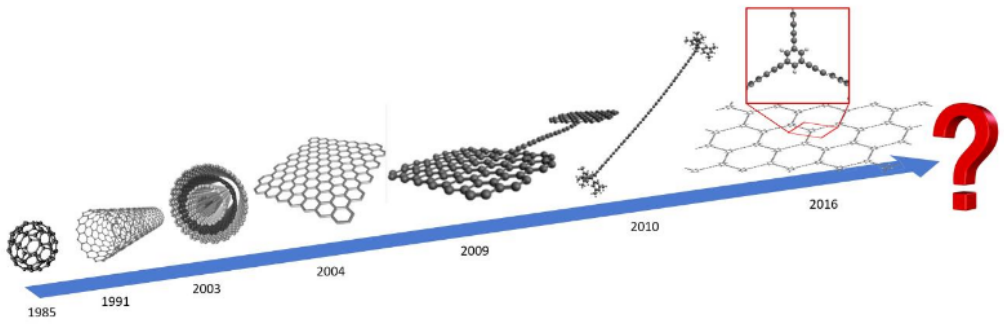

Figure 1.2: Progress on carbon nanostructures development and further studies [1]

synthesized by Tykwinski and Chalifoux [13], still very far from the idealized infinite carbyne.
In the recent years the focus of research has generally shifted from this topic to the possibility of synthesis and characterization of short length carbon atom wires (CAWs).
Also the potential applications have receive attention, especially on molecular electronics, this was pushed by recent achievements on the research of graphene structures and on the development of hybrid sp - sp^2 systems.
CAWs [1] are studied not only for the exceptional mechanical (Young modulus of 32TPa [14]) and electrical properties (electron mobility $> 10^5 \frac{cm^2}{Vs}$ [15]) but also for the ability to tune the electronic properties [8] [1] with chain length and end-chain group, they have an high surface area ($> 10.000 \frac{m^2}{g}$ [16]).
Another property not so prominent for potential applications is that CAWs are in general highly reactive and tend to undergo chain-chain crosslinking reaction tending to sp^2 hybridization.
Their high electron-phonon coupling allow us to determine the length and endgroups of a specific wire based on spectroscopic techniques such as Raman and UV-vis.

1.0.2 Properties of polyynic and cumulenic CAWs

The carbon atom wires can be divided into two types, polyynes and cumulenes (or poly-cumulenes) .
The classification depends in particular on the nature of their intrachain bonding for the infinite carbyne and we can classify them accordingly; if we have an important alternation of 'quasi single' - 'quasi triple' bond on the chain (that corresponds to high bond length alternation - called BLA) we will have a polyynic structure, otherwise if we have an equalized with no alternation we will have a cumulenic structure.
For the infinite carbyne there is also an effect called Peierls distortion (which was at first studied for polyacetilene polymers) that affects the electric character (metallic/semiconducting) of polyconjugated wires.
This is not relevant for short chains and become important only with more than 52 carbon atoms in the chain, this was demonstrated by Yang et al. [17], thus it will not generally be taken into account in this thesis work and we will introduce just the principles.

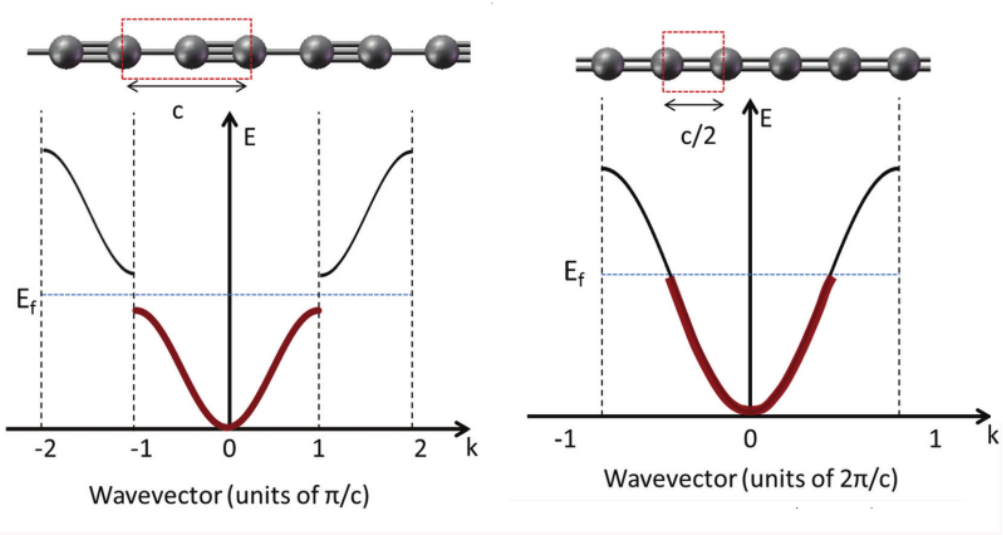

Figure 1.3: Theoretical E(k) dispersion relation for the infinite 'polyyne' (or carbyne- α), in the left, and infinite 'cumulene' (or carbyne - β) in the right [2]

As we can see in figure (1.3) in a perfect 1D equalized structures we will have the crystalline cell consisting only on a single atom, this will have a metallic character for the infinite crystal.
For the structure consisting on the single-triple bond alternation we will have a 2 atom crystalline cell and the opening of a band gap which will put the

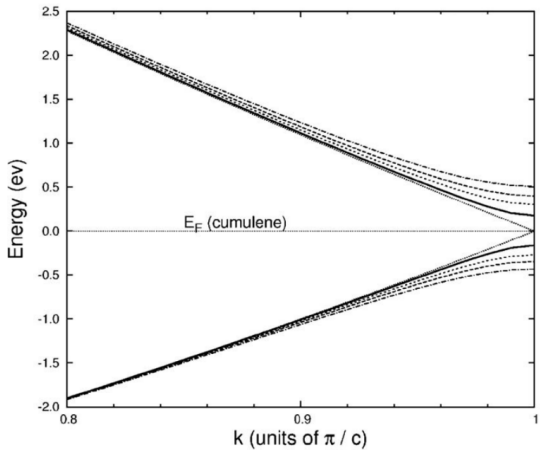

Figure 1.4: Phonon dispersion relation representing the opening of a gap for the theoretical infinite carbyne

system on a semiconducting character, this effect can be seen clearly in figure (1.4).
The polyyne or cumulene structures can be favored one to another depending on the type of terminal group that we have on the chain, that can induce a triple bond on the terminal C atom thus favoring a single - triple bond alternation (thus a polyyne) or a double bond on the terminal C that lead to an equalized double bond structures (or a cumulene).
In particular, for the molecules that we studied on this thesis, CAWs with H, phenyl and diphenyl endgroups will be classified as polyynes and with O , S , C , CH_2 will be regarded as cumulenes. This will be devised by the studies on both the bond length alternation and Raman analysis.
In fact the difference on these type of structure are not only related to the difference bond length inside the chain , but also on their electrical properties and Raman activity , cumulenes structures were initially thought to be undetectable by Raman spectroscopy because in the model cumulenic structure they don't present optical phonon branches, but in the recent years through density functional analysis it has been demonstrated the presence of Raman peaks also in this type of structures correlated to intrachain symmetric/ asymmetric stretching [9]. The CAWs are polyconjugated systems and the molecular orbital of the ground state is characterized by a conjugated π orbital delocalized over all the molecule, this is consisting of an alternation of π_u (ungerade delocalized π orbitals) and π_g (gerade delocalized π orbitals) both on the x and y direction (note that in general π_{ux} and π_{uy} are degenerate forms) [18].
They form an elliptical like isosurface which surround the 1D molecule [19].

Lafferty et al. [20], through detailed analysis of a combination band determined finally that O-cumu[n] do possess the expected $D_{\infty h}$ linear structure after the suppositions that this type of structure would assume a typical bent configuration as we have in CO_2 [21].

1.0.3 Production techniques

The processing techniques can be classified into two main categories: the physical and the chemical techniques.

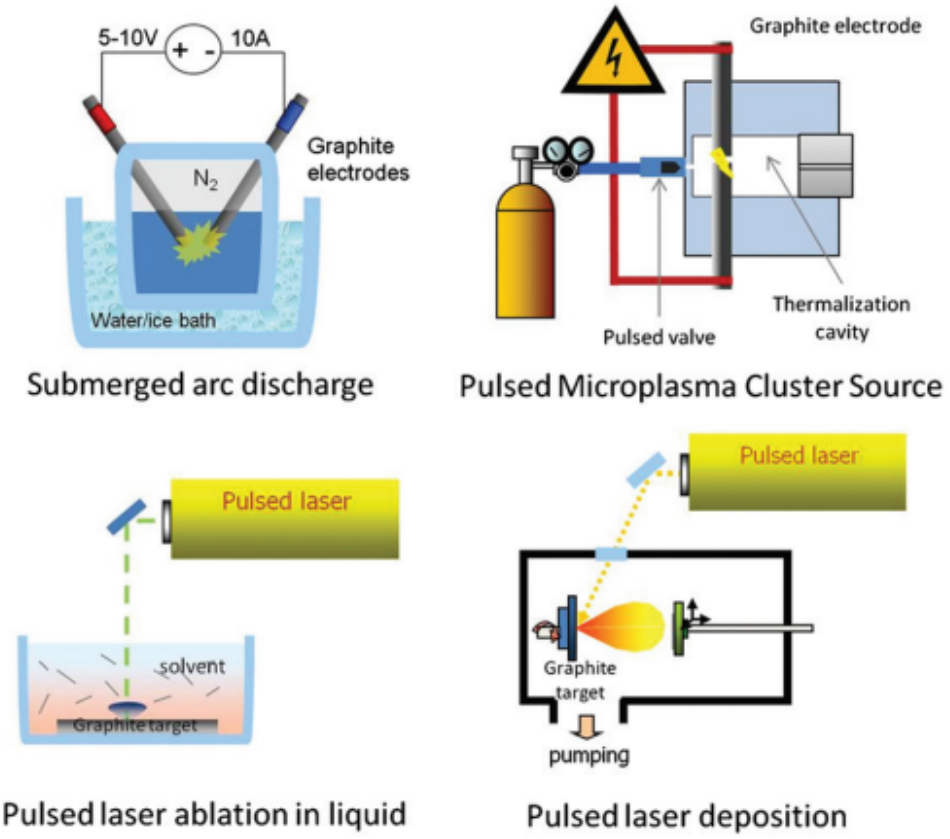

Figure 1.5: Some of the most important physical fabrication techniques [2]

Some of the physical techniques (partially showed in figure (1.5) include electric arc discharge on graphite rods submerged in organic solvents or water (this graphite rods can be coupled with other materials yielding the terminal atom, such as in the case of sulfur end-capped chains), fast cooling of carbon

vapour systems and in general on laser ablation procedures such as PLD of graphite or fullerene structures suspended in organic solvents [22].
The chemical techniques instead involve chemical reactions and are usually divided in two categories [2], the first one involves a polymerization strategy, reviewed by Kudryavtsev [23] and the second one involves molecules with a defined length and specific terminals, and is often carried out with the dimerization reaction of ethynyl groups, or Glaser reaction [24].
On the specific analysis of S-cumu[n] structures , they have been generated in laboratory by laser ablation of mixed sulfur– graphite pellets and also by pulsed discharge of acetylene/carbon disulfide /argon compounds [25].
One of the important problem of these structures is their instability even at room T (they tend to undergo interchain crosslinking reaction forming mixed sp - sp^2 structures) and have to be connected at the end with bulky groups [26] or to be deposited over an Ag substrate [27] in order to limit the crosslinking effect and improve stability.
CAWs are stable also on carbon nanostructures such as carbon nanotubes (which can have stable carbyne structures on the internal part with up to 6000 carbon atoms in chain [12]) , between planar carbon structures such as graphene [2] and in liquid solutions (for structures of up to 16 carbon atoms).
In particular the even-numbered S-cumu[n] clusters were found to be extremely unstable [28].

1.0.4 Characterization techniques

The fabrication techniques reported in the previous section in general aren't able to produce all molecules with a specific chain length but typically we have a variety of structures that must be characterized in order to define, in the case of CAWs, which is its length and termination.
Spectroscopic and visualization techniques are an important probe to assess the electronic and structural character for these polyconjugated systems.
To identify the carbon chains structure we can use imaging microscopes such as AFM [3] (atomic force microscopy), STM (scanning tunneling microscopy) and TEM (transmission electron microscopy).
Also spectroscopy techniques such as Raman([29]), UV-vis and ^{13}C NMR (nuclear magnetic resonance [30]) can give precious information of the systems due to the high electron-phonon coupling.
A lot of different carbon structures can nowadays be identified through Raman spectroscopy as we can see from fig.(1.7), and the difference between each pattern is known and clear.

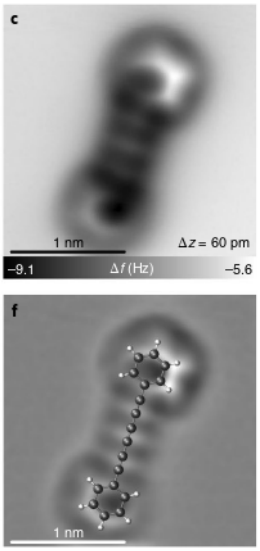

Figure 1.6: AFM images of Ph-Py[6],(c) is constant-height CO-tip AFM images of the precursor and (f) is the corresponding Laplace-filtered AFM images with structural ball-and-stick models overlaid as a visual aid done by Pavlicek et al [3]

The Raman spectra of H-Py[n] show a similar pattern as polyenes, with an intense line that corresponds to the ECC mode (corresponding to the anti-symmetric stretching of adjacent CC bonds) and a second minor band (the β peak) is usually observed, this modes usually are found in the 1800–2300 cm^{-1} spectral region.
Cumulene wires displays only acoustic phonon branches and it was theorized that the system would not present any optical activity [31, 32] and therefore it wouldn't be possible a characterization through Raman spectroscopy.
However this is only true for infinite cumulene, for CAWs this selection rule will be relaxed, making it possible for the identification of some cumulenes through Raman spectroscopy.

The S-cumu are important also in astrochemistry since they initially have been observed on DIB (diffuse interstellar bands) and in the atmosphere of Titan, which is a moon of saturn, through spectroscopic detection.
In particular in some cases we will find them mixed with heteroatoms such as O and S [33] providing them with the structure that will be very important for our specific study.
Small $C_n - S$ species (n=1-3-5) have been observed in particular on interstellar medium [4]. But the $S - C_n - S$, which is part of the thesis, remain undetected , because of their negligible dipole moments.

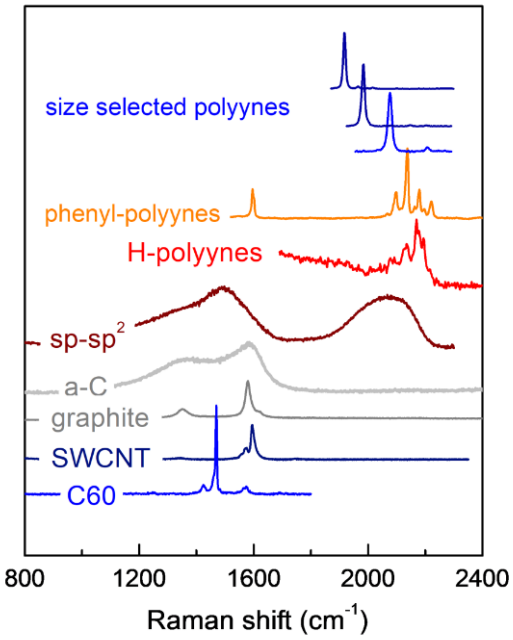

Figure 1.7: Several different structures identified by Raman spectroscopy

Clusters $C_2 - S$ and $C_3 - S$ were initially detected only by millimeter and submillimeter spectroscopy [25] and then seen by a different spectroscopy technique which is radio frequency spectroscopy on DIB_s.

1.0.5 Potential applications

The most recent developments regarding the potential applications for these CAWs are mainly focused on the molecular electronic field, where other carbon structures such as graphene and carbon nanotubes have already been used for the fabrication of transistors for microelectronics, due to the extraordinary electron mobility yielded by these carbon structures at room T. Considering the problem of stability of these wires it is clear that the integration with the current silicon technology can be difficult, and usually transistor based on finite length carbynes are generally considered integrated between graphene planes.
In this structure in fact they are naturally relatively stable, acting as graphene interconnectors [34] in sp - sp^2 systems.
Other applications aside from microelectronics include the possibility to use CAWs in hydrogen storage systems [16] and recently also on supermultiplexed optical imaging and barcoding [35].

Chapter 2

Fundamentals of density functional theory

In this chapter we will be briefly explain all the fundamentals about density functional theory (DFT).
The theoretical background will take a cue from M.Tommasini's "physical properties of molecular materials" lecture notes, A. Milani slides about the basis of DFT calculations, the handbook of conducting polymers [36], Innocenti's thesis and article [9] and Ziegler work. [37]
Starting from the concept of the wave function and the Schrödinger equation, with a brief introduction of the Hartree-Fock method we will elaborate also the basis of the Kohn-Sham equations, the basis of the density functional theory.
This will be extended to time dependent DFT through the concept of Runge-Gross theorem and the time dependent Kohn-Sham equations.
We will introduce all the important parameters used for the calculus, especially the basis set (cc-pVTZ) and the exchange-correlation functional used: B3LYP [38], CAM-B3LYP [39] , PBE1PBE (PBE0) and HSE1PBE (HSE06) both for DFT and time dependent DFT [40].

2.1 Wave function and Schrödinger equation

The Schrödinger equation is an important relation used to define the wave-function $\Psi = \Psi(\mathbf{r}, t)$ describing a certain system of particles.
Its time dependent form is:

$$i\hbar\frac{\partial\Psi}{\partial t}(\mathbf{r}, t) = \hat{H}\Psi(\mathbf{r}, t) \tag{2.1}$$

Where $\hat{H} = (-\frac{\hbar^2}{2m}\nabla^2 + \hat{V})$ is the Hamiltonian operator, $\hbar$ the reduced Plank constant ($= 10^{-34}$ Js) and $\mathbf{r}$,$\mathbf{R}$ are the position vectors.
The time independent form (2.2) for $\Psi = \Psi(\mathbf{r})$ is:

$$E\Psi(\mathbf{r}) = \hat{H}\Psi(\mathbf{r}) \tag{2.2}$$

Where E is the total energy of the system , sum of both the kinetic and potential contribution.
This is the classical quantum mechanical eigen-value problem , where Ψ are a complete set of orthonormal eigen-vectors and E is completely known and determined.
We know that one of the important properties of the $|\Psi(r, t)|^2$ is that is equal to the probability density as devised by Max Born and therefore:

$$\int_{-\infty}^{\infty} |\Psi(\mathbf{r}, t)|^2 d\mathbf{r}dt = 1 \tag{2.3}$$

The time dependent Schrödinger equation will give us the full information on a quantum mechanical system and its evolution through time but it is very difficult to solve analytically even for simple diatomic system , that is why to elaborate the practical molecular orbital models we will need at first to introduce several approximation to simplify step by step the quantum mechanical problem.
In fact if we consider even the simplest molecule that we are going to analyze , $H - C_4 - H$, we will have 6 nuclei and 26 electrons to take into account , which will give a partial differential eigen value equation with 96 variables.

Let's first consider a generic Hamiltonian of a polyatomic molecule with N nuclei and M electrons in which we divide the Hamiltonian operator into other entities corresponding to the kinetic ($\hat{T}$) and potential ($\hat{V}$) operators.

$$\hat{H} = \hat{T}_e(\mathbf{r}) + \hat{T}_n(\mathbf{R}) + \hat{V}_{ee}(\mathbf{r}) + \hat{V}_{en}(\mathbf{r}, \mathbf{R}) + \hat{V}_{nn}(\mathbf{R}) \tag{2.4}$$

$\hat{T}_e$ is the operator corresponding to the sum of all kinetic contributions coming from electrons , we note from 2.5 that $\hat{T}_e = \sum_i \hat{t}_{ei}$ so it's a summation over the independent values of the kinetic energy for each particle (i), so it can be regarded as a one body operator:

$$\hat{T}_e = -\frac{\hbar^2}{2m_e} \sum_{i=1}^{M} \nabla_i^2 = \sum_{i=1}^{M} \hat{t}_{ei} \tag{2.5}$$

$\hat{T}_n$ instead is the operator corresponding to the sum of all kinetic contributions coming from nuclei and is also a one body operator

$$\hat{T}_n = -\frac{\hbar^2}{2M_n} \sum_{i=1}^{N} \nabla_i^2 = \sum_{i=1}^{N} \hat{t}_{ni} \tag{2.6}$$

For the potential energy we take into account all the different Coulomb interaction among charged particles , in particular $\hat{V}_{ee}$ is the operator corresponding to the sum of all potential energy contributions coming from electron - electron interactions and is a 2 body operator, it involves two particle position in the same sum.

$$\hat{V}_{ee} = \frac{e^2}{4\pi\epsilon_0} \sum_{i\neq j}^{M} \frac{1}{|\mathbf{r}_i - \mathbf{r}_j|} = \sum_{i\neq j} \hat{v}_{eij} \tag{2.7}$$

$i \neq j$ is in general accounted to exclude the non-physical self coulombic attraction-repulsion, $\mathbf{r}_i - \mathbf{r}_j$ describe the distance between the electron i and j, under the same description we have

$$\hat{V}_{nn} = \frac{e^2}{4\pi\epsilon_0} \sum_{i\neq j}^{N} \frac{Z_i Z_j}{|\mathbf{R}_i - \mathbf{R}_j|} = \sum_{i\neq j} \hat{v}_{nij} \tag{2.8}$$

where $\mathbf{R}_i - \mathbf{R}_j$ describe the distance between the nuclei i and j, and finally

$$\hat{V}_{en} = -\frac{e^2}{4\pi\epsilon_0} \sum_{i,I}^{N,M} \frac{Z_I}{|\mathbf{r}_i - \mathbf{R}_I|} = \sum_{i,I}^{N,M} \hat{v}_{i,I} \tag{2.9}$$

This term is a two body operator that can be turned into a one body operator if we consider the electron positioned in a field generated by all the nuclei that we have in our molecule, in practice

$$\hat{V}_{en} = -\frac{e^2}{4\pi\epsilon_0}\sum_{i,I}^{N,M}\frac{Z_I}{|\mathbf{r}_i - \mathbf{R}_I|} = -\frac{e^2}{4\pi\epsilon_0}\sum_{i}^{M}\left(\sum_{I}^{N}\frac{Z_I}{|\mathbf{r}_i - \mathbf{R}_I|}\right) = \sum_{i}^{M}\hat{v}_n(\mathbf{r}_i) \tag{2.10}$$

2.2 Born Oppenheimer approximation

The Born-Oppenheimer approximation let us separate the degrees of freedom related to electrons from the ones related to the nuclei, this is an important simplification for the eigen-value problem of molecules.
In practice we will say that we are in a position where "independent" electrons orbit in a quasi static field generated by quasi-immobile nuclei.
This can justified by the fact that if we have the same momentum for electron and nuclei , $p_e = p_n = p$ we will have that the velocity of nuclei will be negligible with respect of those of electrons , as stated in equation 2.11 , with m_e (mass of electrons) being negligible with respect of the nuclei mass M_n.

$$\frac{p_e}{m_e} = \frac{p}{m_e} = v_e >> v_n = \frac{p}{M_n} = \frac{p_n}{M_n} \tag{2.11}$$

This justification lead to an important quantum mechanical approximation , called Born - Oppenheimer approximation , in which the overall wave function for the system (Ψ) is divided in a electronic contribution $\psi_e(\mathbf{r}|\mathbf{R})$ in which the position of the electron r is parametrically depending on the position of the nuclei R and in a nuclei contribution $\psi_n(\mathbf{R})$ independent on the position of electrons r.

$$\Psi(\mathbf{r}, \mathbf{R}) = \psi_e(\mathbf{r}|\mathbf{R})\psi_n(\mathbf{R}) \tag{2.12}$$

We will consider an eigen-value equation (2.13), in which only the operators relative to the energetic contributions coming from electrons is accounted, specifically we will consider the hamiltonian relative to electrons, $\hat{H}_e = \hat{T}_e + \hat{V}_{ee} + \hat{V}_{en}$ which get rid of the purely nuclear terms $\hat{V}_{nn}$ *and* $\hat{T}_n$.

$$\hat{H}_e(\mathbf{R})\psi_e(\mathbf{r}|\mathbf{R}) = \epsilon_e(\mathbf{R})\psi_e(\mathbf{r}|\mathbf{R}) \tag{2.13}$$

$\psi_e(\mathbf{r}, \mathbf{R})$ will be the eigen-function of electrons related to this eigen-value

problem.
$\psi_n(\mathbf{R})$ will be an eigen-function of an effective nuclear Hamiltonian called H_n which is equal to $T_n(\mathbf{R}) + V_{nn}(\mathbf{R}) + \epsilon_e(\mathbf{R})$. In this context we can see that the nuclei fell an overall potential coming both from the quasi-static field generated by the other nuclei ($V_{nn}(\mathbf{R})$) and the field generated by the electrons ($\epsilon_e(\mathbf{R})$) so the total potential field will be

$$V(\mathbf{R}) = V_{nn}(\mathbf{R}) + \epsilon_e(\mathbf{R}) \tag{2.14}$$

This take into account the effect of the electron distribution with the multiple effect of shielding the nuclear coulombic repulsion and generating attraction forces between nuclei when $\psi_e(\mathbf{r}|\mathbf{R})$ is localized in the bonding region. V(R) will be called interatomic potential. This simplify our overall eigen-value problem , if the electronic eigen value problem is solved , thus we know the value of $\epsilon_e(\mathbf{R})$ and the eigen-vector ψ_e we can evaluate the interatomic potential V(R) and then we can solve the nuclei eigen value problem , finding the value for the ψ_n eigen vectors, then combining the two ψ we will find the overall wavefunction for our system.

2.3 LCAO

LCAO (linear combination of atomic orbitals) is another important concept in which we will have to focus before starting the discussion of the Hartree-Fock method.
In this method the molecular orbitals ($|\Psi_j\rangle$) are built as a linear combination of atomic orbitals ($|\psi_i\rangle$).

$$|\Psi_j\rangle = \sum_i c_{ij} |\psi_i\rangle \tag{2.15}$$

2.4 Approximations of the Hartree-Fock method

In this section we will introduce two of the main approximations for the Hartree-Fock method, the mean field and the Slater determinant approximation.

2.4.1 Mean field approximation

Mean field approximation is a simplification that we are going to apply to the Schrödinger equation, it is a particular technique in which we convert the many body hamiltonian problem to a one body problem.
One of this mean field approximations is the Hartree-Fock approximation, in which we split the effective potential of each electron in a coulombic and exchange part. So to start the discussion we will try to convert all the operators contained in the electronic hamiltonian $\hat{H}_e$ into sum of one-body operators relative of each electron that we have in the system.

$$\hat{T}_e = -\frac{\hbar^2}{2m_e}\sum_{i}^{M}\nabla_i^2 = \sum_{i=1}^{M}\hat{t}_{ei} \tag{2.16}$$

and $\hat{V_{en}}$ as we have already seen

$$\hat{V}_{en} = -\frac{e^2}{4\pi\epsilon_0}\sum_{i,I}^{N,M}\frac{Z_I}{|\mathbf{r}_i - \mathbf{R}_I|} = -\frac{e^2}{4\pi\epsilon_0}\sum_{i}^{M}\left(\sum_{I}^{N}\frac{Z_I}{|\mathbf{r}_i - \mathbf{R}_I|}\right) = \sum_{i}^{M}\hat{v}_n(\mathbf{r}_i) \tag{2.17}$$

The last term in the electronic Hamiltonian will be the potential of electron -electron interaction $\hat{V}_{ee}$, this term cannot be turned into a one-body operator since it involves the sum of interaction terms of two electrons at the same time.
So if we put together what we discover until now it will be:

$$\hat{H}_e = \sum_{i=1}^{M}\left(\hat{t}_{ei} + \hat{v}_n(\mathbf{r}_i)\right) + \sum_{i\neq j}^{M}\hat{v}_{eij} \tag{2.18}$$

In which the sum of $\left(\hat{t}_{ei} + \hat{v}_n(\mathbf{r}_i)\right)$ is also called as core hamiltonian for the electron or $\hat{h}_0(i)$.
The purpose of the mean field approximations (also of the Hartree fock approximation) is to reduce the two body-operators into an effective one-body

operator which is able to reproduce effectively the energy and eigen-functions of the real (non-approximated) system.
This can be developed by defining the modulated average of $\hat{v}_{eij}$ as an effective one-body operator potential of the type:

$$\hat{v}_{eff}(i) =< \hat{v}_{eij} > \tag{2.19}$$

The electrons are no more explicitly interacting one with the other: they do interact with the mean field created by all the other electrons in the system which approximately replace the explicit electron-electron interaction as an average term of all the contributions.
So we are finally reducing the electronic hamiltonian to a contribution of approximated effective electronic one-body hamiltonians for each electron on the system, so:

$$\hat{H}_e = \sum_{i=1}^{M} (\hat{h}_0(i) + \hat{v}_{eff}(i)) = \sum_{i=1}^{M} \hat{h}_{eff}(i) \tag{2.20}$$

This important conclusion give the electronic hamiltonian a peculiar one-body term, this simplify enormously the Schrödinger equation and is the second step to determine an effective computational formulae for calculators

2.4.2 Slater determinant approximation

One of the other important approximations, is that the eigen-functions will be described by a single Slater determinant, this is used to take into account the effect of the exchange between electrons.
Let at first consider a single body hamiltonian

$$\hat{h}_{eff}(i)\chi_k(i) = \epsilon_k \chi_k(i) \tag{2.21}$$

In which $\chi_k(i)$ will be a one -electron wave function , the total wavefunction of all the electrons can be constructed as a product of all the wavefunctions for each of the electrons in the system, this is the so called Hartree approximation:

$$\psi_e(1, 2, ..N) = \chi_a(1)\chi_b(2)..\chi_n(N) \tag{2.22}$$

1,2 .. N represent the electron coordinates, instead χ_n represent a single spin

orbital.
In a 3 electron system for example

$$\hat{H}_e\psi_e(1,2,3) = \sum_{i=1}^{3}\left(\hat{h}_{eff}(i)\chi_a(1)\chi_b(2)\chi_c(3)\right) = \tag{2.23}$$

$$= \epsilon_a\chi_a(1)\chi_b(2)\chi_c(3) + \chi_a(1)\epsilon_b\chi_b(2)\chi_c(3) + \chi_a(1)\chi_b(2)\epsilon_c\chi_c(3) = \tag{2.24}$$

$$= (\epsilon_a + \epsilon_b + \epsilon_c)\chi_a(1)\chi_b(2)\chi_c(3) \tag{2.25}$$

This can be easily extended for system of N electrons.
The important principle given by this calculation is that the Hartree product is eigenfunction of the many body Hamiltonian with associated energy eigenvalue given by the sum of the energies of the (χ) spin orbitals which compose the Hartree product:

$$E_e = \epsilon_a + \epsilon_b + ... + \epsilon_n \tag{2.26}$$

Under this assessment we note that any permutation between 1,2 .. N doesn't change the overall energy of the system.
More precisely the N! possible permutations of the N electron coordinates on the available N spin orbitals is degenerate (with the same energy level).
Hence we may form any linear combination of the available N! Hartree products to form a legitimate many-body wave function, still eigenfunction of $\hat{H}_e$, with energy given by the sum of orbital energies.
The construction of this many body wavefunction will take into account firstly that for electron under permutation of the electron into the different spin orbitals we will have a change in sign , in particular with respect to the Hartree approximation $\psi_e = \chi_a(1)\chi_b(2)...\chi_n(N)$ we will need to introduce the anti-simmetry principle for fermions (such as electrons):

$$\psi_e(1,2) = -\psi_e(2,1) \tag{2.27}$$

and so this type of wavefunction can be easily described by

$$\psi_e(1,2) = N\left(\chi_a(1)\chi_b(2) - \chi_a(2)\chi_b(1)\right) \tag{2.28}$$

upon proper normalization N , this will permit the construction of the so called Slater determinant that in the general form will be :

$$\psi_e(1,2..N) = \frac{1}{\sqrt{N!}} \begin{vmatrix} \chi_a(1) & \chi_b(1) & ... & \chi_n(1) \\ \chi_a(2) & \chi_b(2) & ... & \chi_n(2) \\ ... & ... & ... & ... \\ \chi_a(N) & \chi_b(N) & ... & \chi_n(N) \end{vmatrix} \tag{2.29}$$

One of the observable effects of this matrix interpretation is the fact that upon changing the position of two electrons we will change two rows of the matrix, therefore changing the sign of the many body wave function, this is what we expected from (2.27). Also if we have two completely identical column on the matrix we will have that the determinant will be 0 , this represent the Pauli exclusion principle , which states that we can't have two electrons in the same orbital with same multiplicity (corresponding to same set of quantum numbers).
The Slater determinant is an approximated representation of the many body wavefunction.

2.5 The Hartree-Fock method

For the hartree-fock method all the approximations introduced in the previous section will be necessary, as a briefing we have 5 major approximations

- the Born-Oppenheimer approximation
- the many body wavefunction assumed to be described by the Slater determinant
- the mean field approximation (in particular HF approximation)
- the assumption that relativistic effects are negligible
- the assumption that the variational solution will be a linear combination of a basis set that will be complete and finite

For the HF approximation (a particular mean field approximation) the term $\hat{h}_{eff}$ is represented by the so-called fock operator or $\hat{f}$ which is the operator relative to the single electron eigen value problem:

$$\hat{f}(i)\psi_e(i) = \epsilon(i)\psi_e(i) \tag{2.30}$$

In this approximation the mean field or V_{eff} is separated into a Coulomb operator ($\hat{J}$) and an exchange operator ($\hat{K}$).

$$\hat{f}(i) = \hat{h}_0(i) + \hat{v}_{eff}(i) = \hat{h}_0(i) + \sum_{j\neq i}^{M} \hat{J}(j) - \sum_{j\neq i}^{M} \hat{K}(j) \tag{2.31}$$

J operator (or Coulomb operator) represent the coulombic repulsion between the electron relative to the fock equation (2.30) and all the other electrons (j) of the system.
K operator (or exchange operator) describes the interchange between two electrons.
The solution of this problem is iterative and undergoes the so called self consistent field (SCF) that we will introduce after a brief introduction on the Roothann-Hall equations and on the basis sets.

2.5.1 The Roothann-Hall equations

The Roothann-Hall equations start from the position only problem and doesn't take into account the spin multiplicity as in eq. (2.30), in practice:

$$\hat{f}_r(\mathbf{r}_1)\psi_r(\mathbf{r}_1) = \epsilon_r\psi_r(\mathbf{r}_1) \tag{2.32}$$

The fock operator will be modified in this sense:

$$\hat{f}_r(i) = \hat{h}_0(i) + \sum_{j\neq i}^{M/2} 2\hat{J}(j) - \sum_{j\neq i}^{M/2} \hat{K}(j) \tag{2.33}$$

It is still not possible to solve the equation (2.32) nowadays , but Roothann developed a method in order to convert the Hartree-Fock equation into a matrix problem that can be solved by simple matrix algebraic methods.
In particular he thought to produce the molecular orbitals as a linear combination of atomic orbitals, or LCAO.
The atomic orbitals will be also approximated in a linear combination of Gaussian and contraption of gaussian for the gaussian-type basis set and in general by a set of independent and orthonormal basis functions.
So introducing a set of known basis functions K we will expand the molecular orbital (ψ_r) into a combination of atomic orbitals

$$\psi_i = \sum_{\mu=1}^{K} C_{\mu i}\phi_\mu \quad i = 1, 2, ..K \tag{2.34}$$

If the basis set was complete we will have an unapproximated matrix representation of the molecular orbitals , but in order to have a finite time for the calculations we will have to define a finite basis set.
So combining the 2 previous equation (2.32) and (2.34) we will obtain the final matrix representation:

$$\sum_{\nu} F_{\mu\nu}C_{\nu i} = \epsilon_i \sum_{\nu} S_{\mu\nu}C_{\nu i} \; for \; i = 1, 2, ..K \tag{2.35}$$

With S that will be called as the overlap matrix that will be a representation of how the various atomic orbitals are superimposed one to the other and F , or fock matrix that will be the value of the fock operator evaluated between two basis.

The complete integral representation of the two matrices will be:

$$S_{\mu\nu} = \int \phi_\mu^*(1)\phi_\nu(1)dr_1 \tag{2.36}$$

and

$$F_{\mu\nu} = \int \phi_\mu^*(1)f(1)\phi_\nu(1)dr_1 \tag{2.37}$$

The Fock matrix can also be divided into two contributions, one containing information about the electron - nuclei potential and the electron momentum, $H_{\mu\nu}^{core}$ or core hamiltonian matrix and $G_{\mu\nu}$ will give us information of the coulombic and exchange electron - electron interaction.

$$F_{\mu\nu} = H_{\mu\nu}^{core} + G_{\mu\nu} \tag{2.38}$$

so the final matrix equation or Roothann-Hall equation will be:

$$\mathbf{FC} = \mathbf{SC}\epsilon \tag{2.39}$$

2.5.2 The construction of the basis set

Roothann-Hall equations and the basis sets that lead to a matrix representation from the integro-differential equations of the eigen value problem are used in general for computation , and in particular both for the Hartree fock method and in Density functional theory that we will introduce later.
The basis set is usually formed by atomic orbitals (on the quantum chemistry approach) and are divided in three main types: Gaussian-type orbitals, Slater-type orbitals, or numerical atomic orbitals.
The basis set that we used for the thesis is the cc-pVTZ which is the Dunning's correlation consistent basis set with triple Z, it is built up by adding shells of functions to a core set of atomic Hartree-Fock functions, in our particular case we will have three (T = triple) added shells and (V) indicates it is a valence only basis set.
Each function present in a single shell contributes very similar amounts of correlation energy in an atomic calculation.
The 'cc-p' in the first part, stands for 'correlation-consistent polarized' , in

fact in this set polarization functions are added as non-contracted Gaussians and add a significant amount of computational costs. This polarization functions are used to describe polarization of the electron density distribution of each the atom in molecules, they add flexibility to the basis set, permitting molecular orbitals to be more asymmetric with respect the nuclei, this is important for the correct calculations of the interaction with other atoms, since the bonding distort the simmetry of each single atomic orbital , distorting the overall distribution and giving it an asimmetrical character.
One downgrade to this sets is that the correlation-consistent (cc) basis sets described above are sub-optimal regarding the optimization of the calculation time for density-functional theory, because the correlation-consistent cc-pVXZ sets have been designed mainly for Post Hartree–Fock methods, while density-functional theory exhibits much more rapid basis set convergence.
These basis sets have been optimized recently, with some redundant functions removed and they have been rotated in order to increase computational efficiency [41].
The cc-pVTZ is permitted in particular on light atoms from hydrogen to argon excluding some elements like Li, Na , Mg so it can be used for the atoms considered in this thesis.
Analysis of the basis sets is not part of this thesis, in fact we will not analyze in detail all the Slater type basis sets (STO_s) or the Gaussian type basis sets (GTO) aside from our chosen cc-pVTZ basis set, this was considered valid for studies regarding similar molecules [9].

2.5.3 SCF method

This method relies firstly on choosing arbitrarily the wave function of the electron $\psi_e(i)$, this eigen function will be composed by a spatial ($\psi_r(i)$) and a spin ($\psi_s(i)$) part.
In general the spatial wave function ψ_r can be defined starting from a basis set, this define the accuracy and time of a specific calculus, the bigger the basis set, the higher the accuracy corresponding to a decrease on the energy of the fundamental state ϵ_0 until it reaches a minimum on the so-called Hartree-fock limit , beyond this limit the accuracy of the calculation will not increase.
With the electron wave function determined we will build the Fock matrix using the Roothann-Hall relation (2.37), this will be diagonalized to determine a new electronic wave function to build another Fock matrix, this iterative procedure is carried out until $\psi_e(i)$ have converged.

2.6 Density functional theory

DFT, or density functional theory is a first principles computational method that starts from a very different approach from the one that we analyzed for the HF method and Schrodinger equation, and have the fundamental concepts based on the density distribution of electrons rather than the wave function.
It yields a very important simplification from the 3N differential equation in the system of N electrons because the density distribution only depend on the 3 spatial coordinates and represent all the system of N electrons.
In this analysis the 'unsolvable' many-body problem of interacting electrons in a static external potential is reduced to a problem of non-interacting electrons that are moving on an effective potential.
This effective potential includes both the external potential and the effects of the exchange and correlation interactions.
The property of the fundamental state will be functionals of the electronic density.
We will start the elaboration of the DFT theory on the Thomas - Fermi theorem.

2.6.1 The Hohenberg-Kohn theorems

The first to use the concept of density distribution of electrons for the analysis of the molecular many body problem were Llewellyn Thomas and Enrico Fermi in 1927, in their Thomas-Fermi model.
It is a very rough model in which neither the exchange nor the correlation interaction is considered and the electron - electron pair wise interaction is only the one generated by coulombic repulsion.
This model is only exact for atoms of infinite nuclear models and for real system it fails to reproduce even the most simple ones.
It is indeed not exact and just a concept precursor to the much more interesting Kohn-Sham model.

Hohenberg and Kohn have elaborated two fundamental theorems that will evolve this primitive model and will lead to the Kohn-Sham formulation.
In the Hoheneberg and Kohn models electron are subjected to an external potential $\hat{V}_{ext}$ which is equivalent to the $\hat{V}_{en}$ of the nuclei - electron interaction

and we recall it is equal to :

$$\hat{V}_{en} = -\frac{e^2}{4\pi\epsilon_0}\sum_{i,I}^{N,M}\frac{Z_I}{|\mathbf{r}_i - \mathbf{R}_I|} = -\frac{e^2}{4\pi\epsilon_0}\sum_{i}^{M}\left(\sum_{I}^{N}\frac{Z_I}{|\mathbf{r}_i - \mathbf{R}_I|}\right) = \sum_{i}^{M}\hat{v}_n(\mathbf{r}_i) \tag{2.40}$$

On the point of view of a single particle $\hat{v}_n(r_i)$ is the external potential felt by each electron and generated by all the other nuclei.
This external potential will be the most important point for the Kohn-Sham model.

Theorem 1 *The external potential $V_{ext}(\boldsymbol{r})$, and hence the total energy, is a unique functional of the electron density $\rho(\boldsymbol{r})$.*

Not only the potential energy $V_{ext}(\mathbf{r})$ is determined by the electronic density, but the electronic density also determines the external potential.

Theorem 2 *The ground-state energy can be derived with variational methods: the density that minimizes the total energy is the exact ground-state density.*

In particular :

$$E[\rho(\mathbf{r})] = \int \rho(\mathbf{r})V_{ext}(\mathbf{r})d\mathbf{r} + F_{HK}[\rho(\mathbf{r})] \tag{2.41}$$

E will be the energy of the state to be minimized and ρ (r) is the electron density at a certain position (r), and F_{HK} is an unknown , but universal functional of the electron density.

This important theorems are valid only under specific conditions :

- the ground state is not degenerate , if we have more than one eigen function associated to the ground state in fact one can no longer talk about the uniqueness of the ground state expectation value of operators, and thus the first theorem cannot be demonstrated

- the ground / excited state density remain V-representable during the calculation, which means that it can always be associated to an Hamiltonian with an external potential V_{ext}

- the integral of the density must always give a constant number N

$$\int \rho(\mathbf{r}) d\mathbf{r} = N \tag{2.42}$$

This important principles will define the Kohn-Sham equation.

2.6.2 Kohn- Sham equation

Kohn and Sham starting from eq.(2.41) derived a set of differential equation able to find the ground state electron density $\rho_0(\mathbf{r})$.
This technique is based on a fictitious system of non-interacting electrons, since the expression of the kinetic energy for this particles is known, this allow to set up simpler and more accurate DFT calculations.
This fictitious system is constructed in such a way that its density is equal to the one of the real system with interacting electrons.
The Kohn–Sham equation (2.43) precisely is a one electron Schrödinger-like equation of a fictitious system of non-interacting particles that generate the same density (2.45) as any given system of interacting particles.

$$\left[-\frac{\nabla^2}{2} + V_{eff}(\mathbf{r})\right] \psi_i^{KS}(\mathbf{r}) = \epsilon_i \psi_i^{KS}(\mathbf{r}) \;\; with \;\; \rho_{KS}(\mathbf{r}) = \sum_i^N |\psi_i^{KS}(\mathbf{r})|^2 \tag{2.43}$$

This Kohn-Sham system , represented by Kohn-Sham orbitals ψ_i^{KS} is put in a local effective (fictitious) potential $V_{eff}(\mathbf{r})$, also called Kohn-Sham potential , in which the non-interacting particles move.

$$V_{eff}(\mathbf{r}) = V_{ext}(\mathbf{r}) + \frac{1}{2}\int \frac{\rho(\mathbf{r}')}{|\mathbf{r} - \mathbf{r}'|} d\mathbf{r}' + V_{xc}(\mathbf{r}) \tag{2.44}$$

where V_{xc} is the exchange correlation potential and is defined as $V_{xc} = \frac{\partial E_{xc}(\rho)}{\partial \rho}$, we also observe that

$$\int \rho_{KS}(\mathbf{r}) d\mathbf{r} = \int \rho(\mathbf{r}) d\mathbf{r} = N \tag{2.45}$$

as noted before. And the orbital of the fictitious system will correspond both to the real and KS electronic density

$$\rho_{KS}(\mathbf{r}) = \sum_{i=1}^{N} |\psi_i(\mathbf{r})|^2 = \rho(\mathbf{r}) \tag{2.46}$$

This is very important property of the fictitious orbitals, they will correspond

at any moment of the iteration to the real electronic density.
In practice the contribution F_{HK} will be separated into three components:

$$F_{HK}[\rho(\mathbf{r})] = T_s[\rho(\mathbf{r})] + E_H[\rho(\mathbf{r})] + E_{xc}[\rho(\mathbf{r})] \tag{2.47}$$

with T_s defined as the kinetic energy of the non interacting electron gas :

$$T_s[\rho] = -\frac{1}{2}\sum_{i=1}^{N}\int \psi_i^*(\mathbf{r})\nabla^2\psi_i(\mathbf{r}) \tag{2.48}$$

This is not defined and requires several approximations as the exchange-correlation energy functional E_{xc}.
E_H is the so called Hartree energy, representing the classical coulombic repulsion between electrons and precisely:

$$E_H[\rho(\mathbf{r})] = \frac{1}{2}\iint \frac{\rho(\mathbf{r})\rho(\mathbf{r}')}{|\mathbf{r}-\mathbf{r}'|}d\mathbf{r}d\mathbf{r}' \tag{2.49}$$

The total energy of the system, corresponding to the many-body wave functions represented by a Slater determinant and corresponding to the Hamiltonian $\hat{H}_0 = \sum_i^N (T_{ei} + V_{eff}(\mathbf{r}_i))$ will be expressed as a summation of the eigen values of the equation (2.43) over all the electron in the system representing all the energies of the single orbitals, the coulombic contribution of the e-e interaction in the system, and exchange-correlation terms:

$$E_{KS}(\rho) = \sum_i^N \epsilon_i - E_H(\rho) + E_{xc}(\rho) - \int \frac{\partial E_{xc}(\rho)}{\partial \rho}\rho(\mathbf{r})d\mathbf{r} \tag{2.50}$$

This problem is therefore reduced to a problem of N coupled single particle equations.
The KS fictitious orbitals are generally considered just as a computational artifact, but can be approximated to the wavefunctions of a single particle.
With all this said the iterative procedure that undergoes the density functional theory is the following:

$$\rho_n(\mathbf{r}) \longrightarrow V_{eff}(\mathbf{r}) \longrightarrow \hat{H}_O \longrightarrow \psi_i^{KS} \longrightarrow \rho_{n+1}(\mathbf{r}) \tag{2.51}$$

The principles are very simple, we start from the initial guess on the fictitious wave functions, ψ_n^{KS}, this will be related to the electronic density ρ_n^{KS}, that is equal to the real electronic density ρ_n and will give us information on the V_{eff} as stated by the 1^{st} Hohenberg-Kohn theorem.

Since the kinetic energy of the fictitious system is perfectly known we then by using $\hat{H}_0 = \sum_i^N (T_{ei} + V_{eff}(\mathbf{r}_i))$ we will calculate the eigen-functions of the many-body eigen-value problem, ψ_{n+1}^{KS} to finally find the new values for the electronic density $\rho_{n+1}^{KS}(\mathbf{r})$.
This process is iteratively repeated until the energy of the system is converged.

2.6.3 Exchange and correlation functional

The exchange-correlation functional E_{xc} is an important functional that is not known exactly and represent a correction of the KS fictitious system, in fact for the real state:

$$F_{HK}(\rho) = T(\rho) + E_H(\rho) + E_{nc}(\rho) \tag{2.52}$$

in which $E_{nc}(\rho)$ represent a non-classical correction over F_{HK} , instead for the fictitious orbitals we will have

$$F_{HK}(\rho_{KS}) = T_s(\rho_{KS}) + E_H(\rho_{KS}) + E_{xc}(\rho_{KS}) \tag{2.53}$$

and as we have seen in eq.(2.46) we will have ($\rho = \rho_{KS}$).
So we can see the exchange-correlation functional can be written as a summation of a non classical term plus the difference in kinetic energy between the real and the fictitious state:

$$E_{xc}(\rho) = [T(\rho) - T_s(\rho)] + E_{nc}(\rho) \tag{2.54}$$

This $E_{xc}(\rho)$ is approximated with several different methods , the first one is the LDA, or local density approximation.
In this model the exchange-correlation functional is described as an interaction between electrons on an homogeneous cloud of particles.
This is particularly used in metallic materials in which the situation can be approximated by a system of immobile ions in a homogeneous density distribution of electrons, but can be used also in molecular structures with some degree of success.
The form of the exchange-correlation functional for the LDA approximation is

$$E_{xc}^{LDA}(\rho) = \int \rho(\mathbf{r}) \left[-\frac{3}{4} \left(\frac{3\rho(\mathbf{r})}{\pi} \right)^{1/3} + \epsilon_c(\rho) \right] d\mathbf{r} \tag{2.55}$$

On molecular system in general, to describe better the dishomogeneity of this systems, it is appropriate to use the GGA , or generalized gradient approximation, in this approximation also the gradient of the electron density is taken into account and gives the information necessary to assess the specific variation of electronic density typical of molecular systems, in particular:

$$E_{xc}^{GGA} = E_{xc}^{LDA} - \sum_{\sigma} F \left(\frac{|\nabla \rho|}{\rho_{\sigma}^{4/3}} \right) \rho_{\sigma}^{4/3} d\mathbf{r} \tag{2.56}$$

2.6.4 Hybrid functionals

In hybrid functionals the exchange-correlation E_{xc} is divided in two terms, the purely exchange part, and the purely correlation part. We know that Hartree-Fock provides already a useful analytic expression for the exchange energy without the effects of self-interaction errors.
Even if promising is not convenient to use this expression due to the systematic error cancellations.
However, mixing a fraction of this non-local Hartree-Fock exchange to the DFT energy expression we build the class of the so called non-local functionals.
The first successful hybrid functional was developed by Becke and was based on the adiabatic connection formula.

$$E_{xc}^{hybrid} = \alpha E_x^{HF} + (1-\alpha) E_x^{DFT} + E_c^{DFT} \tag{2.57}$$

This is the general expression for the hybrid functionals such as PBE0, HSE06 and B3LYP.
For B3LYP in particular in these functional the exchange DFT part will be divided into an expression provided by Becke (ΔE_x^{B88}) and a LSDA part to provide local exchange, the correlation part will be divided into a local LSDA correlation and a non-local LYP (Lee,Yang and Parr correlation functional).
We will not go in detail on the other hybrid functionals outside their general expression (2.57), we just note that both PBE0 and HSE06 are usually used as an efficient tool for Raman investigation and are generally suitable in polyconjugated systems.
CAM-B3LYP is a long range correct version of B3LYP using the CAM

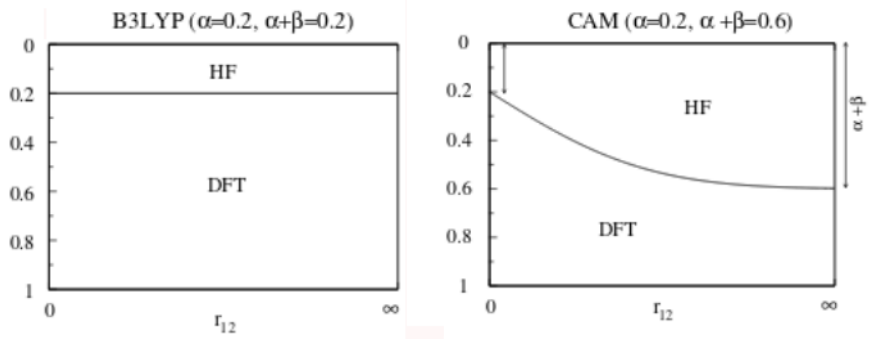

Figure 2.1: B3LYP(left) and CAM-B3LYP (right) α, β parameter dependence on the distance

(Coulomb attenuating method).
In this method the α and the β parameters change accordingly to the distance between electrons, modifying the relative weight of exchange and correlation terms.

2.7 GAUSSIAN input details for the optimization and Raman analysis

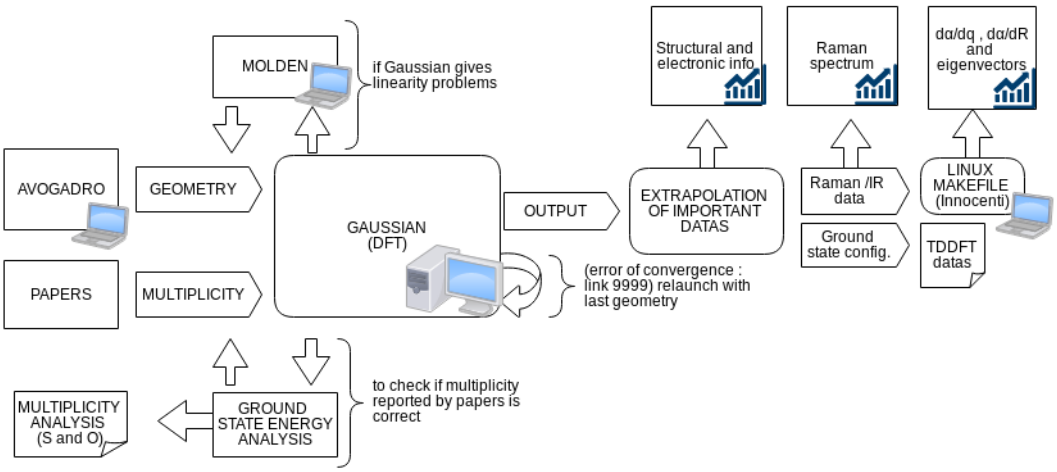

Figure 2.2: Flowchart diagram for the DFT procedure

DFT calculations have been carried out using the Gaussian software [42] to determine the ground state properties of a specific structure, as we can see from fig.(2.2) and fig.(2.3) the input of Gaussian need to know the geometrical un-optimized geometry of the system, which can be built using visualization softwares such as Avogadro [43] and Molden [44].

An input example for the Gaussian DFT procedure can be seen on fig. (2.3). The Gaussian software will at first determine the optimized geometry for the ground state and than the Raman spectra.

Important information such as structural (bond length, BLA), electronic (HOMO-LUMO gap, energy of the ground state) and spectroscopic (Raman intensity of the different peaks) will be determined by this procedure.

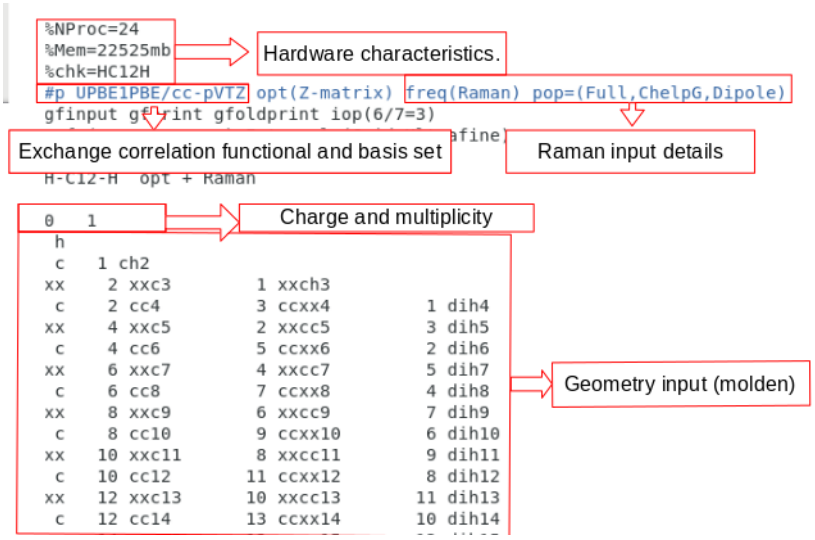

Figure 2.3: Typical input structure for the DFT Gaussian program

2.8 Time dependent DFT

Time dependent density functional theory is an important technique used to evaluate the excited state geometry and vibronic transition properties.
We will start, instead of the time independent Schrodinger equation, on its time dependent form :

$$\hat{H}\left|\Psi(t)\right\rangle = i\hbar\frac{\partial}{\partial t}\left|\Psi(t)\right\rangle \tag{2.58}$$

The first approximation is the one derived by the Runge-Gross theorem.

2.8.1 Runge-Gross theorem

The Runge-Gross theorem is an important theorem of TDDFT, expecially in the spectroscopic studies in presence of scalar fields.
It shows that there exist a correspondence between the potential v_{ks} and the density of the system ρ.
It doesn't hold for all type of potentials and it is correct considering only with an addiction to a purely time-dependent (and not position dependent) function (c(t)).
These have the effect only on changing the wavefunction leaving the density invariant, in fact

$$\left|e^{i\phi}\psi(\mathbf{r},t)\right|^2 = |\psi(\mathbf{r},t)|^2 \tag{2.59}$$

ϕ is an arbitrary phase which represent the shift cause by the position independent c(t) function.
RG theorem is typically applied where the system changes according to an external potential given by a time-varying electric field, such as in spectroscopy, thus TDDFT analysis will be perfect in our field.
It is a parallel concept to those of Hohenberg Kohn for DFT extrapolated in the time-dependent studies and it shows the density again as a fundamental parameter to describe the many-body problem, in this case the time-dependent many-body problem.

2.8.2 Time-dependent Kohn Sham equations

In the time dependent Schrodinger equation, the iterative procedure is focused on finding the stationary point of a quantity analogous to the energy, called quantum mechanical action (A):

$$A[\Psi(t)] = \int_{t_i}^{t_f} \left\langle \Psi(t) \left| i\hbar\frac{\partial}{\partial t} - \hat{H}(t) \right| \Psi(t) \right\rangle dt \tag{2.60}$$

$\Psi(t)$ is the many body wave function.
Given the strict correspondence between density functional and wave function we will have the mechanical action will be directly related to the electronic density (A = $A(\rho)$).
The fictitious Kohn-Sham orbitals are, in this case solutions of the time dependent Schrodinger equation :

$$\left(-\frac{1}{2}\nabla^2 + v_{ks}(\mathbf{r},t)\right)\psi_i(\mathbf{r},t) = i\frac{\partial}{\partial t}\psi_i(\mathbf{r},t) \tag{2.61}$$

The system of KS orbitals is found as the stationary point of the action functional previously reported in eq.(2.60).
The density of the real system can be obtained by the summation over the occupied fictitious orbitals.

$$\rho_{ks}(\mathbf{r},t) = \sum_i |\psi_i(\mathbf{r},t)|^2 = \rho(\mathbf{r},t) \tag{2.62}$$

The Kohn Sham potential v_{ks} is demonstrated to be equivalent to the combination of three components, an external potential term, a coulombic term and an exchange-correlation term as we have seen in the previous section.

2.8.3 Exchange-correlation functions for TDDFT

The concept of exchange-correlation potential is different from the one that we used for DFT and it is related to a so-called action functional $\tilde{A}$, this relation was derived by Leeuwen in 1998 [45]:

$$v_{xc} = \left.\frac{\partial \tilde{A}}{\partial \rho(\mathbf{r}, \tau)}\right|_{\rho(\mathbf{r},t)} \tag{2.63}$$

where τ is the Keldish pseudo-time.
This is not known exactly and an approximation is required to relate exchange-correlation functional used for DFT and extrapolate them into TDDFT, this is the so called adiabatic approximation, which states that the many-body effects are those of the ground-state even if the system is in a excited state. This can be a good approximation if the geometry of the excited state with respect of the one of the ground state remains more or less invariant, but in general it is not successful in systems that in the initial state are not in their ground state level.
The adiabatic approximation is generally appropriate if used for the prediction of the absorption spectrum, since initially the state is in its non-excited form.
Non adiabatic exchange-correlation functionals have been developed but are in general not used.
They are studied theoretically but cannot be implemented in calculators.
Recent development on the theory [40] have studied the decomposition of the exact exchange-correlation potential into an interaction component and a kinetic component.

2.9 GAUSSIAN input details for excited state and vibronic spectra determination

An example of the typical input for The TDDFT is showed in fig.(2.5).
The process undergoes a procedure briefly reported in fig.(2.4).
From the optimized geometry obtained by the DFT optimization of the initial structure, we will start using Gaussian to determine the excited states and vibronic transitions parameters.
Each relevant excited state (which yield a dipole-allowed transition f >> 0) will than be optimized using the Gaussian program using the same geometry of the ground state, this will find optimized values for oscillator strength, peak position and also the electronic transition dipole moment (EDTM).
This calculus will also give the optimized geometry of the excited state (i) that will be used as an input to the UVFC program for all values of gamma, this gamma give an indication of the vibronic coupling between modes and it is strictly related of how the UV- vis spectra will be modulated (we will see this later in detail).
For each optimized transition we will make the individual calculation on the Franck-Condon factors for a maximum amount of gamma's of (7) to limit the computational weight, we will explain this in detail later

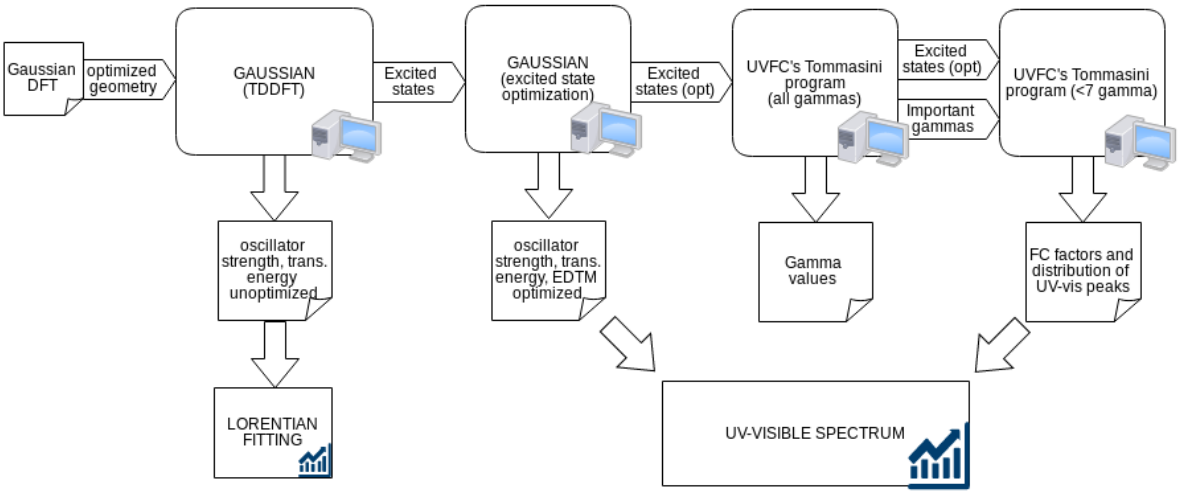

Figure 2.4: Flowchart diagram for the TDDFT procedure

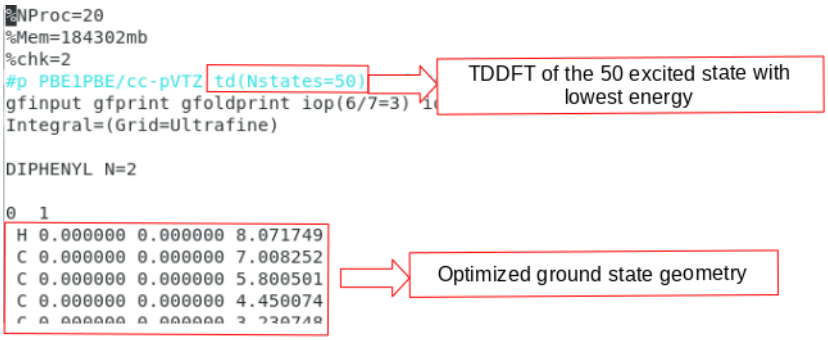

Figure 2.5: Typical input structure for TDDFT Gaussian program

Chapter 3

Fundamentals of Raman and UV-vis spectroscopy

In this chapter we will explain all the fundamentals about vibrational spectroscopy and Raman.
The theoretical detail will be based on Atkins "molecular quantum mechanics" book [46], on Tommasini 'physical properties of molecular materials' lecture notes, on Gierschner [47] and Siebrand [48] work, on Fabrizia Negri lecture notes and on several other works [49–52].

3.1 Vibrational dynamics

In this section we will introduce the fundamental description of the vibrational dynamics of molecules, by adopting a classical approach and the harmonic approximation.
Using cartesian coordinates (x_i) we find that the kinetic energy (T) of a system of N particles with mass m_i can be represented by:

$$T = \frac{1}{2}\sum_{i=1}^{N} m_i \dot{x}_i^2 \tag{3.1}$$

x_i represent the cartesian displacements on the (x,y,z) directions and are 3N in a system on N atoms.
The eq. (3.1) can be represented alternatively in the matrix form:

$$\mathbf{T} = \frac{1}{2}\dot{\mathbf{X}}^T \mathbf{M} \dot{\mathbf{X}} \tag{3.2}$$

$$\dot{\mathbf{X}} = \begin{pmatrix} \dot{x}_1 \\ \dot{x}_1 \\ \cdots \\ \dot{x}_{3N} \end{pmatrix} \tag{3.3}$$

and $\mathbf{M}$ is the diagonal matrix with the values equal to
$(m_1, m_1, m_1, m_2, m_2, m_2, \cdots m_N m_N m_N)$.
The classical representation of the potential instead can be elaborated as a Taylor expansion:

$$V(x_1, x_2, \cdots x_N) = V_0 + \sum_{i=1}^{N} \frac{\partial V}{\partial x_i}\Big|_0 + \frac{1}{2}\sum_{i,j}^{N} \frac{\partial^2 V}{\partial x_i \partial x_j}\Big|_0 x_i x_j + HOT \tag{3.4}$$

In this equation V_0 is arbitrary and we can put it equal to 0, when we are on the minima of the potential energy also the second term $(\frac{\partial V}{\partial x_i}\big|_0)$ for each coordinate.
For small displacements the higher order terms (HOT) can be neglected, this is called as the harmonic approximation.

$$V(x_1, x_2, \cdots x_N) \approx \frac{1}{2}\sum_{i,j}^{N} \frac{\partial^2 V}{\partial x_i \partial x_j}\Big|_0 x_i x_j \tag{3.5}$$

In matrix form this can be represented by:

$$\mathbf{V} = \frac{1}{2}\dot{\mathbf{X}}^T \mathbf{F}^x \dot{\mathbf{X}} \tag{3.6}$$

F^x is the matrix composed by the second order derivatives over the different coordinates and its elements are $f_{ij}^x = \frac{\partial^2 V}{\partial x_i \partial x_j}\big|_0 x_i x_j$, these elements will be called force constants.
In order to solve the dynamical problem, we will have to solve the 3N variable Lagrange equations

$$\frac{\mathrm{d}}{\mathrm{d}t}\frac{\partial T}{\partial \dot{x}_j} + \frac{\partial V}{\partial x_j} = 0 \quad for \quad j = 1, 2, ..., 3N \tag{3.7}$$

The previous classical concepts introduced in eq. (3.1) and (3.5) will be put into the Lagrangian formulae to develop the following 3N equation problem

$$m_j \ddot{x}_j + \sum_{i=1}^{3N} f_{ij}^x x_i = 0 \tag{3.8}$$

A general solution of this equation will be a linear combination

$$x_j = \sum_{i=1}^{3N} L_{ij} cos(\omega_i t + \phi_i) \tag{3.9}$$

The index (i) is relative to all the 3N normal modes, each with frequency ω_i ,phase ϕ_i and oscillation amplitude L_{ij}.
Substituting this solution into (3.8) we obtain :

$$\sum_{i=1}^{3N} \left(f_{ij}^x - \omega^2 m_j \delta_{ij} \right) L_i^x = 0 \tag{3.10}$$

where δ_{ij} is the Dirac delta function, this can be rewritten in matrix form to :

$$\left(\mathbf{M}^{-1}\mathbf{F}^x - \omega^2 \mathbf{I} \right) \bar{L}^x = 0 \tag{3.11}$$

This 3N linear equation eigen value problem can yield non trivial solutions when the determinant of $\left[\mathbf{M}^{-1}\mathbf{F}^x - \omega^2\mathbf{I}\right]$ is equal to 0.
The matrix form of eq. (3.11) can easily be found, $\mathbf{L}$ will be the matrix composed by all eigen vectors $\bar{L}^x$.

$$\mathbf{M}^{-1}\mathbf{F}^x\mathbf{L}^x = \mathbf{L}^x\mathbf{\Lambda} \tag{3.12}$$

Λ is the diagonal matrix of the ω_i for each normal mode (i).
The relation between the generic displacement ($\mathbf{X}$), the eigenvector matrix ($\mathbf{L}^x$) and the normal modes (Q) will be the following:

$$\mathbf{X} = \mathbf{L}^x\mathbf{Q} \tag{3.13}$$

From the point of view of the internal coordinates $\mathbf{R}$, which describe the relative movement of atom inside the chain, we will see that the problem pass from the 3N equations (of all the cartesian coordinates of the N atoms) to the 3N-6 internal coordinates.
In fact the internal coordinates will be referred to a system (molecule) independent on the 3 rotation and 3 translation that this can have with respect to another coordinate reference system.
To shift the problem we will introduce the transformation matrix ($\mathbf{B}$).

$$\mathbf{R} = \mathbf{B}\mathbf{X} \tag{3.14}$$

And the kinetic energy representation over the internal coordinates will be :

$$T = \frac{1}{2}\dot{\mathbf{R}}^T\mathbf{B}\mathbf{M}^{-1}\mathbf{B}^T\dot{\mathbf{R}} \tag{3.15}$$

and the potential energy will be:

$$V = \frac{1}{2}\mathbf{R}^T\mathbf{F}^r\mathbf{R} \tag{3.16}$$

$\mathbf{F}^r$ is the force constants matrix and its elements are the force constants, $f_{ij}^r = \frac{\partial^2 V}{\partial r_i \partial r_j}\big|_{R=0}$ With $\mathbf{G}^{-1} = \mathbf{B}\mathbf{M}^{-1}\mathbf{B}^T$ (called as kinetic matrix) we will have the transformation of eq. (3.12) to:

$$\mathbf{G}\mathbf{F}^r\mathbf{L}^r = \mathbf{L}^r\mathbf{\Lambda} \tag{3.17}$$

And the correspondence between internal coordinates and normal modes will be :

$$\mathbf{R} = \mathbf{L}^r\mathbf{Q} \tag{3.18}$$

Through eq. (3.17) one can find the frequency of each normal mode in the molecule, than find the individual displacements using eq.(3.9).
This will lead us to the final relation; the vibrational frequencies of this modes will be determined on the basis of the solution of a eigenvalue problem:

$$\mathbf{G}\mathbf{F}\mathbf{L}_k = \omega_k^2\mathbf{L}_k \tag{3.19}$$

Where $\mathbf{G}$ is the so called kinetic matrix, $\omega_k = 2\pi f_k$ where f_k is the value of the vibrational frequency of mode k, $\mathbf{L}_k$ is the eigenvector depicting the same mode and $\mathbf{F}$ is the force constant matrix, this equation will be derived and analyzed in the following section.
In the specific case of linear molecules we will analyze a specific subspace of simmetry Σ that represent the stretching coordinates.

3.2 Raman spectroscopy

Density functional theory will be used (with the Gaussian software) to determine the Raman spectrum of the chains studied, we will use the PBE0 exchange correlation functional and the cc-pVTZ basis set, that has been successfully used in our laboratory for the determination of similar structures. [6]
Raman spectroscopy is a vibrational spectroscopy technique based on the interaction of matter and light, in particular on the excitation of a certain molecule from the ground state to an excited virtual state with the configuration of a distorted electron cloud.
From this state the system can go back to the original energy level (Rayleigh scattering or elastic scattering) or absorb / emit a phonon (respectively Antistokes/Stokes inelastic scattering).
The fraction of photons that undergo inelastic scattering is a very limited part ($<< 1\%$) with respect of the elastic scattering (Rayleigh).
In particular only outgoing photon less energetic than the original photon are taken into account, so in practice only the Stokes shift with respect to the Rayleigh scattering frequency is analyzed in the general Raman spectrum.
The Stokes shift, or Raman spectrum is strictly dependent on the type of normal modes that we have in our system, each normal mode will have a specific Stokes band , in particular for the molecules under our study the most important bands will be relative to symmetric / antisymmetric stretching of the chain.
Not only the Raman spectroscopy will be useful to determine the vibration characteristic of the normal modes on the molecule but also to determine the electrical character.
Each normal mode is Raman active if the displacement along the normal coordinate cause a variation of the molecular polarizability ($\frac{\partial \alpha}{\partial Q} \neq 0$) and therefore on Raman transition the polarizability is represented by:

$$\alpha = \alpha_0 + \sum_i \left(\frac{\partial \alpha}{\partial Q}\right)_0 Q_i + \ HOT \ (highest\ order\ terms) \tag{3.20}$$

To determine all the different vibrational characteristic over this type of molecules, alongside with the use of eq. (3.19) we introduce the ECC (effective conjugation coordinate theory) which is important in this field .

3.2.1 Effective conjugation coordinate theory

ECC theory main property is based on defining an important collective vibration for each chain, called R coordinate which gives us information on the fundamental molecular characteristic of polyconjugated systems.
This ECC mode is the most intense mode for polyynes and can be described as an antisymmetric stretching of adjacent CC bonds, corresponding to a stretching / shrinking of adjacent triple / single bonds.
This mode can be also present on cumulenes but with lower intensity.
The variation of the geometry seen on mode R can be demonstrated correspondent to the variation between the ground state geometry and the one of the first excited state.
This important mode can be found both for infinite and finite carbon chain structures.
It is also related to electronic properties (eg. HOMO-LUMO gap) for a system and the electron-phonon coupling is maximized on the coordinate R that define this mode.
π electron conjugation determine the frequency of the R mode because it modifies the force constants between molecules.
We know that in fact with higher conjugation correspond a 'softening' of the force constants and thus a modification of the force constant matrix:

$$F_R = \frac{k_1 + k_2}{2} + \sum_{n \geqslant 1} [f_1^n + f_2^n - 2f_{12}^n] \tag{3.21}$$

Than using eq. (3.17) and eq. (3.18) we will have a relation to the internal coordinates and therefore the ECC line.
In which k_N are the singular force constants between atoms, f_N describe the stretching force constants at different distance (N) and F_R, F_π describes the force constant matrix as seen in equation (3.19),this equations are valid only if we have non negligible f_N (as in the case of polyynes).

3.2.2 Classification of different modes

The dissertation for the modes will not go in detail with the oligomer approach, since it has already been considered extensively by Innocenti, and we won't focus on the phonon dispersion relation.
The importance of this theory for our considerations will be related only to the classification of the peaks.

Modes definition We can divide the mode in our molecule in several different types, my focus was to develop a uniform analysis and a more clear graphical representation of the trends, thus we will not classify the modes only by their static nodes inside the chain but we will use a more general representation:

- the α mode (or R mode) correspond to a LO mode with an alternation of stretching /extension of the single bonds, and the number of nodes in this mode depend on the carbon atoms (n) on the chain (they will be $= (n-1)$, it is the most intense mode for both polyyne chains and even-cumulenic chains.

- the β^* mode correspond to a LO mode with a singular node on the chain(or a singular stretching / extension) , note that this mode is different from the β mode used for the polyyne analysis which is the second peak in intensity for polyyne-type chains.

- the γ mode is defined as a LO mode with 3 nodes on the chain (or 3 stretching /extensions)
- the δ mode is defined as a LO mode with 5 nodes on the chain (or 5 stretching /extensions)
- the ϵ mode is defined as a LO mode with 7 nodes on the chain (or 7 stretching /extensions)
- the ζ mode is defined as a LO mode with 9 nodes on the chain (or 9 stretching /extensions)
- the η mode is defined as a LO mode with 11 nodes on the chain (or 11 stretching /extensions)

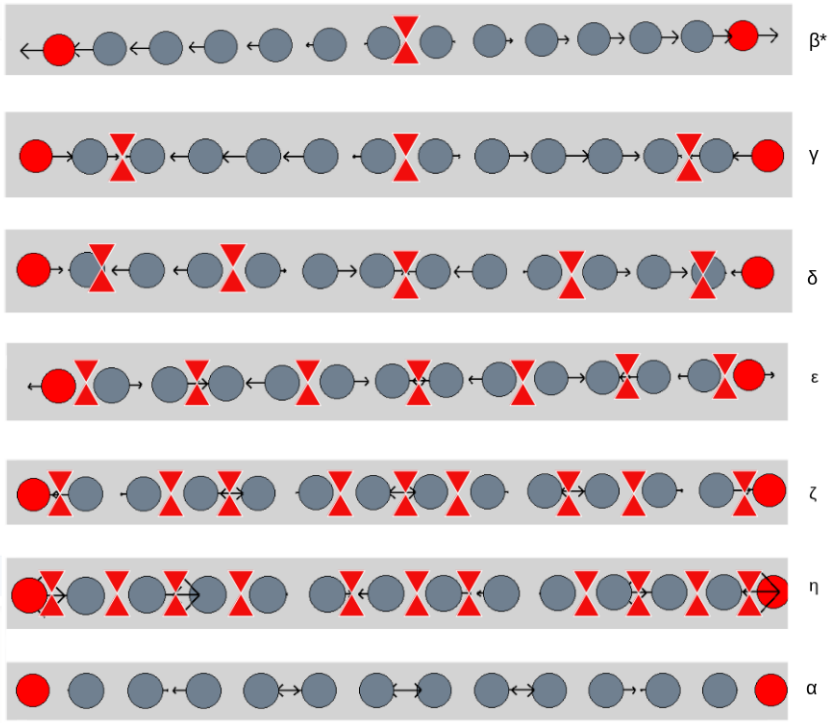

Figure 3.1: All modes present in short chain cumulenes (< 12 carbon atoms in chain) and their node representation

The number of different type of significant modes (M) in our system will be of course related with the n° of carbon atoms per chain and will be $M_{even} = \frac{n}{2}$ for even chains and $M_{odd} = \frac{n+1}{2}$ for odd chains.

The graphical representation of each type of longitudinal mode is pictured on figure (3.1), where we give a more clear representation of the differences between each type of normal mode.

3.3 Basis of quantum transitions and UV-vis spectroscopy

3.3.1 Fermi golden rule

A quantum transition is the variation of the quantum wave function of a system that is represented by the transition from an initial stationary state $|\psi_i\rangle = |i\rangle$ onto a final stationary state $|\psi_f\rangle = |f\rangle$.
The two states are eigen-states of the two different eigen value problems

$$\hat{H}\,|i\rangle = E_i\,|i\rangle \quad and \quad \hat{H}\,|f\rangle = E_f\,|f\rangle \tag{3.22}$$

This will be promoted in general by a time - dependent perturbation

$$\hat{H}'(t) = \hat{V}(t)cos(\omega t + \phi) \tag{3.23}$$

$\hat{H}'$ will be taken as a weak enough perturbation with respect $\hat{H}$, that means that this perturbation doesn't modify the nature of the eigen states of the original hamiltonian for the system.
The Fermi golden rule states that the transition probability (P_{if}) between the initial $|i\rangle$ and final $|f\rangle$ state is:

$$P_{if} = \frac{2\pi}{\hbar}\left\langle i\left|\hat{V}\right|f\right\rangle \delta(E_f - E_i - \hbar\omega) \tag{3.24}$$

The meaning of the Dirac delta function represent the fact that the conservation of the energy of the system must be conserved, thus if $E_f - E_i \neq \hbar\omega$ the transition probability will be 0 as expected.
Also to have a non-zero transition probability we will have to respect the specific selection rules for the transitions, these in reality determine 0 transition probability only if in the system we have only these two specific eigen states $|i\rangle$ and $|f\rangle$, if we have another level $|\gamma\rangle$ from which the selection rules permit both the transitions $|i\rangle \longrightarrow |\gamma\rangle$ and $|\gamma\rangle \longrightarrow |f\rangle$ also P_{if} will be non negligible even if the selection rules doesn't allow $|i\rangle \longrightarrow |f\rangle$, this is called intensity borrowing.
Also the effect of the normal modes in the system, changing the symmetry of the system can have an effect on relaxing the selection rules.
This will be important in the future chapter for the analysis of the UV spectra.
Quantum transitions in a system are divided into three types, from the least energetic one we will have rotational transition, vibrational transition and

electronic transition.

3.3.2 The dipole operator

We will start from the discussion of the perturbation operator ($\hat{H}'$) in order to clarify quantum transitions as a basis to clarify UV - visible spectroscopy. In optical spectroscopies in general we use a photon in between the UV and the infrared range as a probe for the quantum transition.
Neglecting the magnetic component of the plane wave of wave vector **k** the electric field will be oscillating, both along the direction r and in time t:

$$\mathbf{E}(\mathbf{r},t) = \mathbf{E}_0 cos(\mathbf{k}\cdot\mathbf{r} - \omega t + \phi) \tag{3.25}$$

or alternatively

$$\mathbf{E}(\mathbf{r},t) = \mathbf{E}_0 cos(\frac{2\pi}{\lambda}\mathbf{r} - 2\pi\nu t + \phi) \tag{3.26}$$

but knowing that the molecules under our specific study have size of a few Armstrongs and that the wavelength λ has a value in UV - vis spectroscopy typically between 200 nm - 1000 nm we will neglect the position dependence of the electric field, in fact **k**r has to be taken in consideration only for big molecules (not our specific case). Thus we reduce (3.25) into a smaller formulation taking into account only the time - dependent effects:

$$\mathbf{E}(t) = \mathbf{E}_0 cos(\omega t + \phi) \tag{3.27}$$

and the electrical potential Φ can be built up by the scalar product of this oscillating electrical field and the three dimensional vector of position **r**.

$$\Phi(\mathbf{r},t) = -\mathbf{r}\cdot\mathbf{E}_0 cos(\omega t + \phi) \tag{3.28}$$

The energy of all the charged particles (N) on the system (nuclei and electrons) will be of course composed in this form (each charged particle is labelled as (i)) :

$$W = \sum_{i}^{N} q_i \Phi_i \tag{3.29}$$

if we divide the contribution into the one of all the (P) electrons and (Q) nuclei in the system we will have:

$$W = W_e + W_n = \sum_i^P -e\Phi(\mathbf{r}_i, t) + \sum_j^Q eZ_j\Phi(\mathbf{R}_j, t) \tag{3.30}$$

and thus using the relation (3.28) we will find the value for the interaction hamiltonian $\hat{H}'$:

$$\hat{H}' = -\left(-\sum_i^P e\mathbf{r}_i + \sum_j^Q eZ_j\mathbf{R}_j\right)\mathbf{E}(t) = -\hat{\mu}\cdot\mathbf{E}(t) \tag{3.31}$$

Where $\hat{\mu}$ is the dipole operator, introduced as a representation of the electrostatic interaction represented above and represent the magnitude of dipolar migration of charge, it is a summation of two components the electron dipole operator $\hat{\mu}_e$ and the nuclei dipole operator $\hat{\mu}_n$.
We observe that as we have seen in equation (3.23) and (3.38) we can write

$$\hat{V} = -\hat{\mu}\cdot\mathbf{E}_0 \tag{3.32}$$

Thus through the Fermi Golden rule the probability of transition from $|i\rangle$ to $|f\rangle$ (P_{if}) will be related to the electric dipole operator and in particular to the electric dipole transition moment (μ_{if})

$$P_{if} \propto \left\langle i\left|\hat{V}\right|f\right\rangle = -\langle i\,|\hat{\mu}|\,f\rangle\cdot\mathbf{E}_0 = -\mu_{if}\cdot\mathbf{E}_0 \tag{3.33}$$

This is an important result, the probability of transition is directly related through the projection of the transition dipole moment on the polarization vector of the incoming optical field.
The intensity of the absorption peaks (rates of transitions) will also be directly related to the electric dipole transition moment, in fact :

$$for\ spontaneous\ transitions\ R = \frac{8\pi^2}{3\lambda\epsilon_0\hbar}|\mu_{if}|^2 \tag{3.34}$$

$$for\ stimulated\ transitions\ R = \frac{\rho_{rad}(E)}{6\epsilon_0\hbar^2}|\mu_{if}|^2 \tag{3.35}$$

3.3.3 UV - visible spectroscopy

UV – visible spectroscopy refers to absorption spectroscopy caused by photon in the UV - vis spectral region (200-1000 nm).
It is used as an analytical tool to study the optoelectronic properties of conjugated organic compounds.
Photons generate both the electronic and vibrational quantum transitions.
The stationary eigen state will change from an initial one $|i\rangle = |i_{vib}\rangle |i_{el}\rangle$ (under Born-Oppenheimer approximation), with i_{vib}, i_{el} corresponding respectively to a vibration and electronic only wave function.
The final state will be also divided accordingly; $|f\rangle = |f_{vib}\rangle |f_{el}\rangle$.
The initial state will be usually the ground state $|i_{el}\rangle = |g\rangle$, also other initial states can be possible but since they yield less magnitude on the absorption intensity will be in generally not considered.
Also in the initial state we will have $|i_{vib}\rangle = \prod_j |0_j)_g$ the pedix g means that the vibrational states will be of course the one corresponding to the ground state.
We will introduce two approximations important for further discussion, one is that the vibrational frequency on ground state will be equal to those on the excited state and the other will be called harmonic approximation on the vibrational coordinate:

$$V(Q) = V(Q_0) + \left(\frac{\partial V}{\partial Q}\right)_0 (Q - Q_0) + HOT \tag{3.36}$$

So the transition dipole moment under those approximation will be :

$$\mu_{if} = \langle i |\hat{\mu}| f\rangle = \langle i_{vib} |\langle i_{el} |\hat{\mu}| f_{el}\rangle| f_{vib}\rangle = \langle i_{vib} |\mu_{ge}| f_{vib}\rangle \tag{3.37}$$

In which μ_{ge} represent the only electronic transition dipole moment between the initial electronic state (i_{el})(ground , g) and the final excited state (f_{el})(excited, e).
This electronic transition dipole moment will be in general dependent on the normal modes (Q), $\mu_{ge} = \mu_{ge}(Q)$.

3.3.4 Frank-Condon principle

As we have seen previously the electronic transition dipole moment can be seen as dependent on the normal coordinates, if we elaborate it in the means of the Taylor expansion:

$$\mu_{ge} = \mu_{ge}(Q) = \mu^0_{ge}(Q) + \sum_j \left(\frac{\partial \mu_{ge}}{\partial Q_J}\right)_0 Q_J + HOT \tag{3.38}$$

In the Frank Condon approximation only the static value μ^0_{ge}, which is the first term on the Taylor expansion is considered, this means that, as in the Born-Oppenheimer approximation, we will consider the electronic transitions occurring in a field of 'quasi-static' nuclei, the transition moment will be therefore evaluated at equilibrium position of the ground state.
This is justified by the fact that quantum transitions corresponding to absorption phenomenons are very fast and can be carried out in less than 1 fs.
In the transitions which yields a μ^0_{ge} equal to 0 we have to consider also the Herzberg-Teller expansion term that is the second term on Taylor expansion in eq. (3.38), this will consider also the HT vibronic expansion terms $\left(\frac{\partial \mu_{ge}}{\partial Q_J}\right)_0$.
Let us consider the rate of transition under the Franck-Condon approximation :

$$\langle i \left|\hat{\mu}\right| f\rangle = \langle i_{vib} \left|\langle i_{el} \left|\hat{\mu}\right| f_{el}\rangle\right| f_{vib}\rangle = \langle i_{vib} \left|\mu_{ge}\right| f_{vib}\rangle = \mu^0_{ge} \langle i_{vib}|f_{vib}\rangle \tag{3.39}$$

The last point of the previous equation is possible in the Franck-Condon approximation that we analyzed before.
The $\langle i_{vib}|f_{vib}\rangle$ are called as Franck-Condon factors and their evaluation is complicated since the initial vibrational state is localized in the ground state (g) and final vibrational state is on the excited final state (e).
The normal coordinates of ground and excited state , labeled as Q_i and Q_f are related through the Duschinsky rotation:

$$Q_f = JQ_i + \Delta \tag{3.40}$$

with

$$J = L_e^T L_g \quad and \quad \Delta = L_e^T M^{1/2}(x_e^0 - x_g^0) \tag{3.41}$$

Where (J) is the Duschinsky rotation matrix and represent how the normal modes of the excited state are rotated with respect to those of the ground state, Δ is the displacement vector and represent the displacement of these modes.
For simplification the Duschinsky rotation matrix is assumed to be diagonal with all the values equal to 1, thus the final normal modes will not be rotated

with respect to the initial ones , this permit to simplify the multidimensional FC overlap $\langle i_{vib}|f_{vib}\rangle$ into a simpler multiplication of individual FC factors.

$$\langle i_{vib}|f_{vib}\rangle = \prod_k (0_k|n_k) \tag{3.42}$$

Where $|0_k)$ will be located on ground state and $|n_k)$ on the excited state.
So through eq. (3.40) it will be possible to evaluate the FC overlap over all the modes and therefore the intensity (I_{if}) of the transition.

$$I_{if} \propto \sum_k^{3N-6} \left|\mu_{if(k)}\right|^2 = \sum_k^{3N-6} \left|\left\langle i_{vib(k)} \left|\langle g \left|\hat{\mu}\right| e\rangle\right| f_{vib(k)}\right\rangle\right|^2 = \tag{3.43}$$

(using FC approximation of the electronic transition dipole moment)

$$= \sum_k^{3N-6} (\mu_{ge}^0)^2 \left|(0_k|n_k)\right|^2 = \sum_k^{3N-6} (\mu_{ge}^0)^2 e^{-B_k^2/2} \frac{B_k^{2n_k}}{2^{n_k} n_k!} = \sum_k^{3N-6} (\mu_{ge}^0)^2 e^{-\gamma} \frac{\gamma^{n_k}}{n_k!} \tag{3.44}$$

Where $B_k = \left(\frac{\omega_k}{\hbar}\right)^{1/2} \Delta_k$ and is called as dimensionless displacement, and k goes from 1 to the number of linearly independent variables for the internal coordinates
Each individual FC overlap will be dependent on the dimensionless displacement, which is also physically represented by $Q_f^0 - Q_i^0$, which evaluate the difference between geometrical configuration between excited / initial state.
In non totally symmetric modes (NTS) B_k will be 0 so only totally simmetric modes will be important for the calculation of FC factors.
The calculation in eq. (3.43) and (3.44) can be simplified by including only totally simmetric modes, therefore:

$$I_{if} \propto (\mu_{ge}^0)^2 \sum_{k=1}^{TS\ modes} e^{-\gamma} \frac{\gamma^{n_k}}{n_k!} \tag{3.45}$$

The γ parameter is related to the dimensionless displacement, B, that phisically represent the displacement of the normal modes of the ground state with respect to the normal modes of the excited states, in particular $\gamma = \frac{1}{2}B^2$.
With low γ the origin will be more relevant with respect to the $0_g \rightarrow N_e$ peaks because the normal modes won't be significatively displaced.
The intensity of each individual $i \rightarrow f$ excitation (and therefore the modulation of each peak) is in fact strictly dependent on the vibrational coupling and therefore the gamma parameters.

Chapter 4

Investigation of structural and electronic properties for carbon atom wires

4.1 Sulfur cumulenes

In this chapter we will investigate the structural, electronic and vibrational properties of S-cumu[n] (or $S-C_n-S$) wires with n=4,5,..,12 atom in chain by means of density functional theory calculations.
We will mainly focus on short length carbon atom wires, in literature in fact the recent processing techniques allowed the production only of small length sulfur cumulenes [25].
Tommasini et al.[53] and Yang et al.[54] using DFT calculations have already carried out a similar analysis on the relationship between bond length alternation and Raman response for H-Py[n].
We will use the consideration of the effective conjugation theory ([36]) to underline the importance of the α peak as was done in Innocenti thesis work and article [9].

4.1.1 Electronic configuration of ground state for sulfur cumulenes

Multiplicity refers to the spin state of a specific system,.
For a triplet state the total spin S=1 leading to two unpaired electrons on the HOMO level, instead for a singlet state S=0 generating a paired electron configuration.
For our work the multiplicity is an important parameter to determine for DFT calculations, in previous papers it was analyzed to be triplet for even numbered chains and singlet for the odd number ones for this specific type of molecules by Wang et al. [4, 21].
I report the result for the minima of the energy for both the chains with different length and relative triplet / singlet, also I predict the most stable ground configuration, this ground configuration will be the one used later to develop the GAP / BLA and geometry study.
The values of the singlet and triplet energy levels will be given by the following table (4.1).

Sulfur cumulenes					
N°C in chain	Singlet energy	Triplet energy	Δ_{st} (Hartree)	Δ_{st} (kcal/mol)	**Most stable**
N=3	-910,2918	-910,2030	-0,0888	-55,7140	SINGLET
N=4	-948,2853	-948,3071	0,0217	13,6197	TRIPLET
N=5	-986,3758	-986,3105	-0,0653	-40,9915	SINGLET
N=6	-1.024,3824	-1.024,3990	0,0166	10,4387	TRIPLET
N=7	-1.062,4615	-1.062,4142	-0,0473	-29,6808	SINGLET
N=8	-1.100,4754	-1.100,4898	0,0144	9,0112	TRIPLET
N=9	-1.138,5482	-1.138,5072	-0,0410	-25,7537	SINGLET
N=10	-1.176,5672	-1.176,5800	0,0128	8,0166	TRIPLET
N=11	-1.214,6354	-1.214,6015	-0,0339	-21,2608	SINGLET
N=12	-1.252,6582	-1.252,6698	0,0116	7,2897	TRIPLET

Table 4.1: Reported values of the energy minima (in Hartree) for both the singlet and triplet state for all chain lengths, also the difference (Δ) is reported both in Hartree and in kcal/mol, the corresponding most stable ground state multiplicity condition is written in the last column.

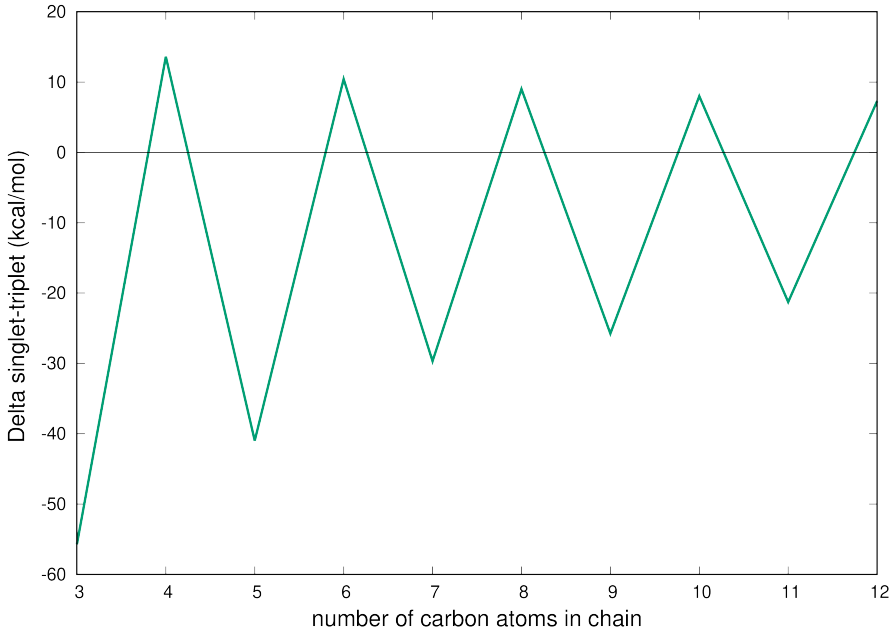

Figure 4.1: Single triplet minima difference over all the different chain lengths

We note several important properties on the S-cumu[n] wire trends present on figure (4.1).

1) *There is an alternation between a favored singlet / triplet state*

As we can see from figure (4.2) the configuration for the delocalized π orbitals in our system will be $\cdots[\pi_{ux}][\pi_{uy}][\pi_{gx}][\pi_{gy}]\cdots$, this is the classical configuration of alternated ungerade and gerade π orbitals along the x and y directions, this is valid for both sulfur and oxygen terminated chains and

n	State	Electronic configuration
1	$^1\Sigma_g$	(Core)$\sigma_g^2\sigma_u^2\sigma_g^2\sigma_u^2\pi_u^4\pi_g^4$
2	$^3\Sigma_g$	(Core)$\sigma_g^2\sigma_u^2\sigma_g^2\sigma_u^2\sigma_g^2\pi_u^4\pi_g^4\pi_u^2$
3	$^1\Sigma_g$	(Core)$\sigma_g^2\sigma_u^2\sigma_g^2\sigma_u^2\sigma_g^2\sigma_u^2\pi_u^4\pi_g^4\pi_u^4$
4	$^3\Sigma_g$	(Core)$\sigma_g^2\sigma_u^2\sigma_g^2\sigma_u^2\sigma_g^2\sigma_u^2\sigma_g^2\pi_u^4\pi_g^4\pi_u^4\pi_g^2$
5	$^1\Sigma_g$	(Core)$\sigma_g^2\sigma_u^2\sigma_g^2\sigma_u^2\sigma_g^2\sigma_u^2\sigma_g^2\sigma_u^2\pi_u^4\pi_g^4\pi_u^4\pi_g^4$
6	$^3\Sigma_g$	(Core)$\sigma_g^2\sigma_u^2\sigma_g^2\sigma_u^2\sigma_g^2\sigma_u^2\sigma_g^2\sigma_u^2\sigma_g^2\pi_u^4\pi_g^4\pi_u^4\pi_g^2\pi_u^2$
7	$^1\Sigma_g$	(Core)$\sigma_g^2\sigma_u^2\sigma_g^2\sigma_u^2\sigma_g^2\sigma_u^2\sigma_g^2\sigma_u^2\sigma_g^2\sigma_u^2\pi_u^4\pi_g^4\pi_u^4\pi_g^4\pi_u^4$
8	$^3\Sigma_g$	(Core)$\sigma_g^2\sigma_u^2\sigma_g^2\sigma_u^2\sigma_g^2\sigma_u^2\sigma_g^2\sigma_u^2\sigma_g^2\sigma_u^2\sigma_g^2\pi_u^4\pi_g^4\pi_u^4\pi_g^4\pi_u^4\pi_g^2$

Figure 4.2: Molecular orbital configuration for both O-cumu and S-cumu [4]

was reported in detail in [4].

The above observation can easily be analized, generally the π delocalized electrons in our chain will be equal to $2n+6$ where n is the number of carbon atom in chain.
Knowing that the configuration of the HOMO and LUMO will be for even chains of (2n) carbon atoms: $\cdots[\pi^2_{ux}][\pi^2_{uy}][\pi^0_{gx}][\pi^0_{gy}]\cdots$ thus yielding typically a singlet state and the HOMO / LUMO configuration for odd chains of (2n+1) carbon atoms is $\cdots[\pi^2_{ux}][\pi^2_{uy}][\pi^1_{gx}][\pi^1_{gy}]\cdots$ (triplet configuration), thus the behaviour is fully justified.

2) *The singlet state is in generally favored and also for even-numbered chains it is close to the ground state energy*

As we have seen before when n is even we will have 14-18-22-26... π electrons for n=4-6-8-10... carbon atoms per chain, thus we will have two SOMO (singly occupied molecular orbitals), where the overall MO configuration will be $\cdots[\pi^2_{ux}][\pi^2_{uy}][\pi^1_{gx}][\pi^1_{gy}]\cdots$, thus the triplet configuration will be favored since π_x and π_y are degenerate, to have the singlet state in fact we will to overcome repulsion between these two electrons, this is not a significant contribution to the energy with respect to the HOMO-LUMO gap, this is the reason for which the triplet state is favored but the singlet state is also close to the ground energy for the system, as it is clearly represented in figure (4.1).
When n is odd we will have 12-16-20-24... π electrons for n=3-5-7... carbon atoms in chain, this numbers are clearly all divisible by 4, thus we will have a fully occupied HOMO configuration :$\cdots[\pi^2_x][\pi^2_y][\pi^0_x][\pi^0_y]\cdots$,the gerade /ungerade HOMO-LUMO combination depend of course on the n°of carbon atoms, for 3-7-11 atoms we will have 12-20-28 delocalized electrons and $\cdots[\pi^2_{ux}][\pi^2_{uy}][\pi^0_{gx}][\pi^0_{gy}]\cdots$ configuration , for 5-9-13 we will have the opposite ungerade /gerade configuration .
This is a clear situation where the singlet state is highly favored, to have the triplet configuration in fact we will have to excite the electrons from the HOMO to the LUMO level to a final state $\cdots[\pi^1_x][\pi^1_y][\pi^1_x][\pi^1_y]\cdots$ thus the triplet state will be highly unfavored.

3) *The Δ_{st} decrease with chain length*

This is an important parameter adding to the fact that this is just and end-chain electronic related to the endgroups.
In fact the effect of the electronegativity [21] of S,O will be in principle localized towards the end of the chain [55], thus for higher chain length the electronic state will not be as highly influenced as for shorter chains.

4.1.2 Modulation of HOMO-LUMO gap and BLA with chain length for S-cumu chains

The values of the HOMO-LUMO gap, BLA and geometry of the ground state for the S-cumu[n] chains calculated by unrestricted PBE0/cc-pVTZ density functional calculations are reported in table (4.2).

Bond lengths The bond length, evaluated for all the specific C-C along the chain and on terminal C-S can give us a general effect on the alternation induced by the terminal atoms and on the conjugation effects.
In the case of S-cumu the terminal bond lengths C-S on both ends shift according to the length of the molecule, in particular for even chains we have values of $> 1.56\mathring{A}$ which is more shifted towards the S-C single bond with respect of the bond values for odd wires, which is $< 1.56\mathring{A}$, thus we will expect an higher bond length alternation for even chains.
The C-C inside the wires are all symmetrical with respect to the center of the chain, for odd chains the center of the chain will be a carbon atom, thus to respect the simmetry the two bonds of these carbon atom should be equal, in fact a double bond, this is another indication of the presence of a very low BLA for shorter chains.
The structure is symmetric and linear, the point group is $D_{\infty h}$ similar to other cumulenes with one-atom terminals, that therefore can yield high linearity.
Even if the structure is cumulenic there is a slightly oscillation on the value of bond lengths along the chain, this alternation becomes more important when we approach the Sulfur endgroups as expected.

Bond length alternation The bond length alternation will be defined in the same description used by Innocenti in its thesis work and article [9]:

$$BLA = \frac{\left[\sum_{i=1}^{N-2} BLA_i\right]}{N-2} \tag{4.1}$$

where N is the number of carbon atoms in the chain, where BLA_i is the difference between the $C_{i+2} - C_{i+1}$ bond length and $C_{i+1} - C_i$ bond length. This eq. (4.1) was used to take into account also odd chains for which the definition of BLA as the difference of the average of'quasi triple bonds' and the 'quasi single bonds' cannot be applied.

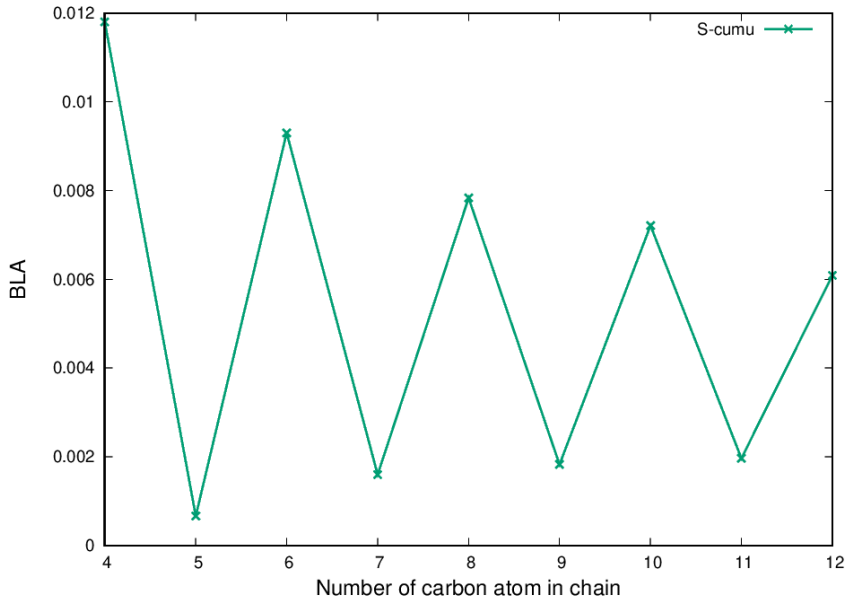

Figure 4.3: BLA behaviour as a function of chain length for S-cumu[n]

We observe in figure (4.3) that the value of the BLA for all the sulfur chains is very low, confirming the cumulenic 'quasi-double bond' structure. The BLA is oscillating depending on the number of sp-carbon atoms, yielding the lowest values for odd-numbered chains.
Another very important observation is that the even numbered chains follow a slight monotic decrease of the BLA, but interestingly the trend is inverted for odd numbered chains where we have a (quasi negligible) monotic increase, leading to a less cumulenic character for higher chain lengths.
This trend and the low BLA yielded for odd wires is non-physical and related on the given definition of BLA and the simmetry of our system, it is an artifact due to the definition of BLA and, as we stated before, the bond lengths of the central atom for odd wiresare equal by simmetry, so the BLA between only these two bonds will be always 0 even for longer chains as we can clearly see from table (4.6).
The effect of the $BLA_i = 0$ on the center of the wire will cause smaller odd wires to have a value of the BLA significantly lower to the expected physical values.
In detail, the equality between consequent bonds, present in the center of the chain of odd wires generates a $BLA_i = |\mathbf{R}_{Ci+1-C_i} - \mathbf{R}_{C_i-C_{i-1}}| = 0$ (with C_i regarded as the central atom).
Aside from the simmetry related effects that exploit the definition of BLA using the requirement for the simmetry of the structure of the chain, the

BLA is almost constant, this is valid also for O-cumu and C-cumu, where this simmetry effect is less evident.

HOMO-LUMO gap The trend for the HOMO-LUMO Gap for the system follow a decreasing function as expected, for higher chain lengths in fact we will increase the $\pi - conjugation$, thus the energy gap will decrease, the interesting behaviour is that this trends are decreasing functions only if we consider chains with the same parity.
The sawtooth trend showed in figure (4.4) is often observed for cumulenes, and it is due to the different behaviour of odd and even chains, both for what concerns the Raman spectra (both for the $\partial\alpha/\partial R$ and the peak intensity) and electronic (ground state multiplicity) and structural (bond length pattern configuration).

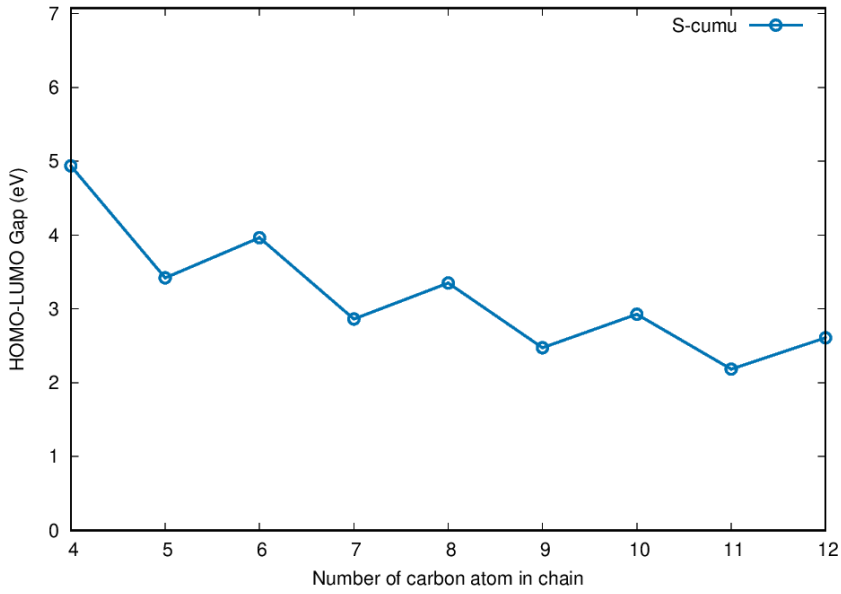

Figure 4.4: HOMO-LUMO gap as a function of chain length for S-cumu[n]

O-cumu[n]									
Bond length values									
	N=4	N=5	N=6	N=7	N=8	N=9	N=10	N=11	N=12
Bond	Triplet	Singlet	Triplet	Singlet	Triplet	Singlet	Triplet	Singlet	Triplet
C1-C2	1,2786	1,2758	1,2780	1,2767	1,2777	1,2770	1,2776	1,2772	1,2776
C2-C3	1,2808	1,2692	1,2774	1,2703	1,2755	1,2709	1,2746	1,2712	1,2740
C3-C4	1,2786	1,2693	1,2736	1,2722	1,2731	1,2727	1,2730	1,2729	1,2730
C4-C5		1,2758	1,2775	1,2722	1,2775	1,2727	1,2767	1,2731	1,2761
C5-C6			1,2780	1,2703	1,2731	1,2727	1,2728	1,2730	1,2727
C6-C7				1,2767	1,2755	1,2727	1,2767	1,2730	1,2762
C7-C8					1,2777	1,2709	1,2730	1,2731	1,2727
C8-C9						1,2770	1,2746	1,2729	1,2761
C9-C10							1,2776	1,2712	1,2730
C10-C11								1,2772	1,2740
C11-C12									1,2776
Energy (Hartree)									
HOMO	-0,2506	-0,2768	-0,2410	-0,2602	-0,2351	-0,2497	-0,2310	-0,2424	-0,2280
LUMO	-0,0124	-0,1044	-0,0604	-0,1254	-0,0886	-0,1382	-0,1069	-0,1469	-0,1196
GAP	0,2382	0,1723	0,1806	0,1348	0,1466	0,1115	0,1241	0,0955	0,1083
Energy (eV)									
HOMO	-6,8178	-7,5313	-6,5590	-7,0799	-6,3982	-6,7944	-6,2861	-6,5958	-6,2034
LUMO	-0,3363	-2,8420	-1,6438	-3,4120	-2,4101	-3,7612	-2,9078	-3,9976	-3,2556
GAP	6,4815	4,6893	4,9152	3,6678	3,9881	3,0332	3,3783	2,5981	2,9478
Bond length alternation									
BLA(i)	0,0022	0,0066	0,0005	0,0064	0,0022	0,0061	0,0031	0,0060	0,0036
	0,0022	0,0001	0,0038	0,0019	0,0024	0,0018	0,0015	0,0017	0,0010
		0,0065	0,0039	0,0000	0,0044	0,0000	0,0037	0,0002	0,0031
			0,0005	0,0019	0,0044	0,0000	0,0039	0,0001	0,0033
				0,0064	0,0024	0,0000	0,00388	0,0000	0,0035
					0,0022	0,0018	0,0037	0,0001	0,0035
						0,0061	0,0015	0,0002	0,0033
							0,0030	0,0017	0,0031
								0,0060	0,0010
									0,0036
BLA	0,0022	0,0044	0,0022	0,0033	0,0030	0,0023	0,0030	0,0018	0,0029

Table 4.2: Computed bond length, BLA and HOMO-LUMO gap values for each of the O-cumu[n] chains with n=4,...,12

4.1.3 Analysis of Raman intensity parameters for S-cumu[n] chains

We will analize the trends of Raman activity for each mode according to the ECC theory [36] that has already been used successfully in this specific field [9].
The partial derivatives of the polarizability ($\frac{\partial \alpha}{\partial Q_i}$) with respect of a specific normal mode for the molecule is directly related to the intensity of the Raman peak for that mode.
We know that:

$$I_k \propto \left(\sum_i \frac{\partial \alpha}{\partial Q_{ik}} \right)^2 \tag{4.2}$$

Where I_k is the Raman activity of a specific mode k and i is the bond order, the sum of the polarizability derivatives over each CC bond with respect to the normal mode k will give us information of the total $\partial \alpha / \partial Q_k$ of the overall molecule.
This factors are composed by the product:

$$\frac{\partial \alpha}{\partial Q_k} = \sum_i \frac{\partial \alpha}{\partial R_i} L_{ik} = \sum_i \frac{\partial \alpha}{\partial Q_{ik}} \tag{4.3}$$

for a specific mode (k), where L_{ik} is the (i)-value of the eigenvector L_k, who represents the amplitude of vibration of the normal mode (k) on internal coordinates R_i.
Thus the $\frac{\partial \alpha}{\partial R_i}$ give us important information of the structural properties of a specific CAWs.
Since in the case of cumulenes the molecular structure consists of a sequence of quasi equalized double CC bonds, the local parameter $\frac{\partial \alpha}{\partial R_i}$ of the singular CC stretching of the collective oscillation mode will yield similar values.
Instead for polyynic wires the $\frac{\partial \alpha}{\partial R_i}$ will have an alternation between a positive and a negative value.
We can see that increasing the length of the chain we will have two effects: a red shift to lower frequencies ([29]) as we commented before, and a monotonic increase on the intensity of the peaks.
In a previous Raman analysis Wang et al [4] suggested an increase of the vibrational frequency of the main peak of S-cumu[n] for $n < 6$, this is only caused because the main peak will be associated to different modes for short chains instead of the ECC line.
If the sum over all the CC bonds is shifted towards negative or positive values we will have an high $|\frac{\partial \alpha}{\partial Q_k}|$ for the chain and so an higher intensity of the

specific normal mode k.
The normal modes considered, labelled for identification as $\beta^*, \gamma, \delta \cdots$, will give also information on the Raman spectra, in fact also the peaks will be identified by the correspondent type of normal mode.

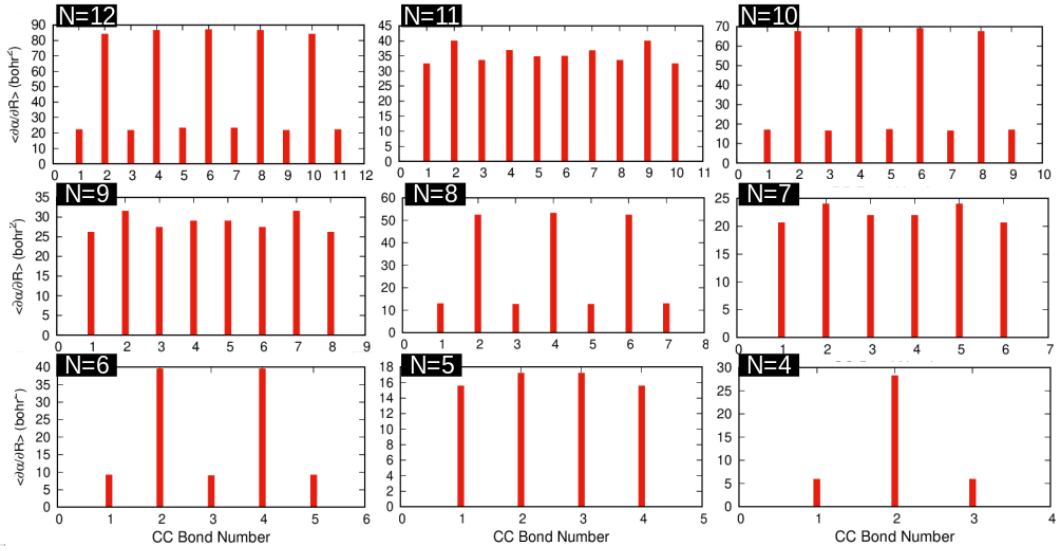

Figure 4.5: Variation of the polarizability with respect of the BLA oscillation, from top left (S-cumu[12]) to bottom right (S-cumu[4])

As we can see in figure (4.5) the $\frac{\partial \alpha}{\partial R_i}$ trend generally show a cumulenic character.
The even chains shows less equalized $\frac{\partial \alpha}{\partial R_i}$ (typical of Vyn-cumu[n] chains [9]), which will explain the overall higher Raman activity of the modes (*this will be explained in detail later considering the eigen-vectors*), the bond also will be less equalized yielding an higher value for the BLA.
The odd chains shows a more equalized $\frac{\partial \alpha}{\partial R_i}$ pattern (typical also of C_n-cumu[n] chains) and a lower bond length alternation.

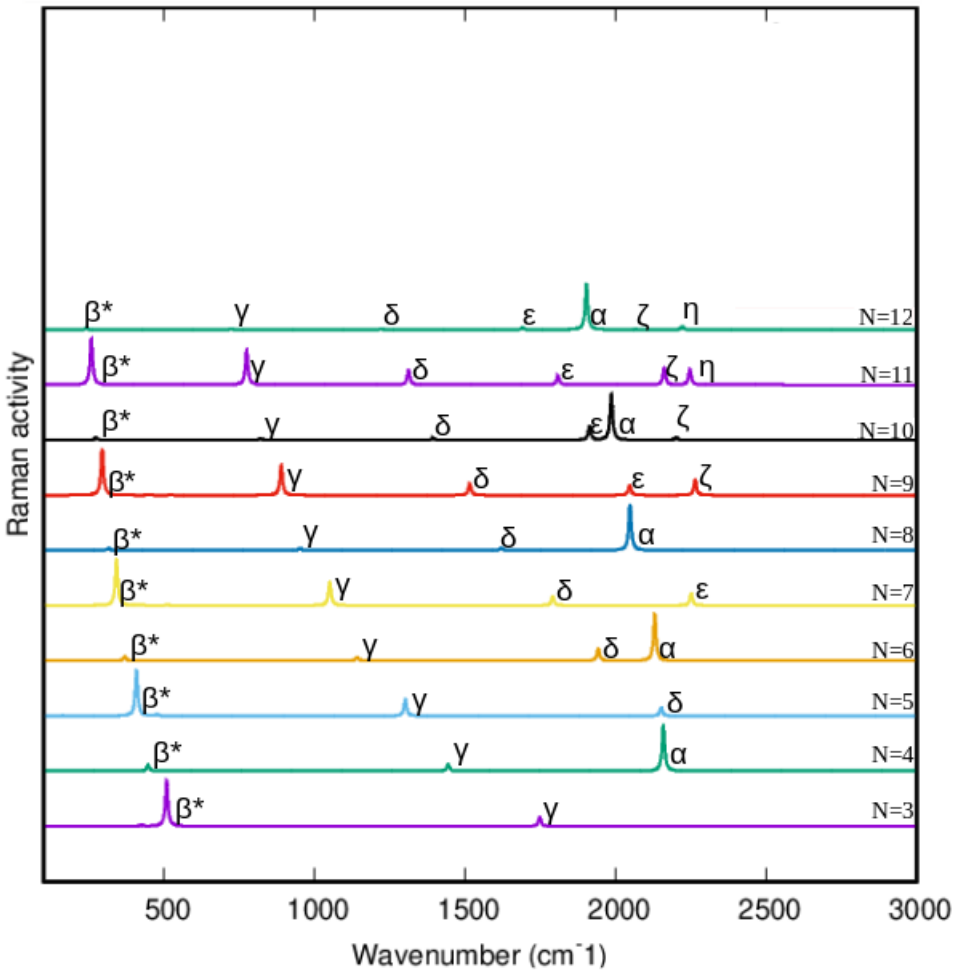

Figure 4.6: Normalized Raman spectrum for all type of chains, the number on the top right refer to the number of carbon atom per chain

From the calculated Raman spectrum on figure (4.6) we note several important observations:

1) *The red shift of all modes is evident: increasing the length of the chain the overall frequency of the stretching vibration will decrease*

This is probably related to the force constants associated to CC stretching coordinates, which for higher chain lengths are known to be 'softer', as a result of the softer CC bonds promoted by conjugation, this generates a decrease on the frequency of each normal mode with chain length.

A more detailed investigation on the force constant in internal coordinates should be required to prove this point.
This is only present on longitudinal normal modes and not normal modes regarding the end-groups such in the case of phenyl (phenyl modes) and vinylidene termination (CH wagging,stretching), in this cases there isn't generally a variation on the wavenumber.
We will see the normal modes related to the presence of these terminations later.

2) *The odd chains show a Raman spectra with several lines of comparable intensity, whereas the even chains present a relatively intense ECC mode (or α peak)*

3) *All the Raman intensities for even chains are significantly higher with respect to the odd chain ones, and they also all follow a monotonic increase with the length of the chain*

This is valid for all the peaks except for the case of the δ for S-cumu[6] and ϵ for S-cumu[10] peaks, this is related to the lower alternation of the $\partial\alpha/\partial Q$ and their high values compared to the other peaks.
Regarding the relative calculated Raman activity between even-odd wires we observe that $\beta^*_{even}(2n) \approx 2\beta^*_{odd}(2n-1)$ both the value refer to the intensity of the peaks for the chain with (n) carbon atoms, this trend is similar for γ modes but the intensities for $\gamma(3)$ and $\gamma(5)$ are extremely low with respect to $\gamma(4)$ and $\gamma(6)$ (respectively 5, 15 times less).
The δ, ϵ and η peak intensities for odd peaks is 1 order of magnitude or less and can be considered negligible.

Even chains

In table (4.3) are reported all the important data for the wavenumber and Raman activity for each significant normal mode for even chains and their assignation.

Even chains			
n° C atoms	Wavenumber $[cm^{-1}]$	Raman activity $[\AA^4/amu]$	Type
12	244	895	β^*
	725	657	γ
	1224	658	δ
	1692	1302	ϵ
	1904	28407	α
	2070	204	ζ
	2221	1872	η
10	276	620	β^*
	822	472	γ
	1396	523	δ
	1915	3782	ϵ
	1987	12750	α
	2202	717	ζ
8	316	414	β^*
	953	327	γ
	1621	460	δ
	2049	8007	α
6	371	264	β^*
	1143	228	γ
	1943	738	δ
	2131	2835	α
4	448	157	β^*
	1445	176	γ
	2160	1168	α

Table 4.3: Calculated data for the wavenumber and Raman activity of significant peaks for even-carbon chains S-cumu[2n]

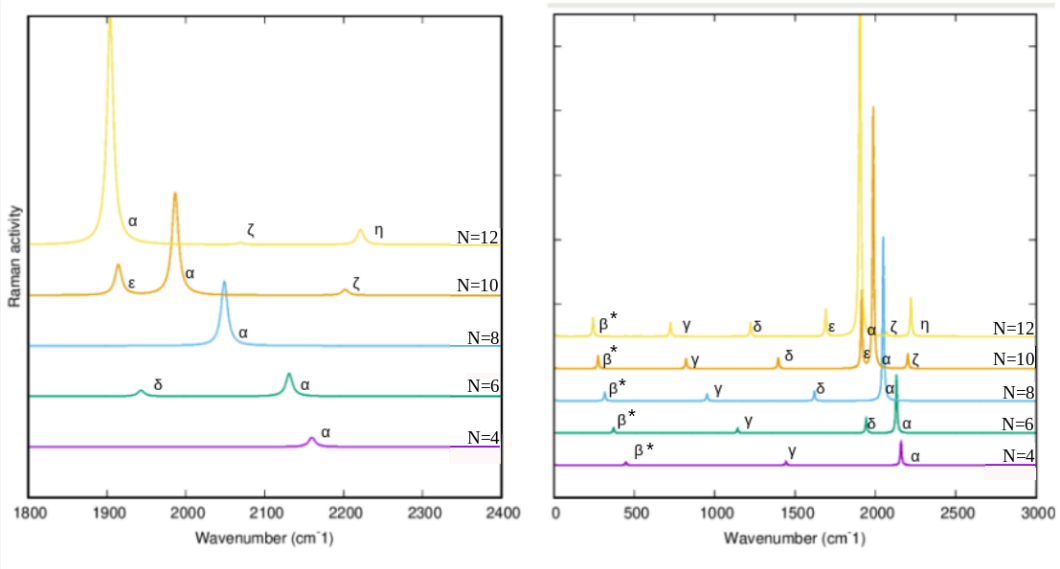

Figure 4.7: Raman spectra over a selected frequency range (on the left) and over all the spectrum (on the right)

In the figure (4.7) all the relevant peaks for even S-cumu[n] wires are depicted, with an indication on the behaviour of the Raman peaks over a selected range (1800 cm^{-1} to 2400 cm^{-1}), a range in which generally the ECC mode line is found for similar systems.
We can see that for even chains that the α peak for even chain is relevant and is inside our selected range.
In the following pages we will analize in detail each mode and its trends and activity behaviours with a detailed analysis also on the polarizability derivatives.

$\beta*$ mode The β^* trends are depicted below:

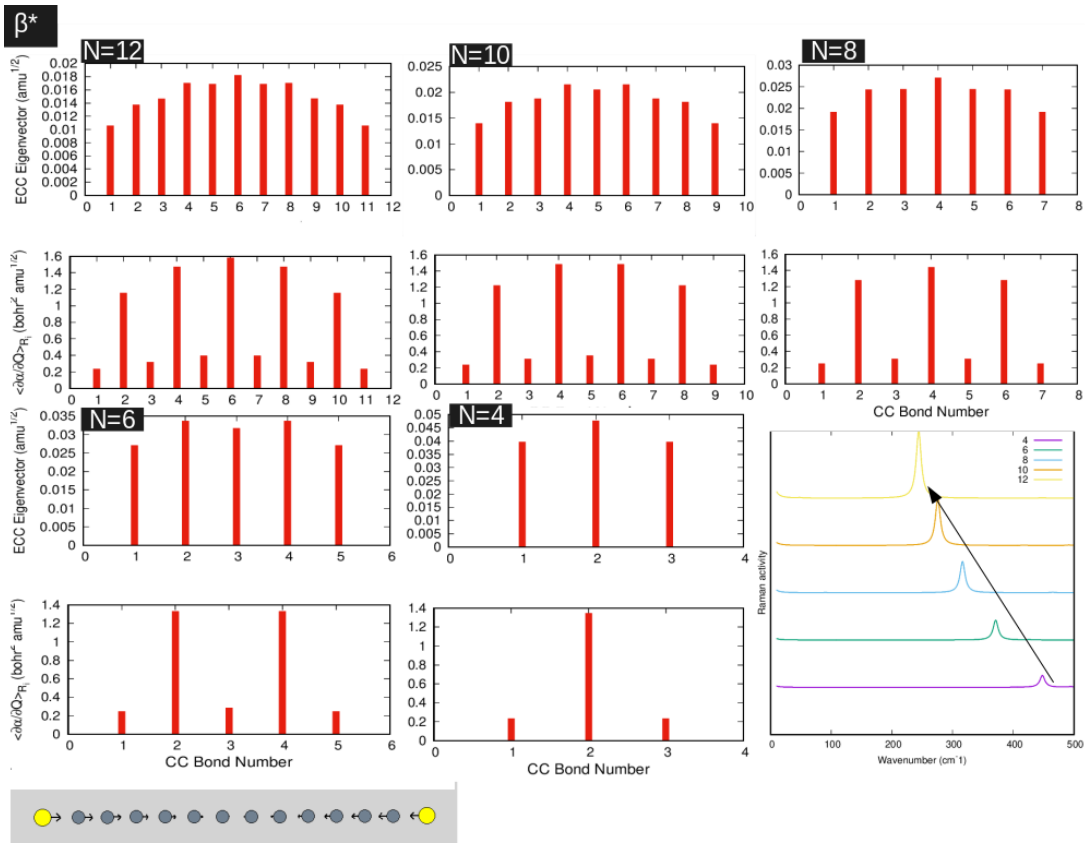

Figure 4.8: β^* mode (even chains)

As we can see in figure (4.8) the β^* mode is characterized by relatively low values of Raman activity ($< 1000[\mathring{A}^4/amu]$) and can become only important for characterization of odd chains since for even chains it is negligible with respect of the main ECC line ($= 28407[\mathring{A}^4/amu]$).
The values of $\partial\alpha/\partial Q$ are all positive, but each CC gives very little contribution to Raman activity, reaching the maximum of $\approx 2[bohr^2 \cdot amu^{1/2}]$.
We note that for the $\partial\alpha/\partial Q$ follows the same alternating pattern of relatively low and high values of the $\partial\alpha/\partial R$, this is a consequence of the eigen-vectors yielding almost constant values. The β^* mode wavenumber is red shifting as expected with increasing chain length and yield values of 448-371-316-276-244 cm^{-1} for 4,6,8,10,12 carbon atom in chain.

γ mode The γ trends are depicted below:

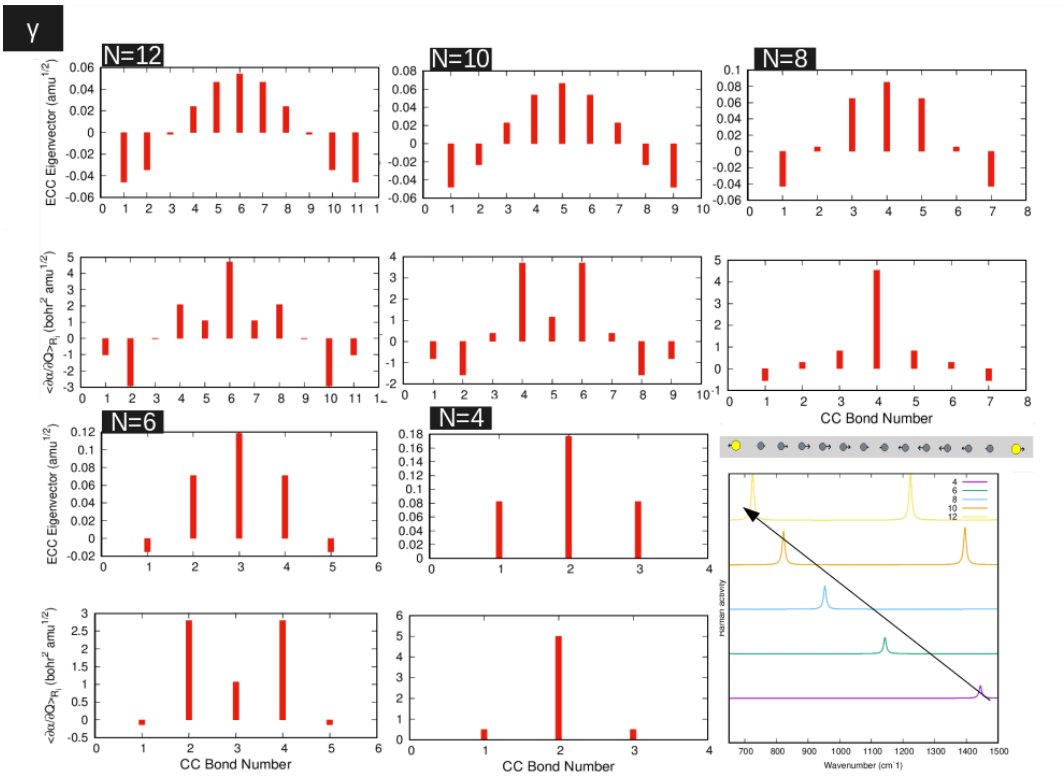

Figure 4.9: γ mode (even chains)

As we can see in figure (4.9) the values of $\partial\alpha/\partial Q$ are alternated, also each CC gives little contribution to Raman activity, reaching the maximum of $\approx 5[bohr^2 \cdot amu^{1/2}]$, this explain the very low values for Raman activity of these modes $< 700[\mathring{A}^4/amu]$.
The γ mode wavenumber is red shifting as expected with increasing chain length and yield values of 1445-1143-953-822-725 cm^{-1} for 4,6,8,10,12 carbon atom in chain.

δ mode The δ trends are depicted below:

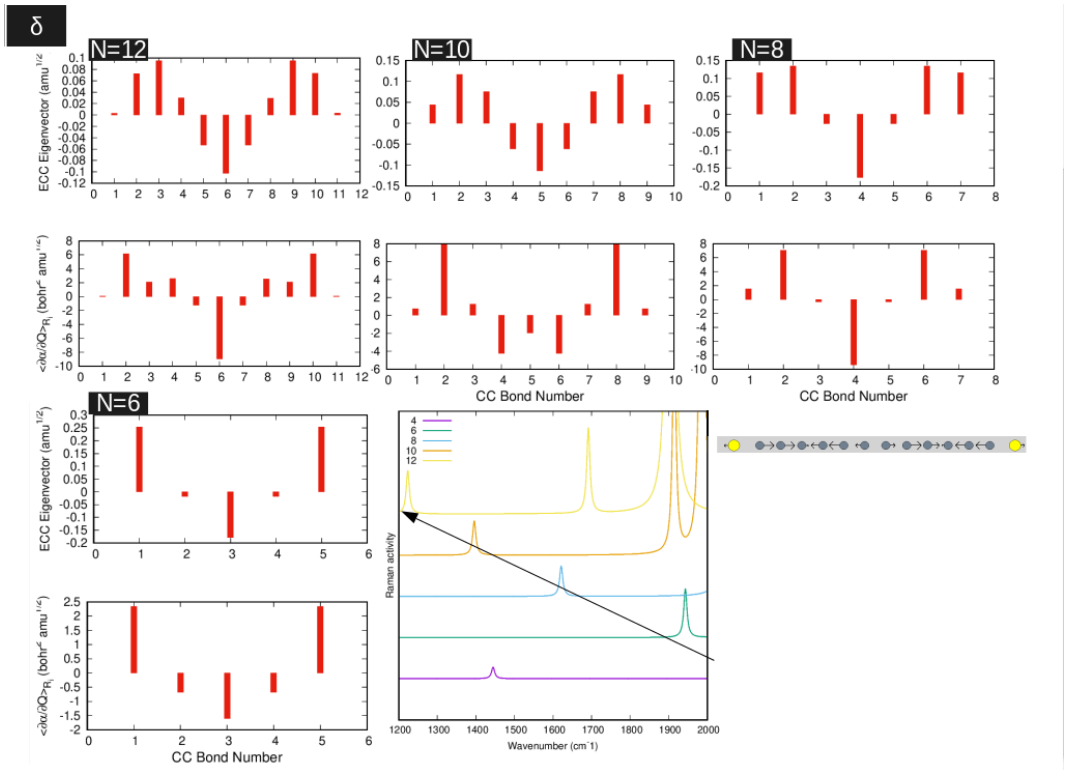

Figure 4.10: δ mode (even chains)

As we can see in figure (4.10) the values of $\partial\alpha/\partial Q_i$ are alternated and each CC gives little contribution to Raman activity, reaching the maximum of $\approx 8[bohr^2 \cdot amu^{1/2}]$.
This explain the very low values for Raman activity of these modes that is less than $800[\mathring{A}^4/amu]$.
In the case of the δ mode for $S-C_6-S$ chains however the value of $\partial\alpha/\partial Q$ are less alternated and shifted towards positive amounts and this explains its higher intensity with respect to the other δ modes, indeed it is the most relevant even compared to the $S-C_{12}-S$ value of δ ($738[\mathring{A}^4/amu]$) compared to ($658[\mathring{A}^4/amu]$). The δ mode wavenumber is red shifting as expected with increasing chain length and yield values of 1943-1621-1396-1224 cm^{-1} for 6,8,10,12 carbon atom in chain.

α mode The α trends are depicted below:

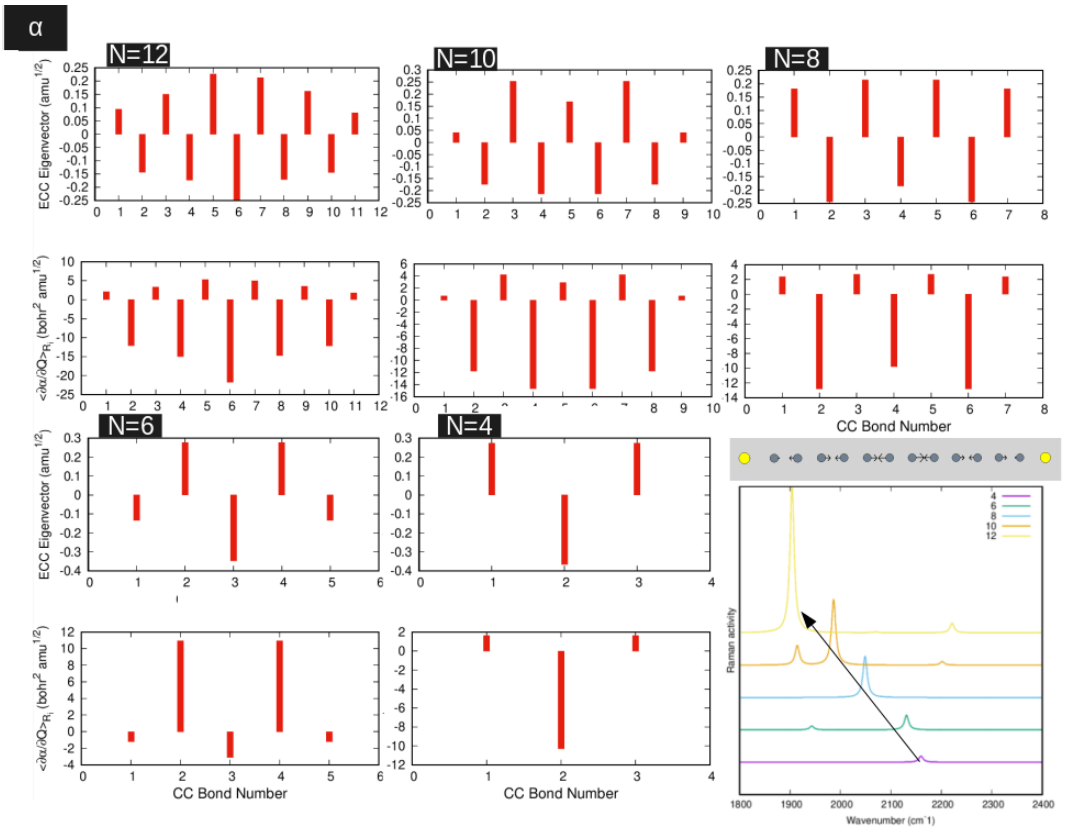

Figure 4.11: α mode (even chains)

As we can see in figure (4.11) the values of $\partial\alpha/\partial Q$ are shifted towards negative values and this is explained by the fact that the $\partial\alpha/\partial R$ are positive but with a significant difference in values: the $\partial\alpha/\partial R$ related to positive eigen-vectors have values ≈ 4 times lower with respect to the ones related to negative eigen-vectors. Thus the positive $\partial\alpha/\partial Q$ will give a contribution ≈ 4 times lower than their negative counterpart. Considering also that the value of $\partial\alpha/\partial Q$ can reach $\approx 90[bohr^2 \cdot amu^{1/2}]$ we will expect an high intensity of these α peaks as expected that reach $28407[\mathring{A}^4/amu]$. The α peak wavenumber is red shifting as expected with increasing chain length and yield values of 2160-2131-2049-1987-1904 cm^{-1} for 4,6,8,10,12 carbon atom in chain. We note that the red shifting is anyway limited compared to the trends for the other peaks and the wavenumber is maintained in the 2200-1900 cm^{-1} range.

ϵ mode The ϵ trends are depicted below:

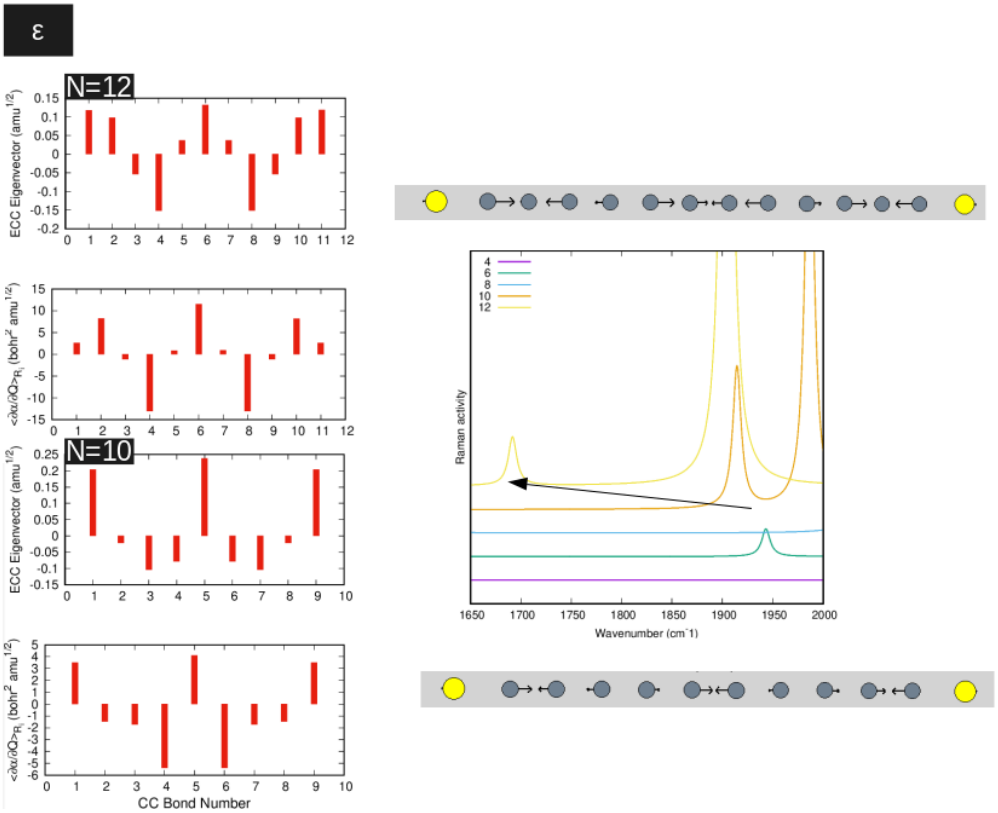

Figure 4.12: ϵ mode (even chains)

As we can see in figure (4.12) the values of $\partial\alpha/\partial Q$ are alternated, each CC gives a contribution to Raman activity with a maximum of $\approx 10[bohr^2 \cdot amu^{1/2}]$.
This explains the medium values of Raman activity of these mode for $S - C_{12} - S$ which is $1302[\mathring{A}^4/amu]$.
In the case of the ϵ mode for $S - C_{10} - S$ chains however the value of $\partial\alpha/\partial Q$ are less alternated and shifted towards negative values and this will explain its higher intensity ($3782[\mathring{A}^4/amu]$) with respect to the other ϵ mode.
This peak is significant with respect also to the ECC line for this specific wire.

ζ mode The ζ trends are depicted below:

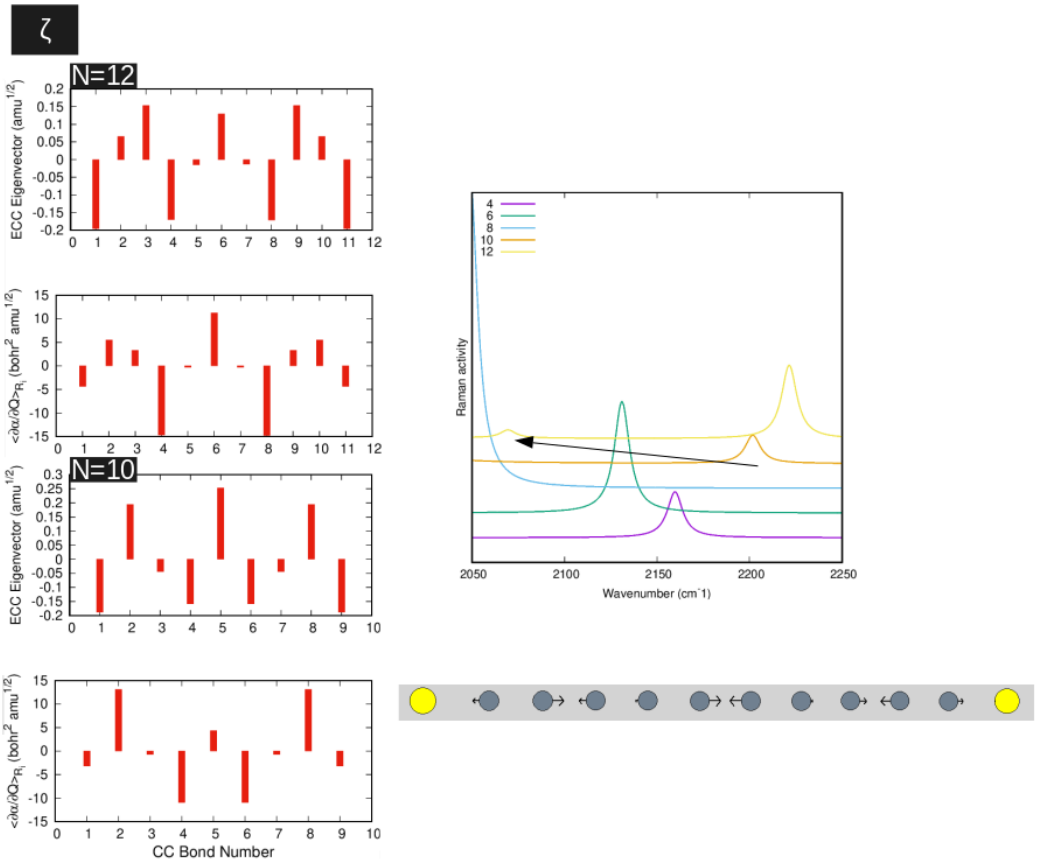

Figure 4.13: ζ mode (even chains)

As we can see in figure (4.13) the values of $\partial\alpha/\partial Q$ are alternated and each CC gives little contribution to Raman activity, reaching the maximum of $\approx 10[bohr^2 \cdot amu^{1/2}]$.
This explains the low values for Raman activity of these modes and especially the value for the ζ peak for $S-C_{12}-S$ is very low ($204[\mathring{A}^4/amu]$) as a result of the high alternation of the $\partial\alpha/\partial Q$.

η mode The η trends are depicted below:

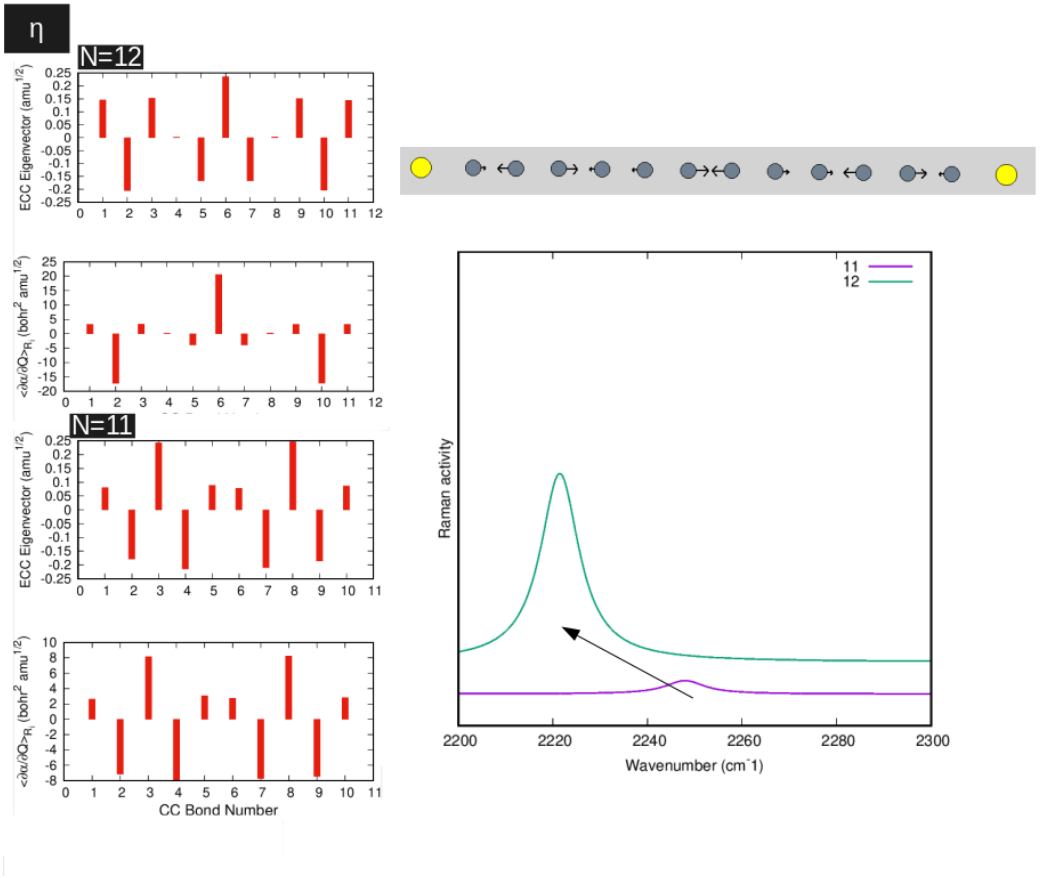

Figure 4.14: η mode ($S - C_{11} - S$ and $S - C_{12} - S$ chains)

As we can see in figure (4.14) the values of $\partial\alpha/\partial Q$ are relatively high with respect of the other peaks, reaching the maximum of $\approx 20[bohr^2 \cdot amu^{1/2}]$, but the values are alternated in the case of $S - C_{11} - S$ and do not give significant Raman activity values.
In the case of $S - C_{12} - S$ they are shifted towards negative values presenting higher values $1872[\mathring{A}^4/amu]$.

Odd chains

In table (4.4) are reported all the important results for the wavenumber and Raman activity for each significant normal mode for odd chains and their assignation.

Odd chains

n° C atoms	Wavenumber $[cm^{-1}]$	Raman activity$[\dot{A}^4/amu]$	Type
11	260	397	β^*
	775	302	γ
	1313	129	δ
	1810	81	ϵ
	2162	143	ζ
	2248	133	η
9	296	285	β^*
	890	184	γ
	1517	72	δ
	2048	62	ϵ
	2265	96	ζ
7	343	192	β^*
	1052	98	γ
	1792	37	δ
	2252	50	ϵ
5	410	117	β^*
	1302	42	γ
	2153	21	δ
3	510	61	β^*
	1749	12	γ

Table 4.4: Calculated data for the wavenumber and Raman activity of significant peaks for odd-carbon chains S-cumu[2n+1]

In figure (4.15) we show the Raman spectra of odd chains:

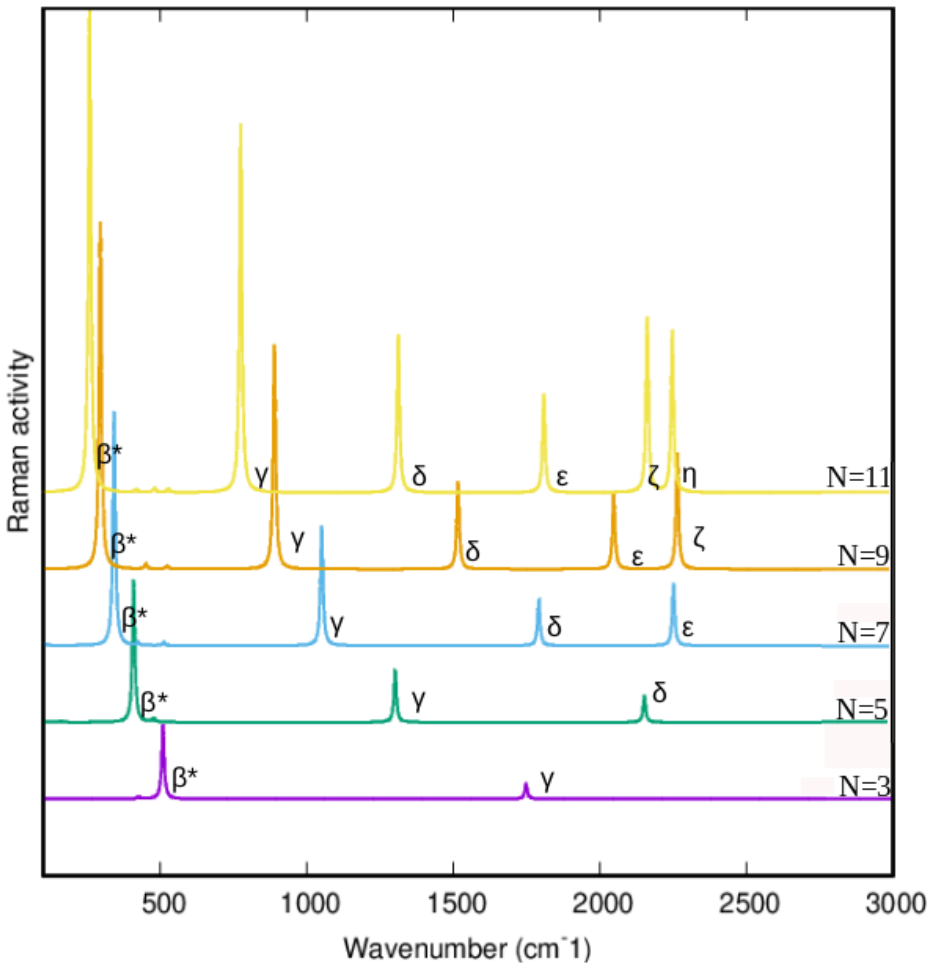

Figure 4.15: Raman spectra for odd chains

This pattern is significantly different from the one found for even chains, in fact the quasi equalized $\frac{\partial \alpha}{\partial R}$ over the structure will give a better alternation of the $\frac{\partial \alpha}{\partial Q}$.
This increase on the regularity, along with the fact that the average values for the singular $\partial \alpha / \partial Q$ for each CC is much lower that in even chains explain the fact that the corresponding intensity of the peaks will be much lower. The value for the Raman intensity of each mode is increasing for longer chains and there aren't any specific modes that don't follow this trend (as found in the case of even chains).

β^* mode The β^* trends are depicted below:

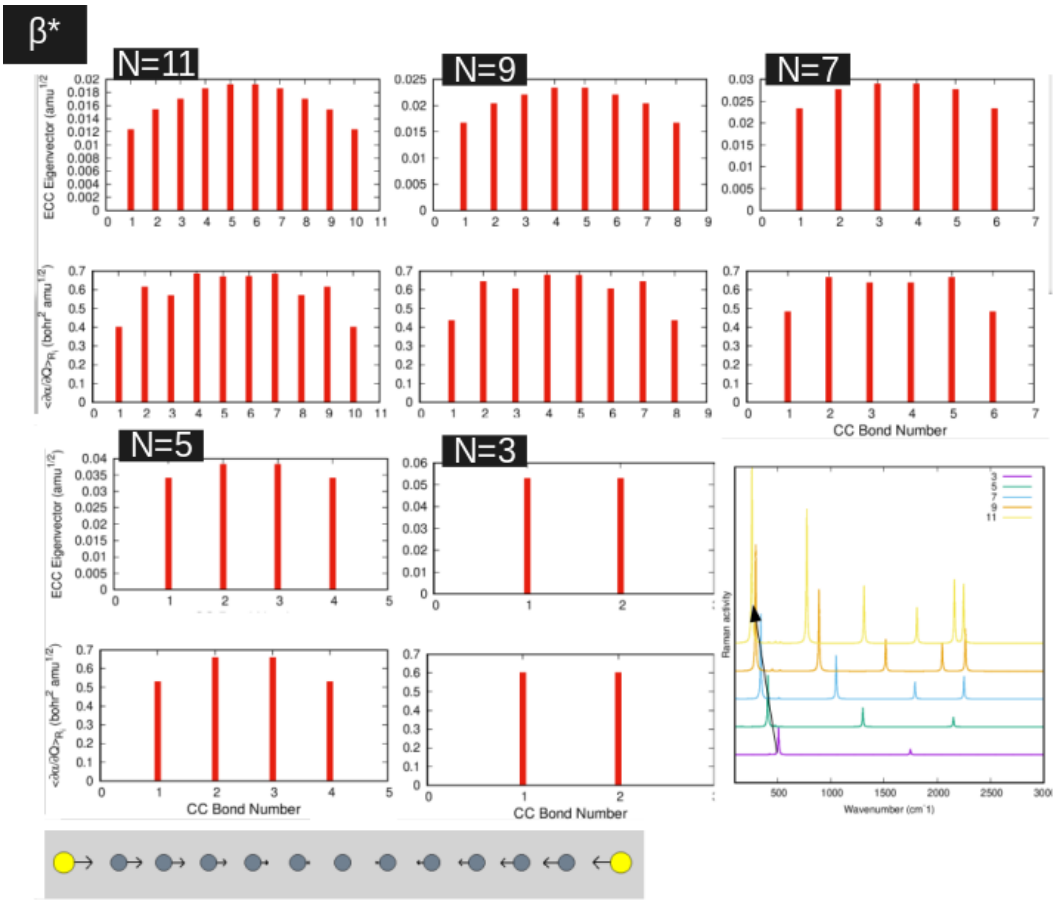

Figure 4.16: β^* mode (odd chains)

In figure (4.16) we can see that this is the only mode not affected by the equalized $\partial\alpha/\partial R$ pattern, in fact there is not a negative contribution of the $\partial\alpha/\partial Q$ and for this fact it becomes the most significant peak for these types of molecules.
The $\partial\alpha/\partial Q$ reach up to $\approx 0.7[bohr^2 \cdot amu^{1/2}]$, which is a very low value. The β^* mode wavenumber is red shifting as expected with increasing chain length and yield values of 510-410-343-296-260 cm^{-1} for 3,5,7,9,11 carbon atom in chain.

γ mode The γ trends are depicted below:

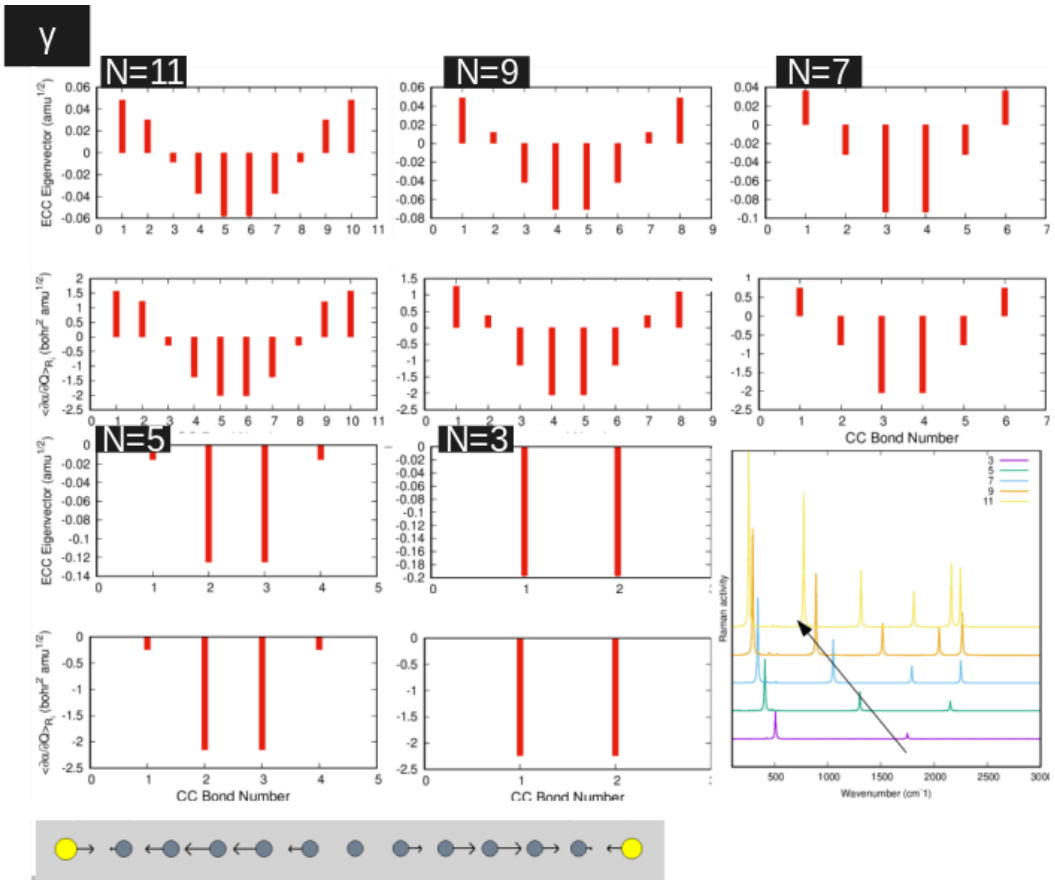

Figure 4.17: γ mode (odd chains)

As we can see from (4.17) the $\partial\alpha/\partial Q$ reach up to $\approx 2[bohr^2 \cdot amu^{1/2}]$, thus we have low intensity for these modes.
For $S - C_5 - S$ this mode show a significant higher intensity with respect to the δ since it has only negative contribution of the $\partial\alpha/\partial Q$ with respect to the alternating pattern of the other mode, even if the singular $\partial\alpha/\partial Q$ for the γ peak reach a value of $\approx 5[bohr^2 \cdot amu^{1/2}]$. The γ mode wavenumber is red shifting as expected with increasing chain length and yield values of 1749-1302-1052-890-775 cm^{-1} for 3,5,7,9,11 carbon atom in chain.

δ mode The δ trends are depicted below:

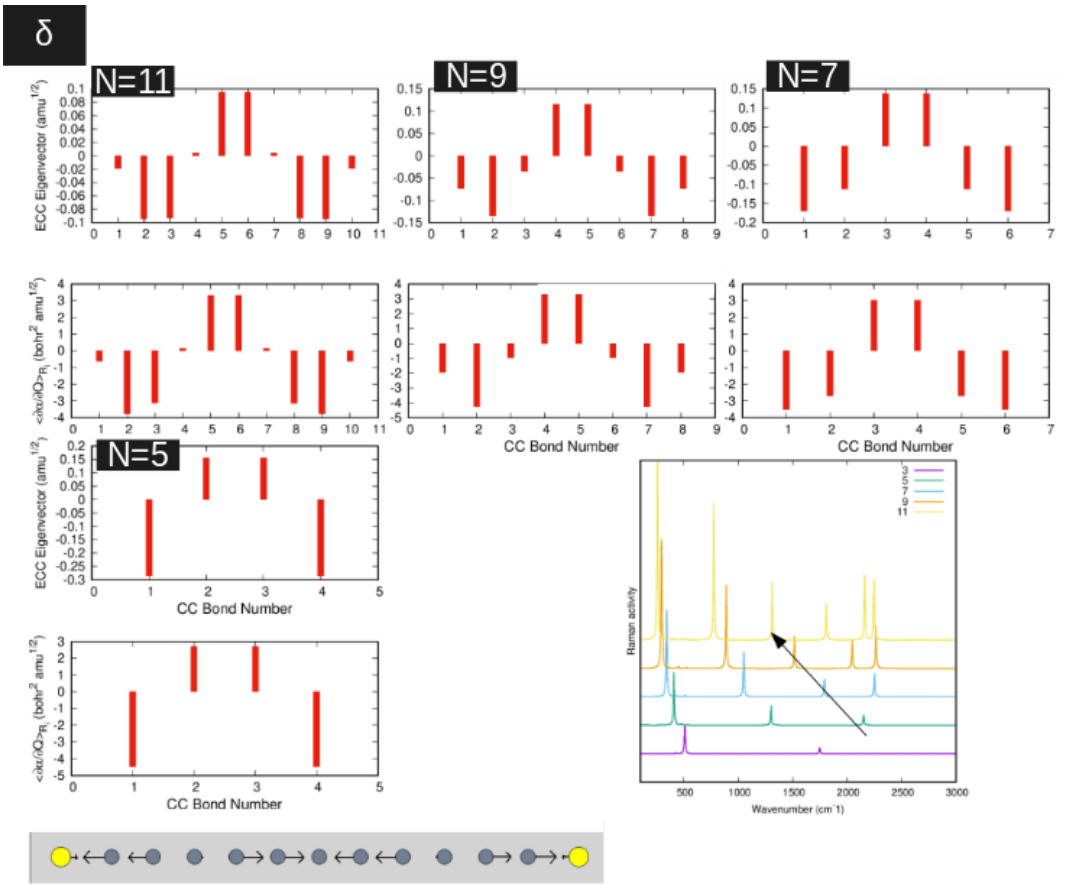

Figure 4.18: δ mode (odd chains)

As we can see from figure (4.18) the $\partial\alpha/\partial Q$ reach up to $\approx 3[bohr^2 \cdot amu^{1/2}]$ for small chains, but with higher alternation with respect to γ modes as we stated before.
Instead for higher chain length it presents very low values for the $\partial\alpha/\partial Q$ of $\approx 4[bohr^2 \cdot amu^{1/2}]$ but also with high alternation. The δ mode wavenumber is red shifting as expected with increasing chain length and yield values of 2153-1792-1517-1313 cm^{-1} for 5,7,9,11 carbon atom in chain.

ϵ mode The ϵ trends are depicted below:

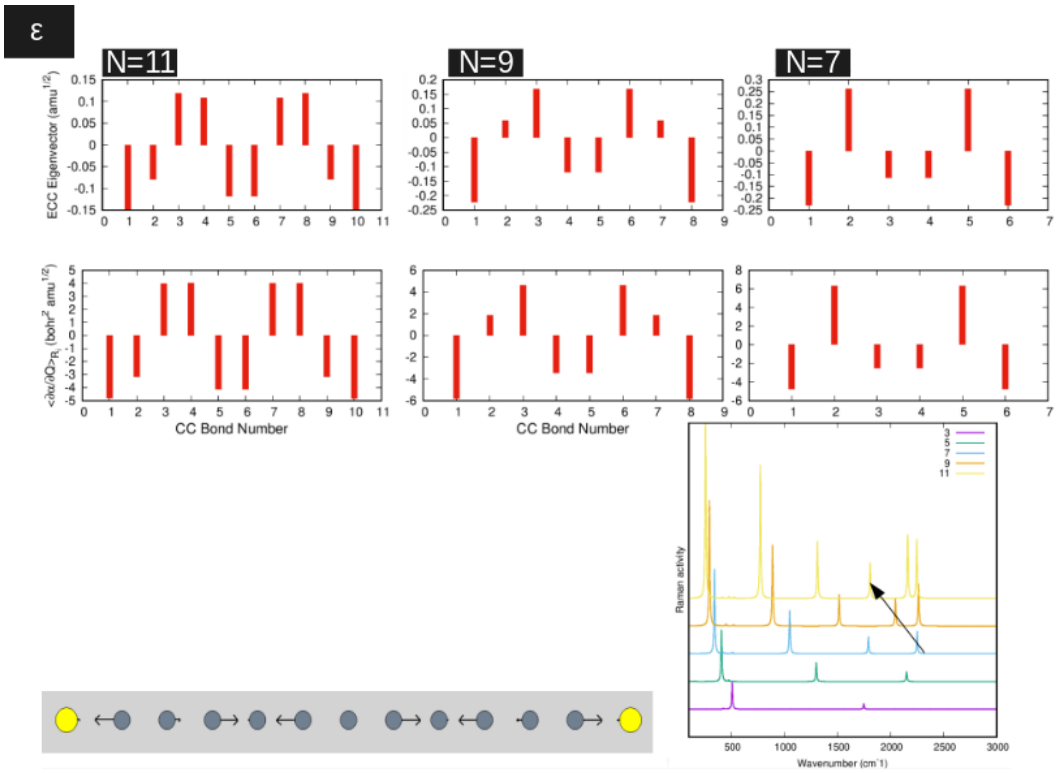

Figure 4.19: ϵ mode (odd chains)

As we can see from figure (4.19) the $\partial\alpha/\partial Q$ has low values and reach up to $\approx 6[bohr^2 \cdot amu^{1/2}]$ and also with high alternation yielding low intensity peaks. The ϵ mode wavenumber is red shifting as expected with increasing chain length and yield values of 2048-1810 cm^{-1} for 9,11 carbon atom in chain.

ζ mode The ζ trends are depicted below:

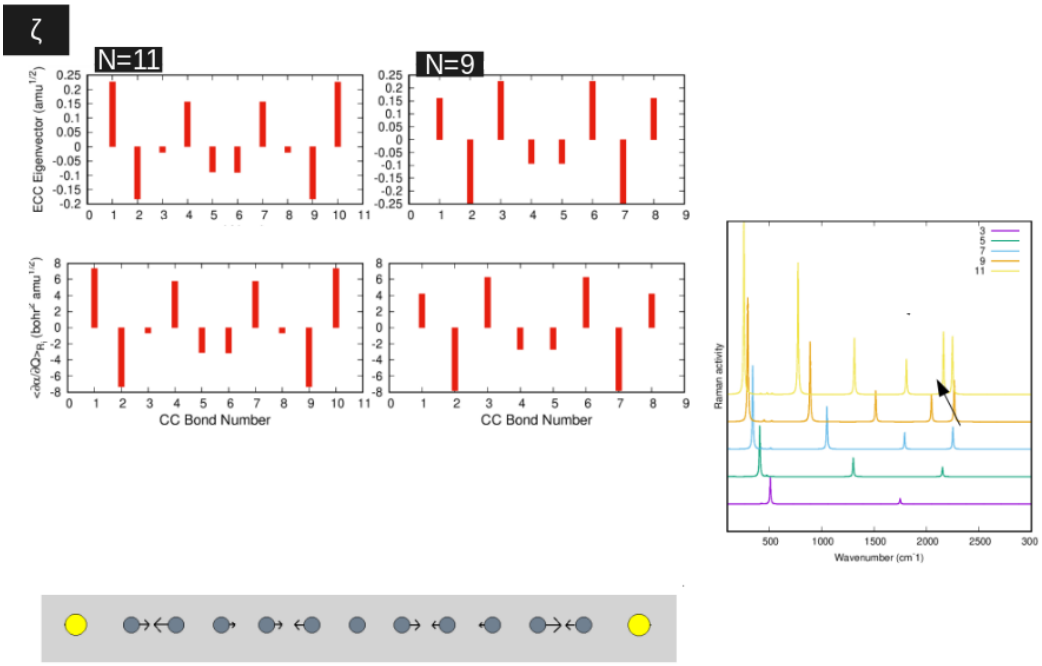

Figure 4.20: ζ mode (odd chains)

As we can see in figure (4.20) the $\partial\alpha/\partial Q$ has low values and reach up to $\approx 7[bohr^2 \cdot amu^{1/2}]$ and also with high alternation yielding low intensity peaks

4.2 Oxygen cumulenes

In this chapter we will investigate the electronic, structural and vibrational properties for oxygen terminated cumulenes (O-cumu[n] or $O-C_n-O$ with n=3,4...,12) by the means of PBE0/cc-pVTZ calculations as we did for S-cumu[n] wires.
We will study in detail the calculated electronic and structural properties of these chains and we will carry a complete study on the Raman spectra, focusing on each relevant mode.

4.2.1 Electronic configuration of ground state for O-cumu chains

Multiplicity considerations also for oxygen-terminated chains was not completely clear in papers [4, 21] and it was necessary to undergo a ground state analysis as for sulfur terminated carbynes.
I report the results for the ground state energy of O-cumu[n], each analyzed in its triplet and singlet state, on the basis of the calculated energies i predict the most stable spin configuration for each wire.
The values of the singlet and triplet energy will be given by the following table (4.5).

We observe a similar behaviour as in the case of sulfur cumulenes, in par-

Oxygen cumulenes					
N°C in chain	Singlet E	Triplet E	Δ_{st}(Hartree)	Δ_{st} (kcal/mol)	**Most stable**
N=3	-264,5247	-264,3731	-0,1517	-95,1691	SINGLET
N=4	-302,4898	-302,5141	0,0243	15,2196	TRIPLET
N=5	-340,6018	-340,5100	-0,0918	-57,6296	SINGLET
N=6	-378,5924	-378,6113	0,0188	11,8194	TRIPLET
N=7	-416,6846	-416,6133	-0,0713	-44,7493	SINGLET
N=8	-454,6887	-454,7044	0,0156	9,8129	TRIPLET
N=9	-492,7698	-492,7149	-0,0549	-34,4543	SINGLET
N=10	-530,7822	-530,7957	0,0135	8,4998	TRIPLET
N=11	-568,8561	-568,8140	-0,0421	-26,4429	SINGLET
N=12	-606,8741	-606,8862	0,0121	7,5806	TRIPLET

Table 4.5: Values of the energy minima (in Hartree) for both the singlet and triplet state for all chain lengths, the difference (Δ_{st}) is reported both in Hartree and in kcal/mol, the corresponding most stable ground state multiplicity condition is written in the last column.

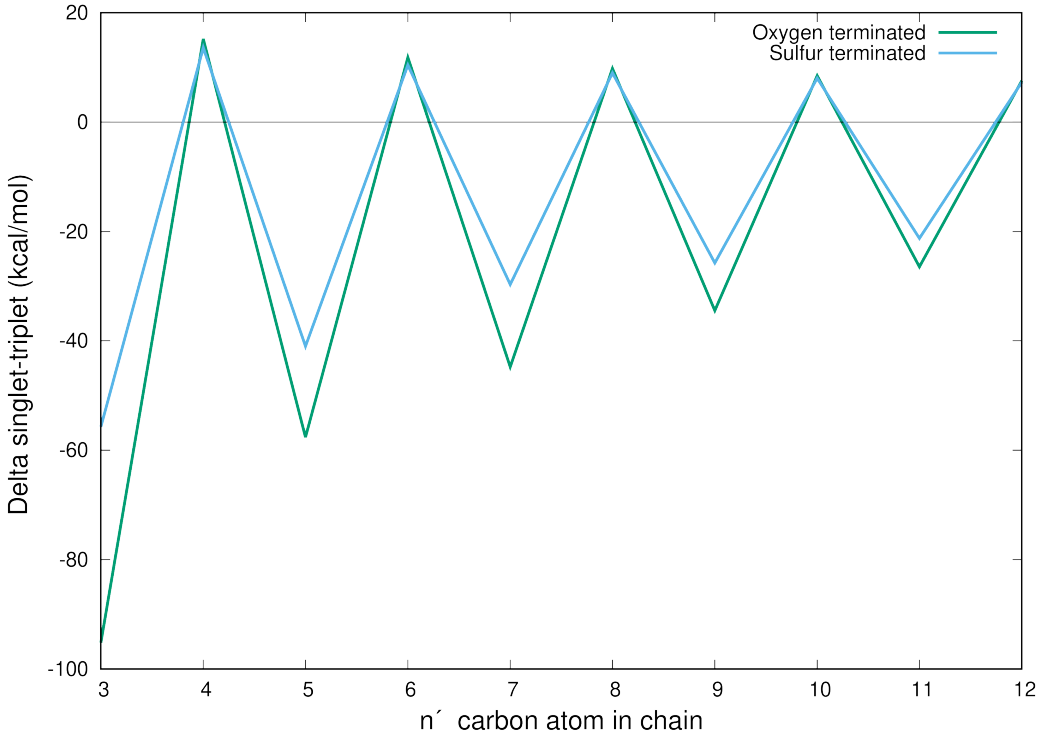

Figure 4.21: Single triplet minima difference over all the different chain lengths, also the previous values for the S-cumu[n] are reported as a comparison

ticular we have the same sawtooth alternation between singlet state for odd chains and triplet state for even ones.
The molecular orbital configuration of degenerate π_x and π_y is the same for oxygen cumulenes as it was for sulfur cumulenes, thus most of the observations regarding the trends of the singlet and triplet energies are still valid for these wires.
The only difference between the two trends is that the difference in energy between the singlet and the triplet state Δ_{st} is higher for oxygen terminated cumulenes than it was for sulfur terminated.
This can be related to the electronic effect of the different types of termination (sulfur and oxygen).
We know that the electronegativity for oxygen is much higher than sulfur, this can lead on modification of the shape and size of molecular orbitals, changing the electronic properties of the system and therefore also the tendency to be in a triplet or singlet state.

4.2.2 Modulation of HOMO-LUMO gap and BLA with chain length for O-cumu chains

The values of the GAP, BLA and geometry of the ground state for the $O - C_n - O$ chains calculated by unrestricted PBE0/cc-pVTZ density functional calculations are reported in table (4.6).

Bond lengths The oxygen-capped chains show a lower degree of alternation on the length of the bonds as we had for S-cumu[n] wires, the oxygen doesn't give a significant alternation of 'quasi single' and 'quasi triple' bonds, showing a more equalized cumulenic structure.
Also in even chains, that for S-cumu[n] showed a significant alternation, is not relevant for O-cumu[n] wires.
The maximum difference between the longest CC and the shortest on a singular molecule in these systems is $\approx 0,006$, instead for S-cumu the value was $\approx 0,011$.

Bond length alternation In figure (4.22) we show the BLA trend for O-cumu wires.

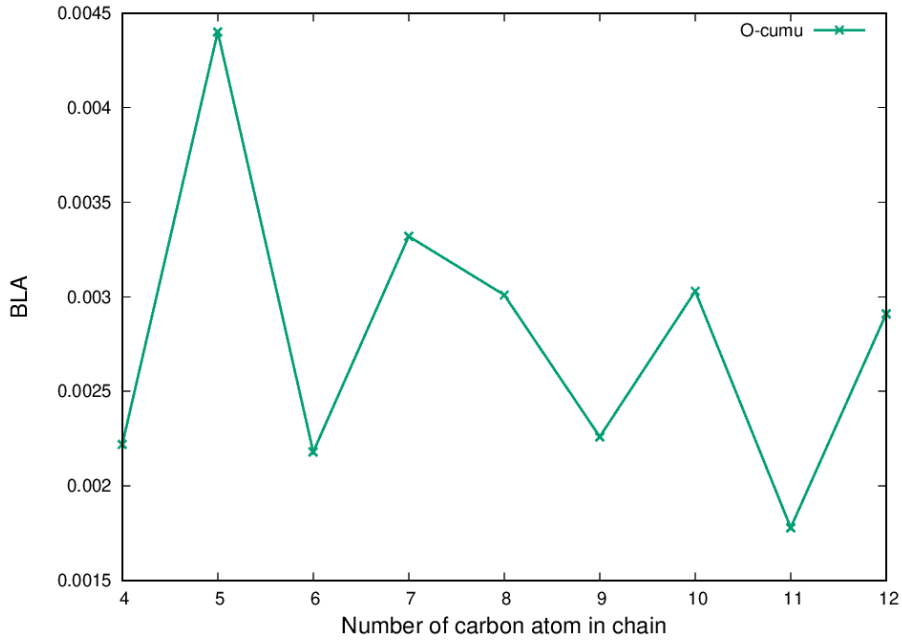

Figure 4.22: BLA dependence on the chain length for O-cumu[n] wires

The trend in the BLA is different from the one of sulfur terminated chains, for O-cumu we have low values for the bond length alternation also for even chains.
This BLA show a quasi-constant behaviour, the variation of this trend are of the order of the numerical errors for the DFT calculations and this values are all between 0.002 and 0.0045.

HOMO-LUMO gap In figure (4.23) we can see the HOMO-LUMO gap trend for O-cumu[n] wires of increasing chain length.

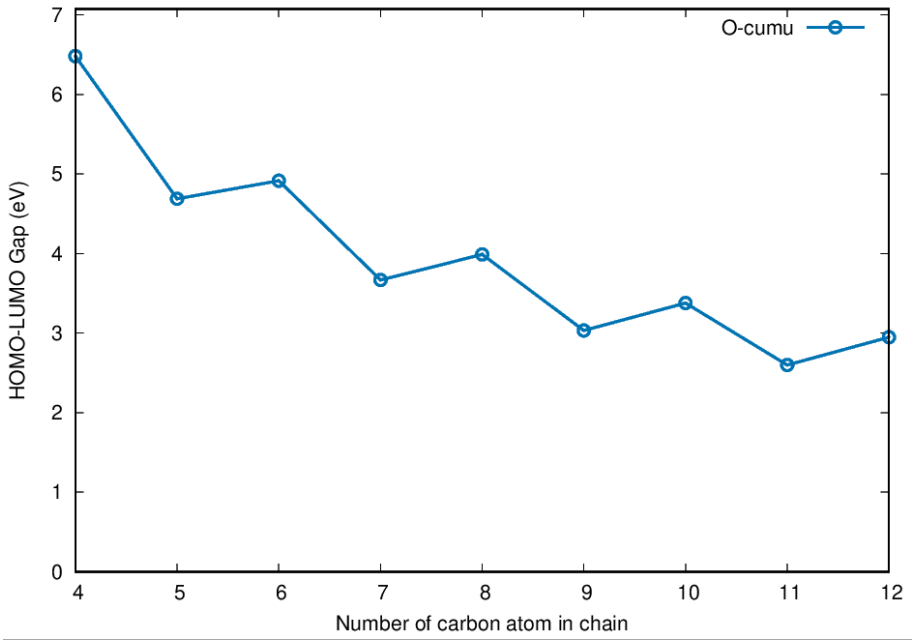

Figure 4.23: HOMO-LUMO gap as a function of chain length for O-cumu[n]

The trend for the gap for the system show a sawtooth trend as expected, with wires of the same parity following a monotonic decreasing function.
We observe values for this gap higher than other cumulenic structures, especially for shorter chains where it reaches the value of 6,64 eV for O-cumu[4] which is high compared to the other values of < 5 eV yielded by the other cumulenic wires and also to the BPh-Py[4] (≈ 4 eV) and Ph-Py[4] (≈ 4.5 eV).
This effect, related to the electronic contribution of the oxygen termination, is significantly reduced with chain length, in longer wires the HOMO-LUMO gap will be similar to the trend devised for the other cumulenic structures.

This is a relatively strange behaviour, we know that the bond length alternation is in general directly related to the value of the HOMO-LUMO gap, but for short wires also the termination can have a significant effect.
For longer chains in fact as expected also the O-cumu[n] will have values of the HOMO-LUMO gap lower than the polyynic wires.

O-cumu[n]									
Bond length values									
	N=4	N=5	N=6	N=7	N=8	N=9	N=10	N=11	N=12
Bond	Triplet	Singlet	Triplet	Singlet	Triplet	Singlet	Triplet	Singlet	Triplet
C1-C2	1,2786	1,2758	1,2780	1,2767	1,2777	1,2770	1,2776	1,2772	1,2776
C2-C3	1,2808	1,2692	1,2774	1,2703	1,2755	1,2709	1,2746	1,2712	1,2740
C3-C4	1,2786	1,2693	1,2736	1,2722	1,2731	1,2727	1,2730	1,2729	1,2730
C4-C5		1,2758	1,2775	1,2722	1,2775	1,2727	1,2767	1,2731	1,2761
C5-C6			1,2780	1,2703	1,2731	1,2727	1,2728	1,2730	1,2727
C6-C7				1,2767	1,2755	1,2727	1,2767	1,2730	1,2762
C7-C8					1,2777	1,2709	1,2730	1,2731	1,2727
C8-C9						1,2770	1,2746	1,2729	1,2761
C9-C10							1,2776	1,2712	1,2730
C10-C11								1,2772	1,2740
C11-C12									1,2776
Energy (Hartree)									
HOMO	-0,2506	-0,2768	-0,2410	-0,2602	-0,2351	-0,2497	-0,2310	-0,2424	-0,2280
LUMO	-0,0124	-0,1044	-0,0604	-0,1254	-0,0886	-0,1382	-0,1069	-0,1469	-0,1196
GAP	0,2382	0,1723	0,1806	0,1348	0,1466	0,1115	0,1241	0,0955	0,1083
Energy (eV)									
HOMO	-6,8178	-7,5313	-6,5590	-7,0799	-6,3982	-6,7944	-6,2861	-6,5958	-6,2034
LUMO	-0,3363	-2,8420	-1,6438	-3,4120	-2,4101	-3,7612	-2,9078	-3,9976	-3,2556
GAP	6,4815	4,6893	4,9152	3,6678	3,9881	3,0332	3,3783	2,5981	2,9478
Bond length alternation									
BLA(i)	0,0022	0,0066	0,0005	0,0064	0,0022	0,0061	0,0031	0,0060	0,0036
	0,0022	0,0001	0,0038	0,0019	0,0024	0,0018	0,0015	0,0017	0,0010
		0,0065	0,0039	0,0000	0,0044	0,0000	0,0037	0,0002	0,0031
			0,0005	0,0019	0,0044	0,0000	0,0039	0,0001	0,0033
				0,0064	0,0024	0,0000	0,00388	0,0000	0,0035
					0,0022	0,0018	0,0037	0,0001	0,0035
						0,0061	0,0015	0,0002	0,0033
							0,0030	0,0017	0,0031
								0,0060	0,0010
									0,0036
BLA	0,0022	0,0044	0,0022	0,0033	0,0030	0,0023	0,0030	0,0018	0,0029

Table 4.6: Computed bond length, BLA and HOMO-LUMO gap values for each of the O-cumu[n] chains with n=4,...,12

4.2.3 Analysis of Raman intensity parameters for O-cumu[n] chains

As we have seen in the S-cumu section the first derivative of the polarization with respect to each CC stretching give us information of whether the chain is cumulenic, with all $\frac{\partial \alpha}{\partial R}$ positive, or polyynic , with an alternation between a positive and a negative value).

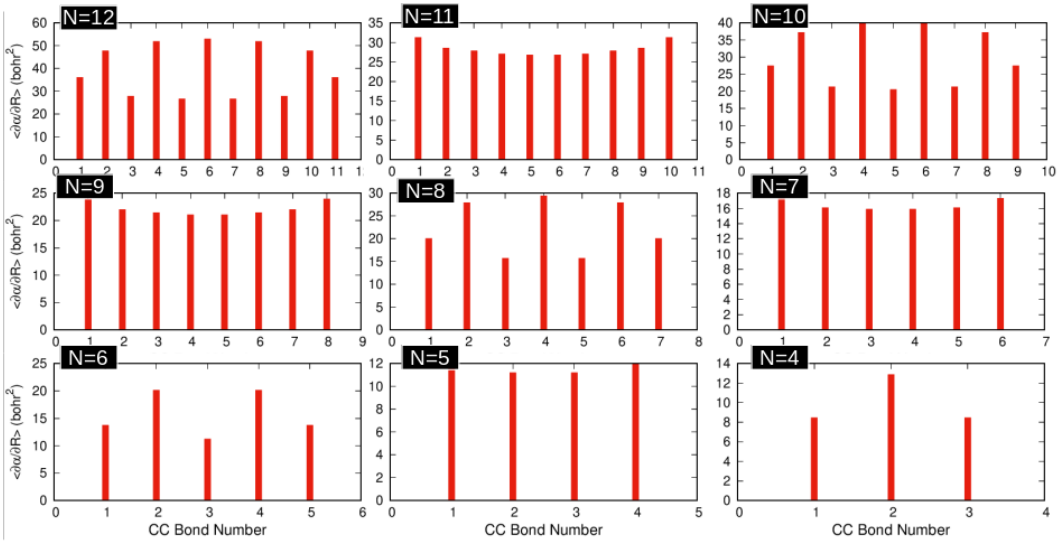

Figure 4.24: Variation of the polarizability with respect of the BLA oscillation, from top left (O-cumu[12]) to bottom right (O-cumu[4])

As we can see in figure (4.24) the $\frac{\partial \alpha}{\partial R}$ of both even and odd chains show a prevalent cumulenic character, with only a slight oscillation due to relatively low polyynic character on even chains, this effect with respect to the $\partial \alpha / \partial R$ of S-cumu is less evident, thus as we expect we will have the presence of a low intensity ECC mode.
From the calculated Raman spectrum observed in figure (4.25) we can draw the following observations:

1) *The red shift of all modes is evident, increasing the length of the chain also the overall frequency of the bands will decrease, the same effect was seen in S-cumu wires*

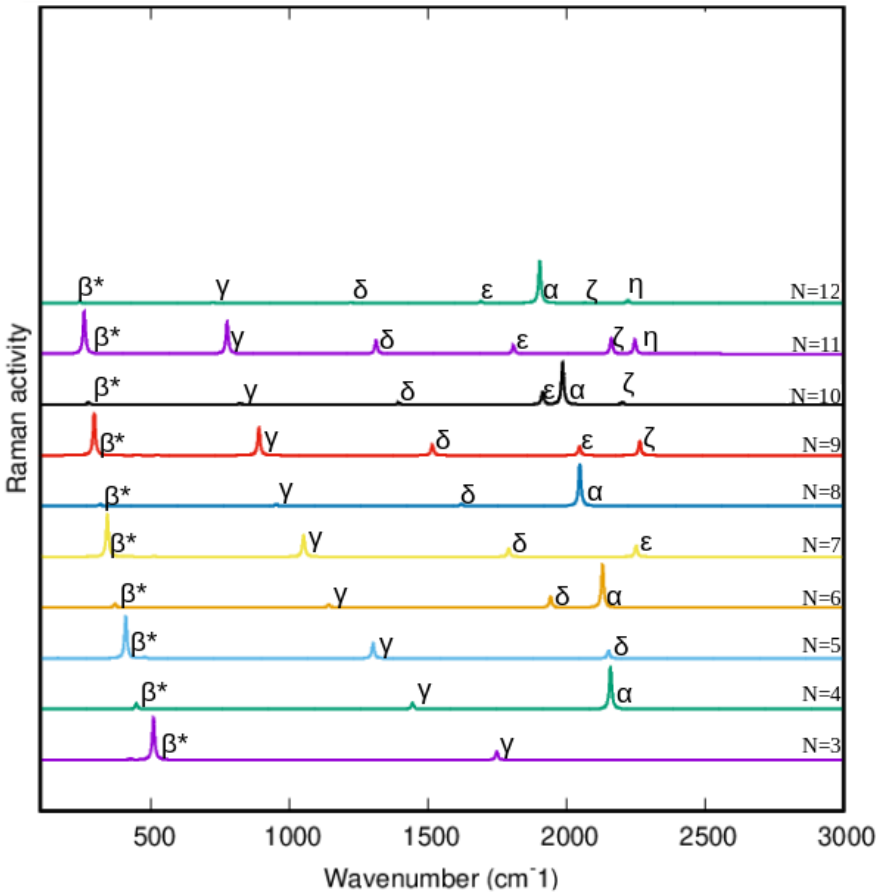

Figure 4.25: Normalized Raman spectrum for all type of O-cumu chains, the number on the top right refer to the number of carbon atom per chain

2) *Both the odd and even chains show lines of comparable intensities*
As we have seen, since the polyynic character for even chains is not relevant, we have the presence of low intensity α modes that reach a maximum of 3304 $[\mathring{A}^4/amu]$ for the O-cumu[12], whereas for S-cumu[12] was higher than 28000 $[\mathring{A}^4/amu]$.
For shorter chain the ECC mode becomes even less relevant showing less intensity with respect to other normal modes in the system (eg. the ϵ mode).

3) *All the Raman intensities for even chains are significantly higher than for the odd chain, and they also all follow a monotonic increase with the length of the chain*

Even chains

In table (4.7) are reported all the important data for the wavenumber and Raman activity for each significant normal mode for even chains and their assignation.

Even chains			
n° C atoms	Wavenumber $[cm^{-1}]$	Raman activity $[\AA^4/amu]$	Type
12	290	541	β^*
	869	450	γ
	1495	395	δ
	1890	289	ϵ
	2011	3304	α
	2188	80	ζ
	2348	1132	η
10	336	360	β^*
	1008	306	γ
	1643	256	δ
	2086	679	α
	2098	817	ϵ
	2351	779	ζ
8	400	227	β^*
	1203	192	γ
	1899	132	δ
	2159	364	α
	2343	626	ϵ
6	494	132	β^*
	1496	110	γ
	2347	439	α
4	648	67	β^*
	1899	41	γ
	2403	161	α

Table 4.7: Calculated data for the wavenumber and Raman activity of significant peaks for even-carbon chains O-cumu[2n]

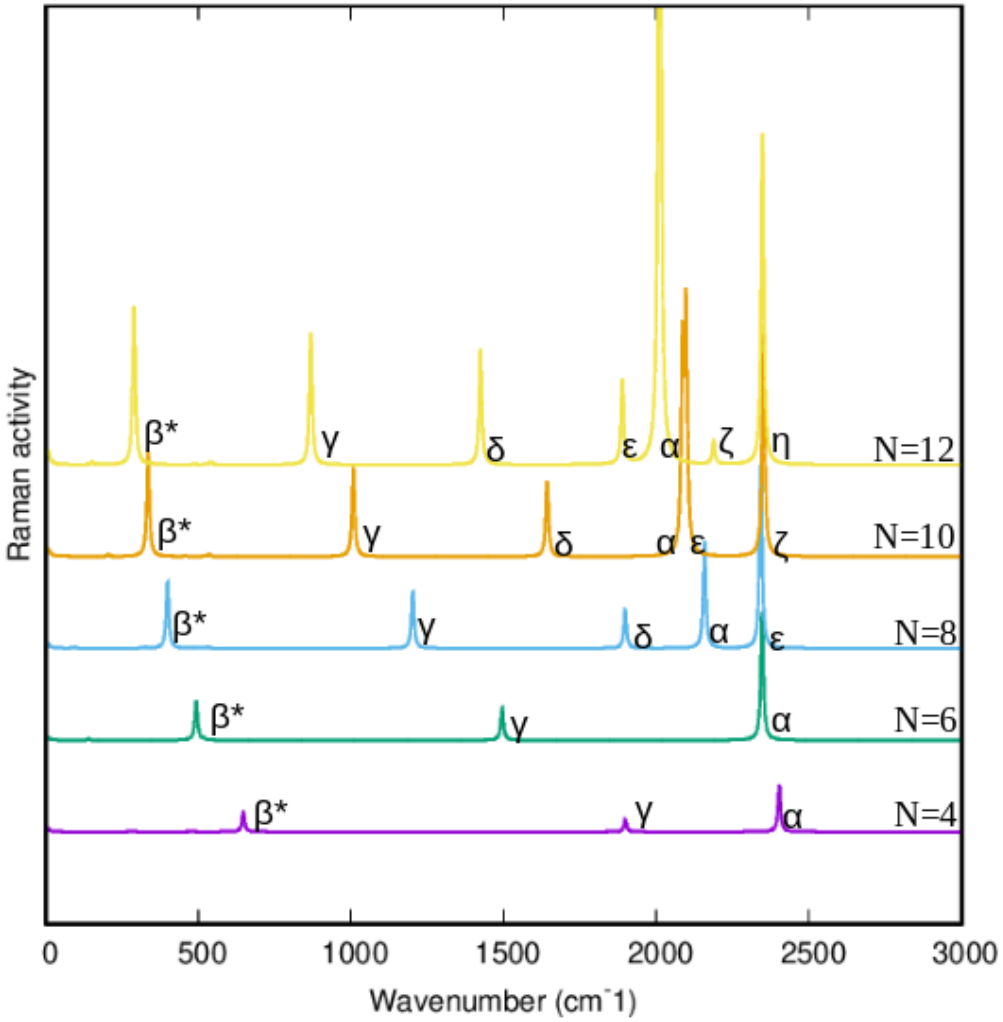

Figure 4.26: Calculated Raman spectra for O-cumu[2n]

As we can see from figure (4.26) the Raman spectrum for even chains show significant difference from the one depicted for S-cumu[n] wires in figure (4.7).
Several observation can be made: The δ peak is not present for $O - C_6 - O$, is negligible with respect to the other peaks and is maintained in the 2100 cm^{-1} - 2500 cm^{-1} range.
The ECC line is weak, especially for short chains, and becomes comparable to the other peak in the spectrum.
For O-cumu[10] the ϵ and the α peak have similar values for the Raman activity (817 and 679 $[\mathring{A}^4/amu]$ respectively), and almost the same wavenumber (2098 and 2086 cm^{-1}).

β^* mode The β^* trends are depicted below:

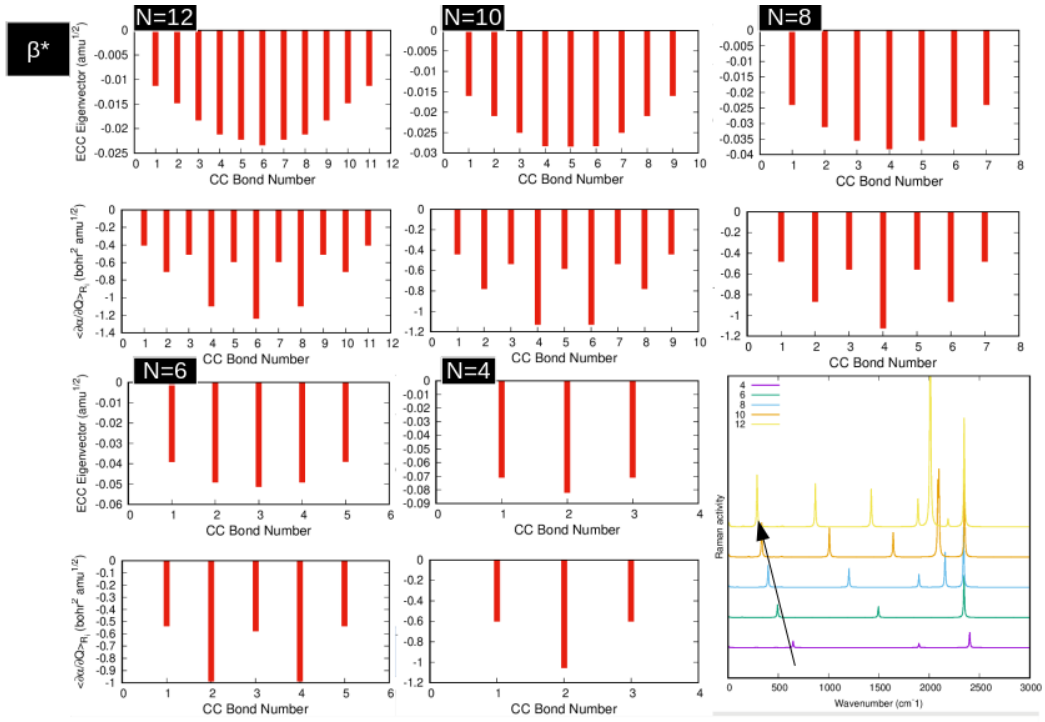

Figure 4.27: β^* mode (even chains)

As we can see in figure (4.27) the β^* mode is characterized by relatively low values of Raman activity ($< 600[\mathring{A}^4/amu]$), it is a longitudinal mode with 1 node, as we have seen in detail for S-cumu[n] wires.
The values of $\partial\alpha/\partial Q$ are all of the same sign, but each CC gives very little contribution to Raman activity, reaching the maximum of $\approx 1.2[bohr^2 \cdot amu^{1/2}]$, lower to the value of $\approx 2[bohr^2 \cdot amu^{1/2}]$ for S-cumu, thus this peak is expected to be less intense with respect to the β^* for S-terminated wires.
We note that the $\partial\alpha/\partial Q$ follows show a slight alternation determined by the $\partial\alpha/\partial R$ pattern, this is a consequence of the eigenvectors yielding almost constant values.
The β^* mode wavenumber is red shifting as expected with increasing chain length and yield values of 648-494-400-336-290 cm^{-1} for 4,6,8,10,12 carbon atom in chain.

γ mode The γ trends are depicted below:

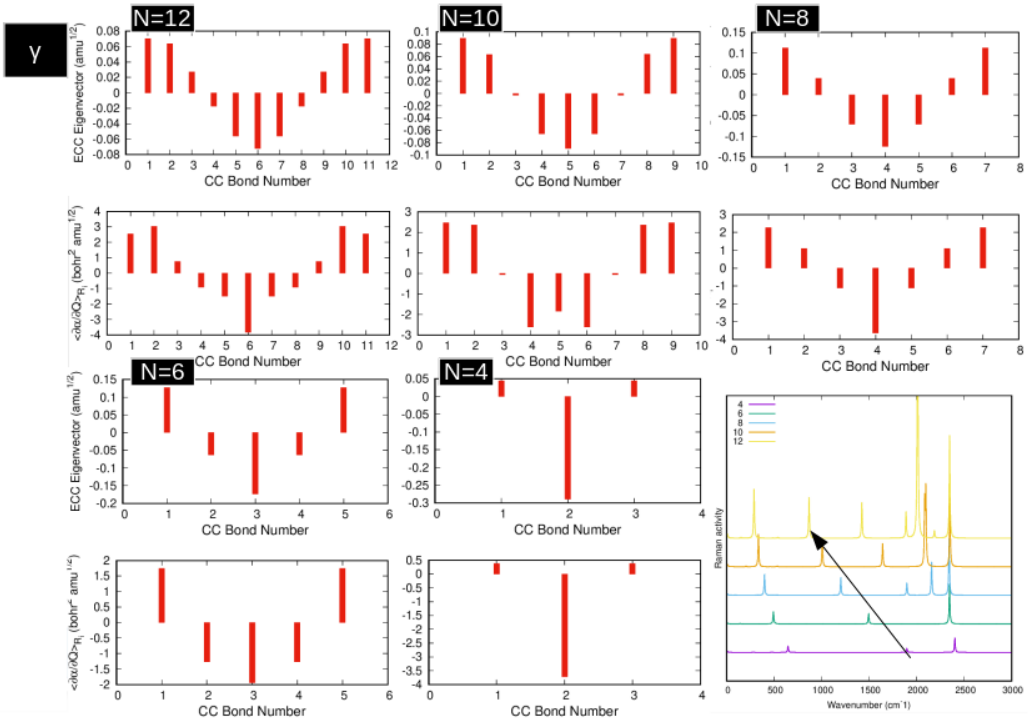

Figure 4.28: γ mode (even chains)

γ is a longitudinal mode with 3 nodes.
As we can see in figure (4.28) the values of $\partial\alpha/\partial Q$ are alternated, also each CC gives little contribution to Raman activity, reaching the maximum of $\approx 3[bohr^2 \cdot amu^{1/2}]$, this explain the very low values for Raman activity of these modes $< 500[\mathring{A}^4/amu]$.
The γ mode wavenumber is red shifting as expected with increasing chain length and yield values of 1899-1496-1203-1008-869 cm^{-1} for 4,6,8,10,12 carbon atom in chain.

δ mode The δ trends are depicted below:

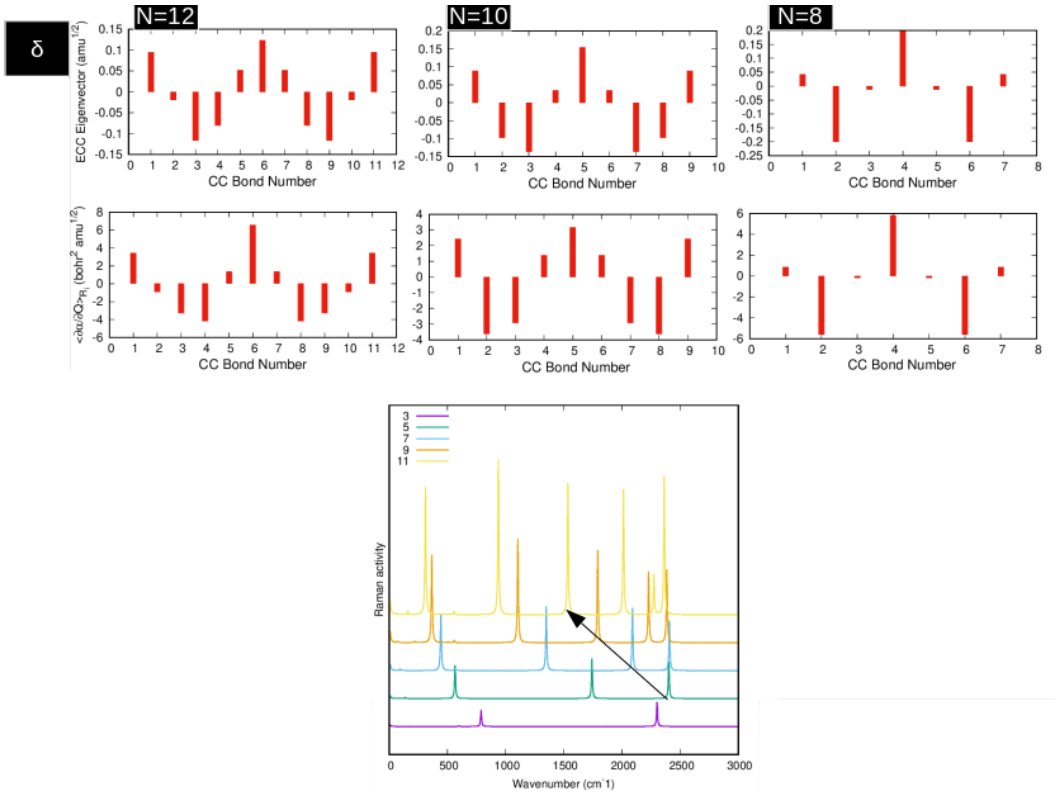

Figure 4.29: δ mode (even chains)

δ is a longitudinal mode with 5 nodes.
As we can see from figure (4.29) the values of $\partial\alpha/\partial Q$ are alternated and each CC gives little contribution to Raman activity, reaching the maximum of $\approx 6[bohr^2 \cdot amu^{1/2}]$, this explain the very low values for Raman activity of these modes $< 400[\mathring{A}^4/amu]$.
The δ mode for $O-C_6-O$ chains is not relevant and negligible with respect of the activity of the other peaks.
The δ mode wavenumber is red shifting as expected with increasing chain length and yield values of 1899-1643-1425 cm^{-1} for 8,10,12 carbon atom in chain.

α mode The α trends are depicted below:

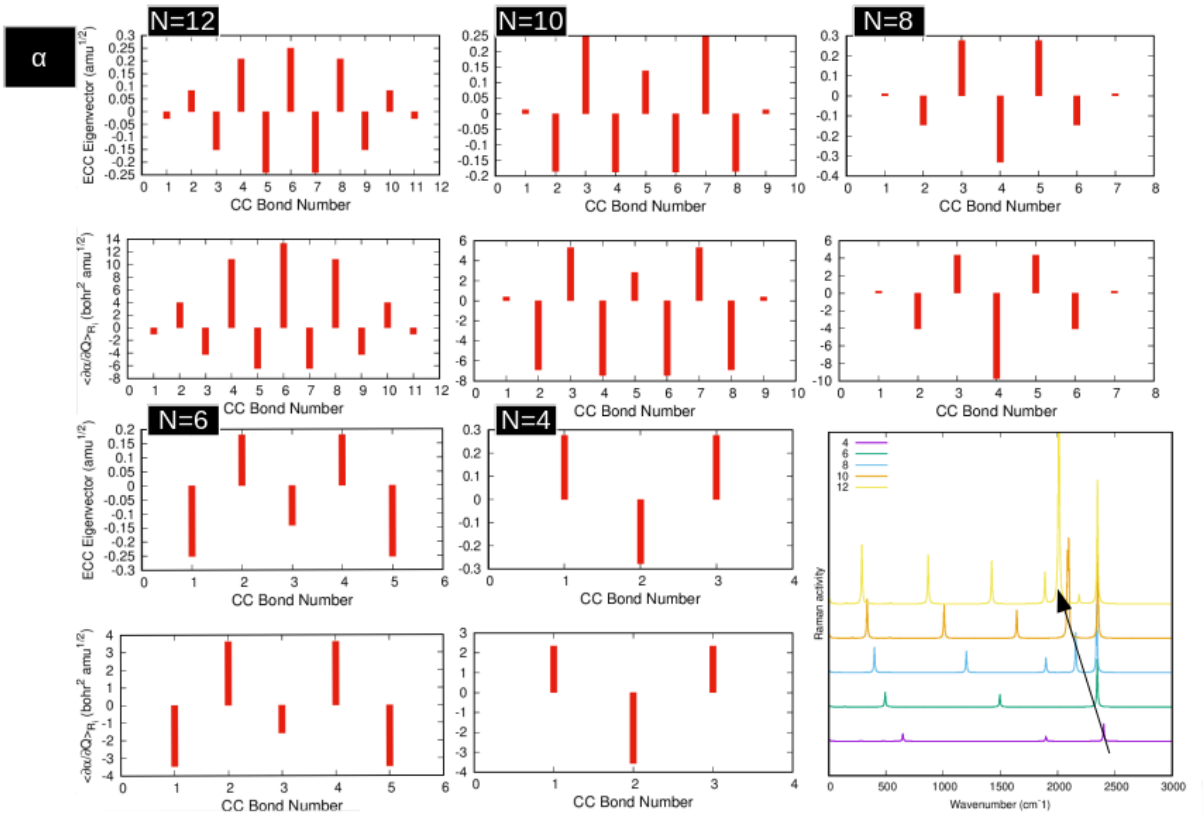

Figure 4.30: α mode (even chains)

The values of $\partial\alpha/\partial Q$ seen in figure (4.30) show an high degree of alternation. For O-cumu[12] we have that the $\partial\alpha/\partial Q$ for this mode can reach up to $\approx 12[bohr^2 \cdot amu^{1/2}]$, thus we expect a relatively high Raman activity for this mode.
The value of $\partial\alpha/\partial Q$ for the other even chains instead can reach only $\approx 6[bohr^2 \cdot amu^{1/2}]$, this low value and the high alternation can explain why this mode is not relevant and is even lower in intensity than the ϵ mode.
The α peak wavenumber is red shifting as expected with increasing chain length and yield values of 2403-2347-2159-2086-2011 cm^{-1} for 4,6,8,10,12 carbon atom in chain, we note that, similarly that in the case of S-cumu, the red shifting is limited compared to the trends for the other peaks and the wavenumber is maintained in the 2400-2000 cm^{-1} range.

ϵ mode The ϵ trends are depicted below:

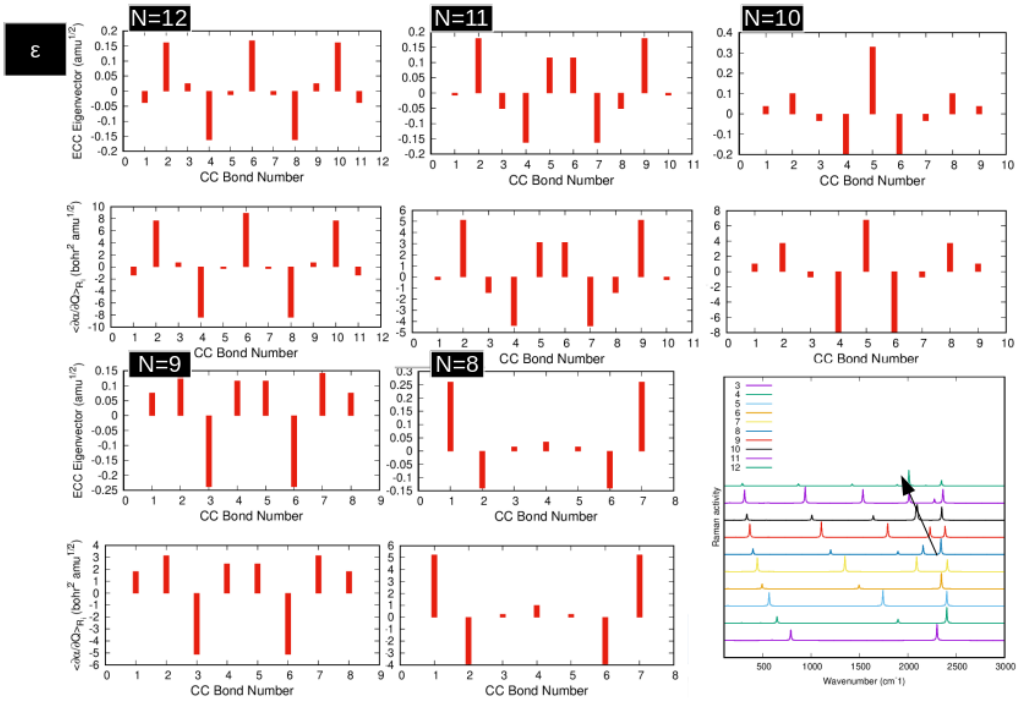

Figure 4.31: ϵ mode (even and odd chains)

ϵ is a longitudinal mode with 7 nodes.
As we can see in figure (4.31) the values of $\partial\alpha/\partial Q$ are alternated and each CC gives a contribution to Raman activity with a maximum of $\approx 10[bohr^2 \cdot amu^{1/2}]$.
This value is big enough to be compared to the one yielded by the ECC line, but the degree of alternation for the $O - C_{12} - O$ is very high, determining a very low value for the Raman activity ($289[\mathring{A}^4/amu]$)
In the shorter chain instead, the relatively high value of the $\partial\alpha/\partial Q$ of the singular CC stretching, combined to the fact that they show a lower degree of alternation, the ϵ will have value of 817 and 626 $[\mathring{A}^4/amu]$, comparable to the ECC line.
The ϵ mode wavenumber is red shifting as expected with increasing chain length and yield values of 2409-2343-2230-2098-2014-1890 cm^{-1} for $7 \cdots 12$ carbon atoms in chain.

Odd chains

In table (4.8) are reported all the important data for the wavenumber and Raman activity for each significant normal mode for odd chains and their assignation.

Odd chains

n° C atoms	Wavenumber $[cm^{-1}]$	Raman activity$[\mathring{A}^4/amu]$	Type
11	312	286	β^*
	939	348	γ
	1536	296	δ
	2014	283	ϵ
	2275	90	ζ
	2364	310	η
9	367	198	β^*
	1106	233	γ
	1793	209	δ
	2230	159	ϵ
	2386	165	ζ
7	445	127	β^*
	1350	144	γ
	2091	141	δ
	2409	111	ϵ
5	567	73	β^*
	1743	88	γ
	2403	83	δ
3	791	35	β^*
	2302	54	γ

Table 4.8: Calculated data for the wavenumber and Raman activity of significant peaks for odd-carbon chains O-cumu[2n+1]

In figure (4.32) we show the Raman spectra of odd chains:

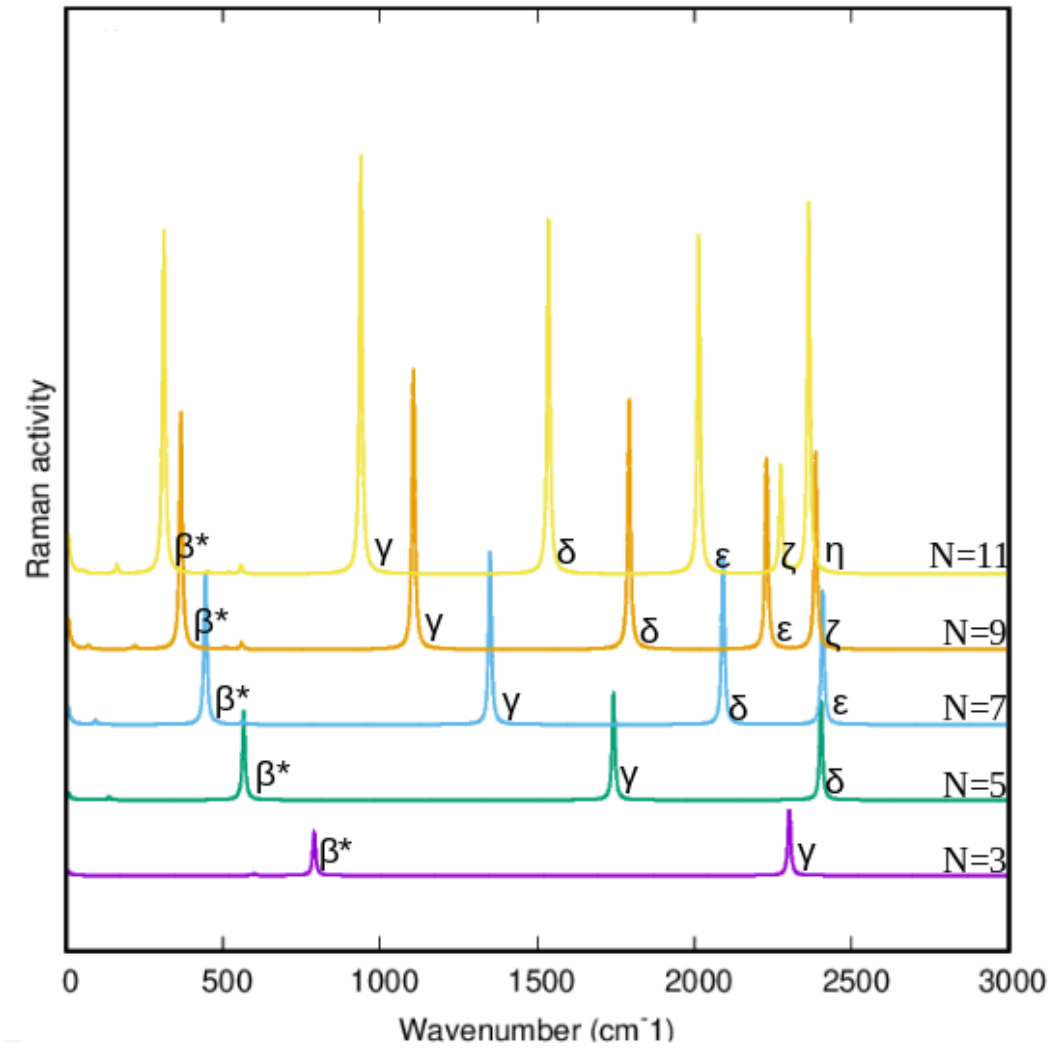

Figure 4.32: Raman spectra for odd chains

This pattern is significantly different from the one devised for even chains, in fact the quasi equalized $\frac{\partial \alpha}{\partial R}$ over the structure will give a more regular alternation of the $\frac{\partial \alpha}{\partial Q}$.
This increase on the regularity, along with the fact that the average values for the singular $\partial \alpha / \partial Q$ for each CC is much lower that in even chains explain the fact that the corresponding intensity of the peaks will be much lower. The value for the Raman intensity of each mode for a single wire yields similar values compared to each other mode, there is not a prevalant ECC line as in the case of odd S-cumu structures.

β^* mode The β^* trends are depicted below:

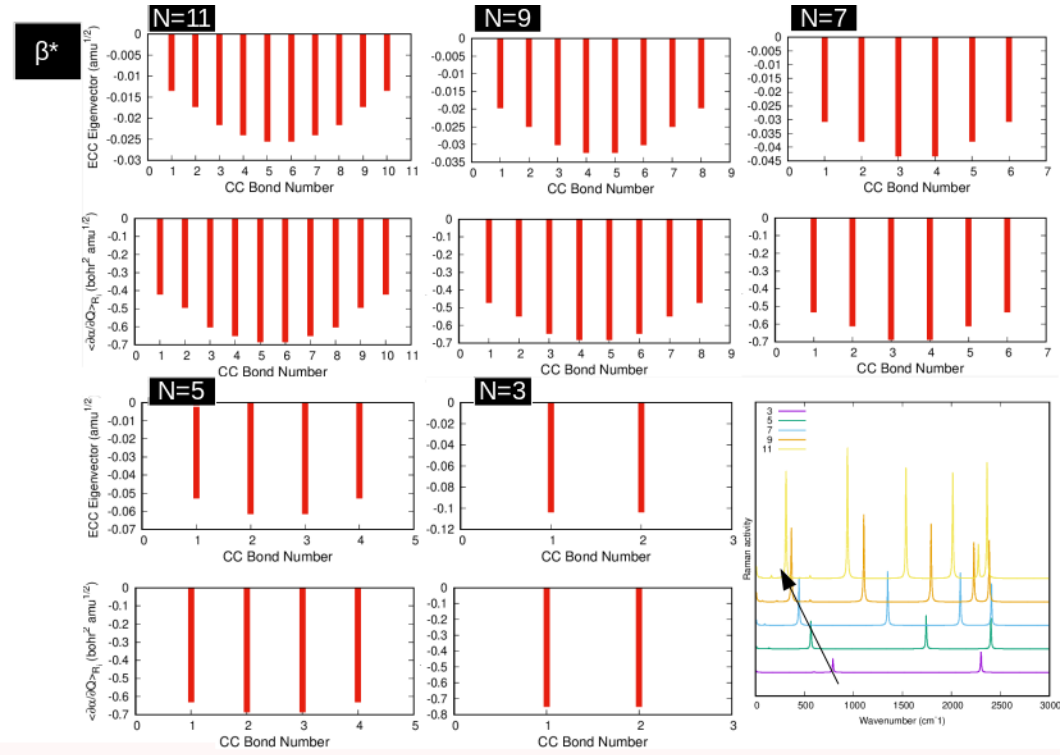

Figure 4.33: β^* mode (odd chains)

β^* is a longitudinal mode with 1 node.
The $\partial\alpha/\partial Q$ as seen in figure (4.33) are oriented towards negative values and reach up to $\approx 0.7[bohr^2 \cdot amu^{1/2}]$, which is a very low value, similar to what we found for S-cumu.
The β^* mode wavenumber is red shifting as expected with increasing chain length and yield values of 791-567-445-367-312 cm^{-1} for 3,5,7,9,11 carbon atom in chain.

γ mode The γ trends are depicted below:

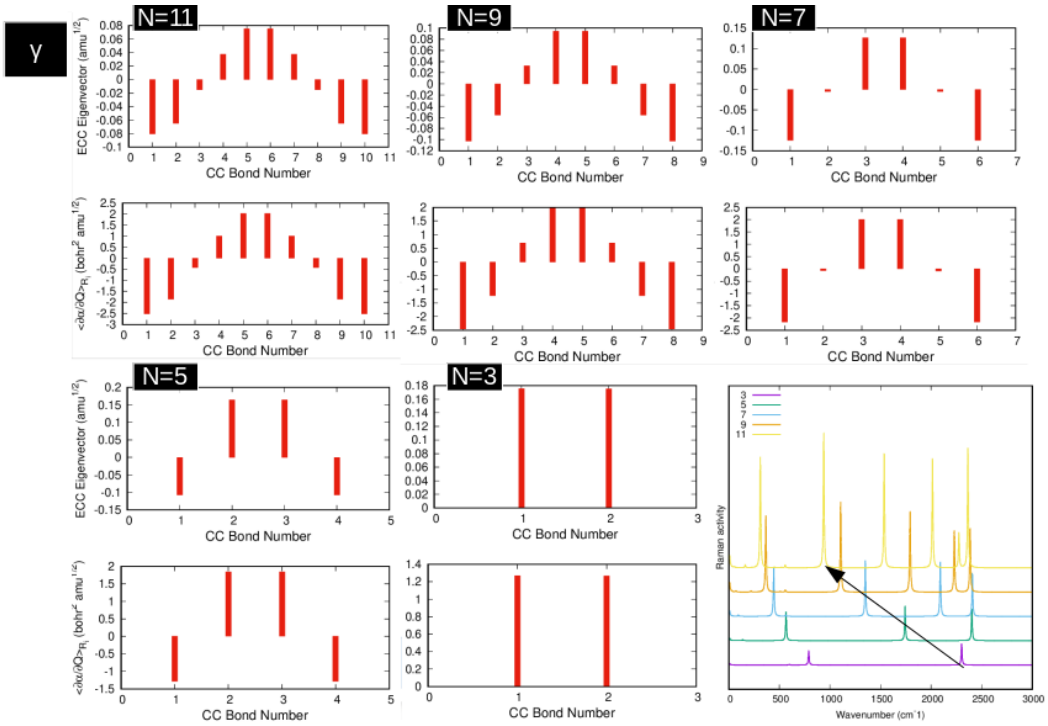

Figure 4.34: γ mode (odd chains)

γ is a longitudinal mode with 3 nodes.
As reported in figure (4.34) the $\partial\alpha/\partial Q$ reach up to $\approx 2[bohr^2 \cdot amu^{1/2}]$, thus we have low intensity for these modes.
The γ mode wavenumber is red shifting as expected with increasing chain length and yield values of 2302-1743-1350-1106-939 cm^{-1} for 3,5,7,9,11 carbon atom in chain.

δ mode The δ trends are depicted below:

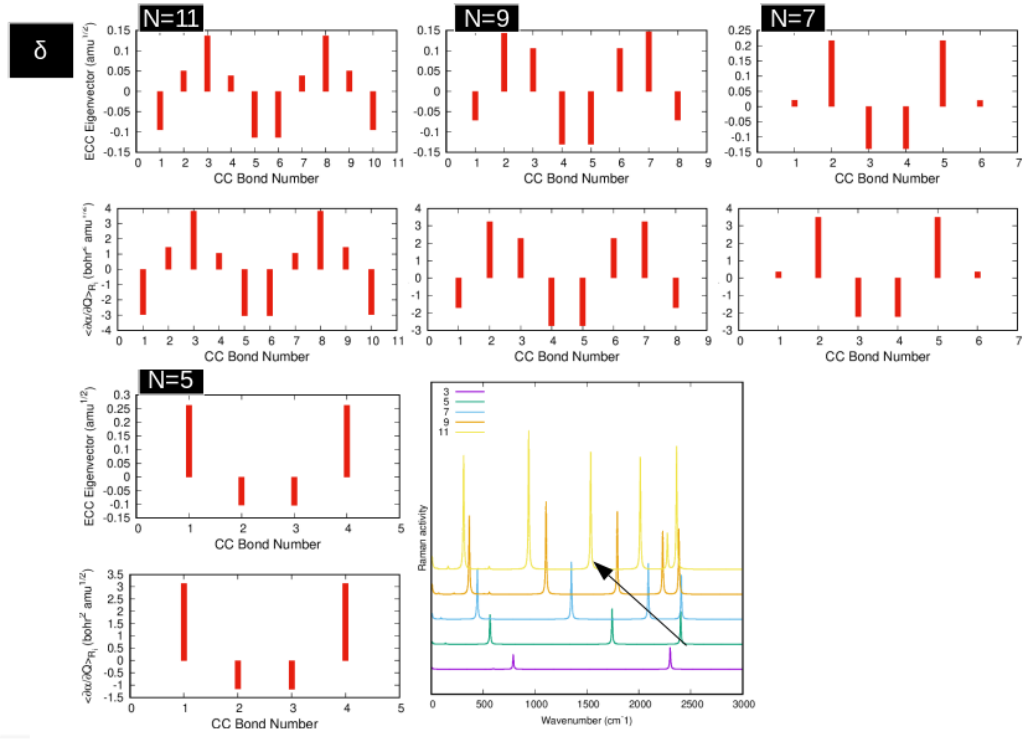

Figure 4.35: δ mode (odd chains)

δ is a longitudinal mode with 5 nodes.
From figure (4.35) we see that the $\partial\alpha/\partial Q$ reach up to $\approx 3[bohr^2 \cdot amu^{1/2}]$ for small chains, but with higher alternation with respect to γ, thus they show slightly less intensity in general with respect to these modes.
The δ mode wavenumber is red shifting as expected with increasing chain length and yield values of 2403-2091-1793-1536 cm^{-1} for 5,7,9,11 carbon atom in chain.

4.3 Discussion on structural and electronic properties of different CAWs

In this section we will carry out a comparison between all structural and electronic properties of different CAWs (eg. the one depicted in figure (4.36)) focusing on their polyynic or cumulenic behaviour both for the bond length alternation and energy gap and giving an interpretation of the Raman spectra.
The numerical values (bond length, BLA and gap) for each molecule (using PBE0/cc-pVTZ calculations) can be found on the appendix.
The comparison will be made for carbon wires with 4 to 12 sp carbon atoms.
The data found in our calculation will be compared to the work done by Milani et al [8] and we will give an interpretation on the trends obtained .
The Raman comparison will be focused on the variation in wavelength of the ECC line, on the intensity of the relative peaks between cumulenes and polyynes to determine if this type of structure can be determined by means of Raman spectroscopy, and also give an indication on the terminal modes.

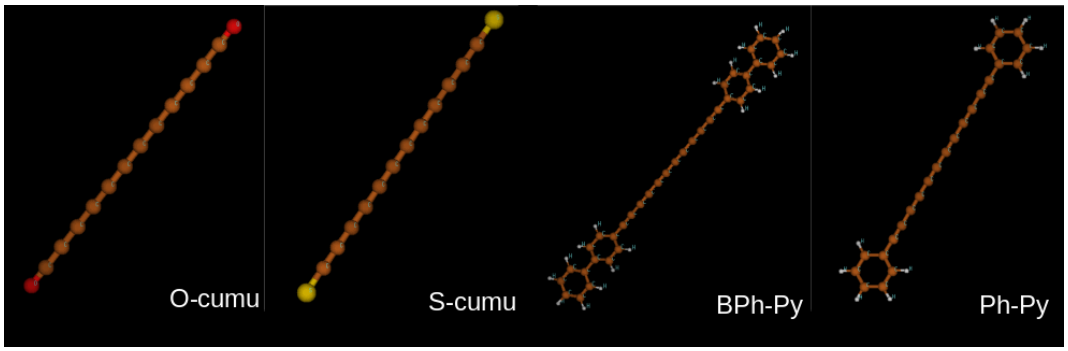

Figure 4.36: Some of the structures compared

4.3.1 Correlation between structural, electronic and vibrational properties

As we said in the introduction the interesting properties of polyconjugated systems such as carbon atom wires is the high degree of electron phonon coupling, the ECC line wavenumber is in fact directly related to the bond length alternation and also to the energy gap.
As we can see from the following figures we have two different behaviours for the cumulenes and polyynic CAWs and the electronic (gap), structural (bla) and spectroscopic (ECC line) will be directly dependent one to another.

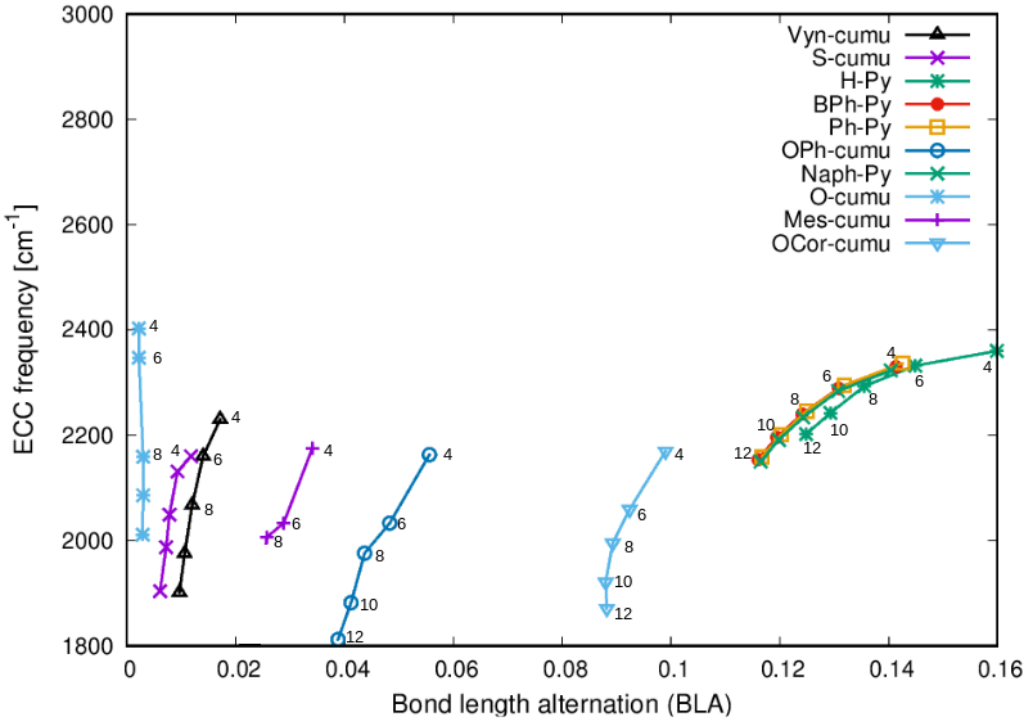

Figure 4.37: ECC mode wavenumber dependence on the bond length alternation, the labels for each point are relative to the number of carbon atoms in chain

For figure (4.37) and (4.38) we took into account values found in our calculations (for O-cumu[n], S-cumu[n], H-Py[n], BPh-Py[n] and Ph-Py[n]) but also computed results found in the literature, in particular OPh[n],Naph[n], OCor[n] and Mes[n] are structures for which the BLA, gap and Raman spectra was calculated in detail using the same set of PBE0/cc-pVTZ functionals

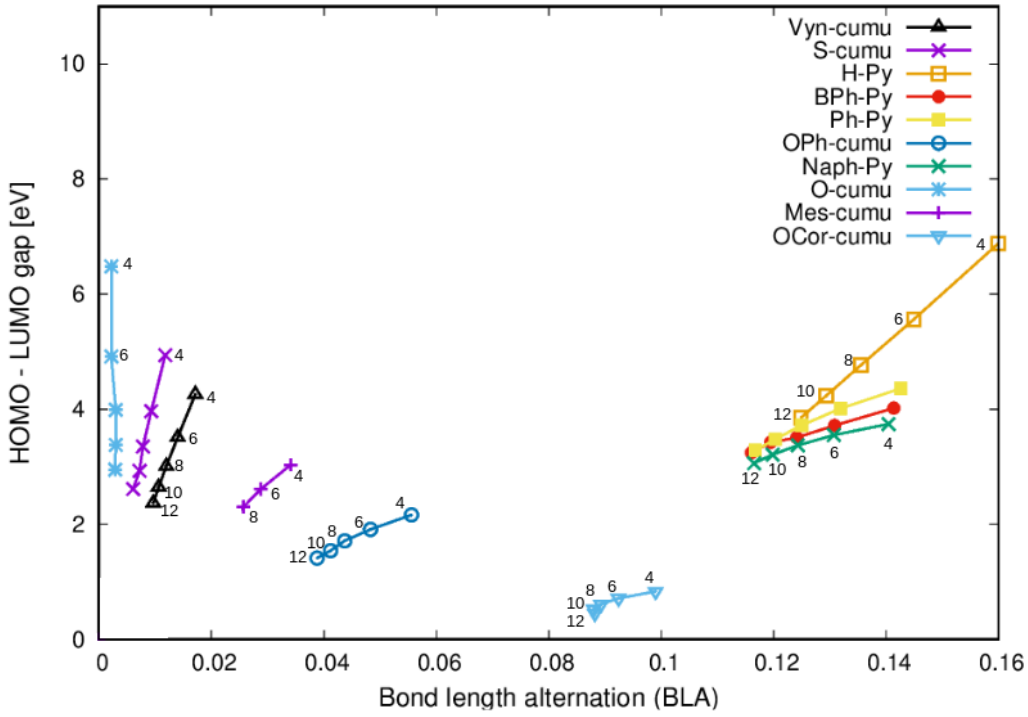

Figure 4.38: HOMO-LUMO gap dependence on the bond length alternation, the labels for each point are relative to the number of carbon atoms in chain

by Milani et al. [8].
OCor[n] and Mes[n] are actual cumulenes that have been synthetized. In figure (4.37) we can see that the ECC frequency is always showed in a selected range (from 1800 cm^{-1} to 2400 cm^{-1}) and is decreasing as expected with chain length for all the structures analized.
The BLA, and HOMO-LUMO gap as seen in figure (4.38) are also decreasing with chain length due to the higher conjugation yielded by longer wires.
We can see also that most of the cumulenes (S-cumu[n], O-cumu[n],Vyn-cumu[n]) are localized on low BLA ranges (< 0.02), whereas polyynes are located at high BLA ranges (> 0.12).
The other 3 structures analyzed (Mes-cumu[n], OPh-cumu[n], OCor-cumu[n]) are localized on intermediate BLA ranges ($0.02 - 0.12$), with relatively high alternation of the 'single-triple' even if they are classified as cumulenes.
Because of these 'intermediate structures' we cannot completely classify CAWs into cumulenes or polyynes just considering the values of the BLA or the HOMO-LUMO gap alone.
Instead the classification should be based on the different relation between

structural and electronic properties for these systems.
One of the most interesting thing we can see from this graph is that for cumulenes with the same number of carbon atoms in chain, with higher BLA that the structure present, we will have lower HOMO-LUMO gap.
This trend is inverted for polyynes that with higher BLA will have an increase on the HOMO-LUMO gap.
This trends allow us to distinguish two different regions of cumulenic and polyynic, and in related to the different shape of the $\partial\alpha/\partial R$ of the internal coordinates for the two systems.

4.3.2 Bond-length alternation (BLA)

In figure (4.39) we analize the values of the bond length alternation for all the cumulenic and polyynic species studied.

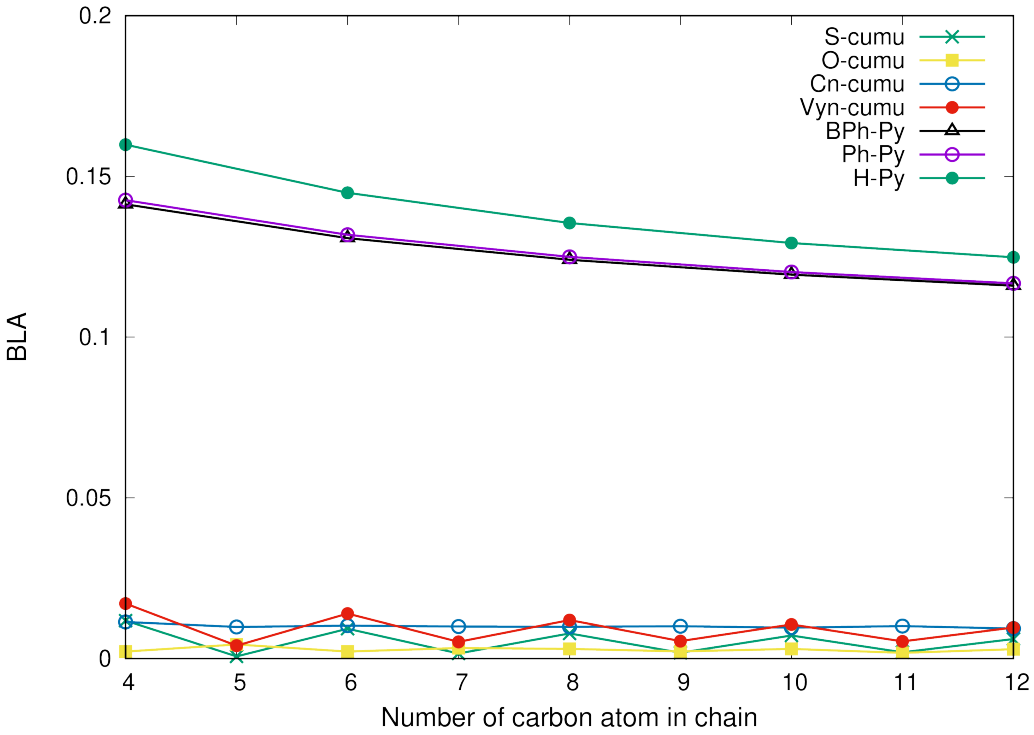

Figure 4.39: Values for the bond length alternation of bis(diphenyl), diphenyl and hydrogen polyynes compared to the BLA of sulfur, carbon , vinylidene and oxygen cumulenes

Two different trends are found for polyyne and cumulenes, we don't observe in the wires studied for the thesis any intermediate structure localized at BLA range $(0.02 - 0.12)$.
The polyynes, as we expect, have higher values for the BLA monotonically decreasing with chain length.
For cumulenes instead, we have low BLA that present an oscillation, especially showed by Vyn-cumu[n] and S-cumu[n] wires, and, as we can see from (4.40) we have an almost constant BLA for O-cumu[n] ($\approx 0,003$) and Cn-cumu[n] ($\approx 0,01$) cumulenes, indicating that O-cumu[n] is the structure with less bond length alternation(in general)
Only for S-cumu[2n] and Vyn-cumu[2n] (even wires) we have an appreciable

decrease on the BLA with chain length.
Even if cumulenic, we have seen in the previous discussion that S-cumu[n] show similar trends with respect to Vyn-cumu[n] wires, with a slightly induced 'quasi triple-quasi single' character, for *even* chains which is showed both on the trend on the BLA (monotonically decreasing and slightly higher) and on the oscillating $\partial\alpha/\partial R$, this trend is not present in odd chains, with almost constant values for the $\partial\alpha/\partial R$ and a prevalent cumulenic character.
It should be noted that the calculated BLA for vinylidene and carbon terminated cumulenes show lower values with respect to other works [9], that is because for the calculation of the BLA I didn't include the carbon atom present on the terminals. For example the C_{12} chain (showed in Innocenti work) will have 2 terminal carbon atoms, in fact it is a $C-C_{10}-C$ chain, that in our discussion will be called C_{10} cumulene, the vinylidene with (12) carbon atoms in chain in our discussion will be a $CH_2-C_{12}-CH_2$), with the carbon atom directly linked in the end group not counted as 'carbon atom in chain', this was used to provide a better relation between the different type of CAWs.

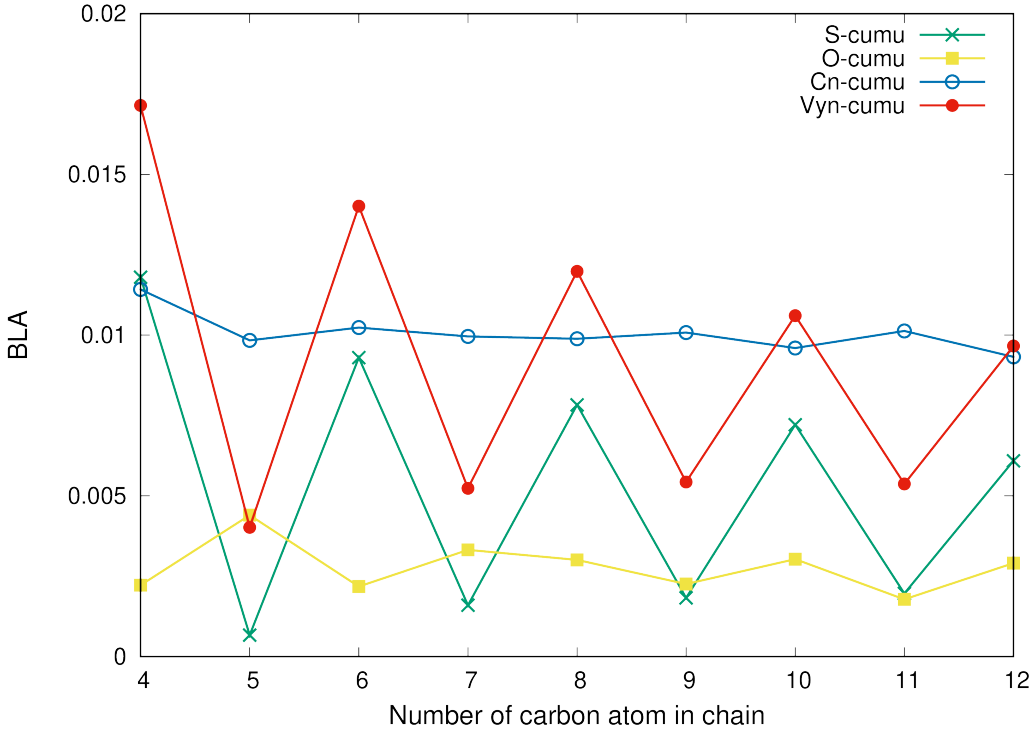

Figure 4.40: BLA behaviour for cumulenes

4.3.3 Energy gap and conjugation

The energy gap of these systems is strictly related to their conjugation, increasing the chain length we will have more π-delocalized electrons (2 for each additional carbon atom) and thus more frontier orbitals that generates a lower energy gap. The general trends can be depicted on figure (4.41):

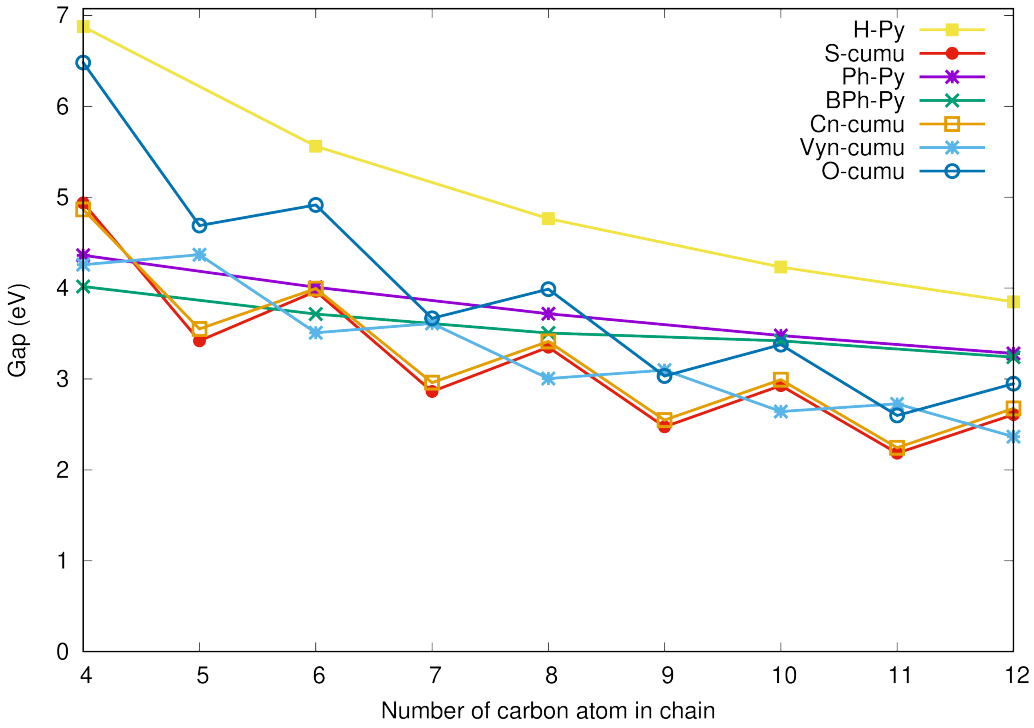

Figure 4.41: Values of the gap for different carbon atom wires

As we can see from figure (4.41) we have an overall decrease of the HOMO-LUMO gap with chain length for all wires with a significant alternation on cumulenes, the alternation on polyynes isn't showed because we didn't analize the situation for odd wires. We observe that for longer chains the gap will be generally lower in cumulenes than in polyynes, for short wires instead the highly conjugated phenyl groups generated a lower HOMO-LUMO gap for BPh-Py[n] and Ph-Py[n] with respect to some cumulenes. In fact BPh-Py[4] and Ph-Py[4] values of the gap is lower than O-cumu[4], S-cumu[4] and Cn-cumu[4] and BPh-Py[6] gap is lower than Cn-cumu[6], S-cumu[6] and O-cumu[6].
The hydrogen atom at the end of the chain doesn't participate to the delocalized π molecular orbitals since it has only an s atomic orbital and will

create a localized σ orbital with the adjacent carbon.

4.3.4 Identification of Raman activity between cumulenes and H terminated chains

In figure (4.42) the Raman activity for the cumulenes taken into consideration and the polyyne are compared, including also the analysis on the $\partial\alpha/\partial Q$ of the singular longitudinal CC stretching.

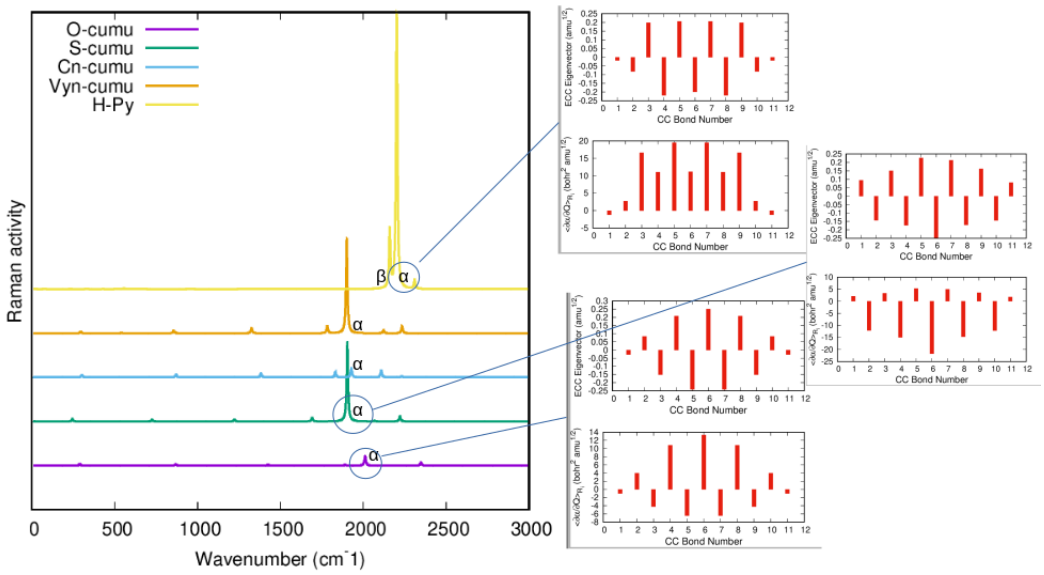

Figure 4.42: Computed values of Raman activity of several different wires: S, O, C, vynilidene terminated cumulenes and H terminated polyynes with 12 carbon atoms in chain

We know that one of the most important features to take into account by a Raman spectroscopist is the identifiability of these type of chains.
As we know in the past cumulenes wires weren't supposed to have any ECC line or a significant Raman signal, for a theoretical infinite carbyne chain we will have in fact a singular atom per unit cell, therefore generating the impossibility to have any longitudinal phonon and any alternation of a quasi single - quasi triple bond.
Instead, some cumulenic CAWs can be identified through Raman and can present a relatively relevant alternation of 'quasi single - quasi triple' CC bonds showing an ECC line, which can even be compared to the intensity of

the ECC for some polyynic wires.
In fact as we can see from figure (4.42) we have that the α peak of sulfur and vinylidene cumulenes yields a non negligible intensity with respect to the α peak of H-Py and they are also higher than its β peak.
Thus we expect that even S-cumu and Vyn-cumu chains can be identified through Raman spectroscopy, for odd S-cumu and Vyn-cumu wires that is not the case as we analyzed in detail for sulfur cumulenes in the previous section.
Taking into account the pattern of the $\partial\alpha/\partial Q$ we can easily explain why. The eigen-vectors of the α peak show a perfect alternation, the $\partial\alpha/\partial R$ are switching between low and high values, so we have, as we have seen in detail for the α peak of sulfur, that the $\partial\alpha/\partial Q$ of singular CC stretching are shifted to negative values as we can see in figure (4.42).
This determines that the $|\partial\alpha/\partial Q|$ for the overall molecule, strictly related to the intensity, will be relatively high .
For hydrogen polyynes we see that the α peak is more intense since we have almost all the $\partial\alpha/\partial Q$ with positive values that reach also $\approx 20[bohr^2 \cdot amu^{1/2}]$.
A similar alternation for the eigen-vectors (of the ECC line) is found for Cn-cumu and O-cumu, this structures also present a quasi constant value for the $\partial\alpha/\partial R_i$.
This reflects on the alternation also on the singular $\partial\alpha/\partial Q_i$ leading to an overall $\partial\alpha/\partial Q$ only slightly shifted towards positive values for the overall molecule, this will cause this wires to yield a very low Raman intensity for the ECC line that can be even compared to the peak intensity of the other longitudinal modes.
For this reason the Cn-cumu and O-cumu both in odd and even chains will be very difficult to detect through Raman spectroscopy won't present any relevant lines, especially for short wires.
In figure (4.43) we can clearly see the difference for the polyynes, which present only relevant α and β peaks (and other additional terminal modes) to the cumulenes, that generally present a lot of similar peaks (intensity wise).
We see also that for bis(diphenyl) and phenyl polyyne we have the presence of phenyl modes around 1600 cm^1 [8], for vinylidene cumulenes we have the presence of CH_2 scissoring near 3100 cm^{-1} and also CH_2 bending at around 1400 cm^{-1} [9],these mode is relevant even with respect to the main ECC line.

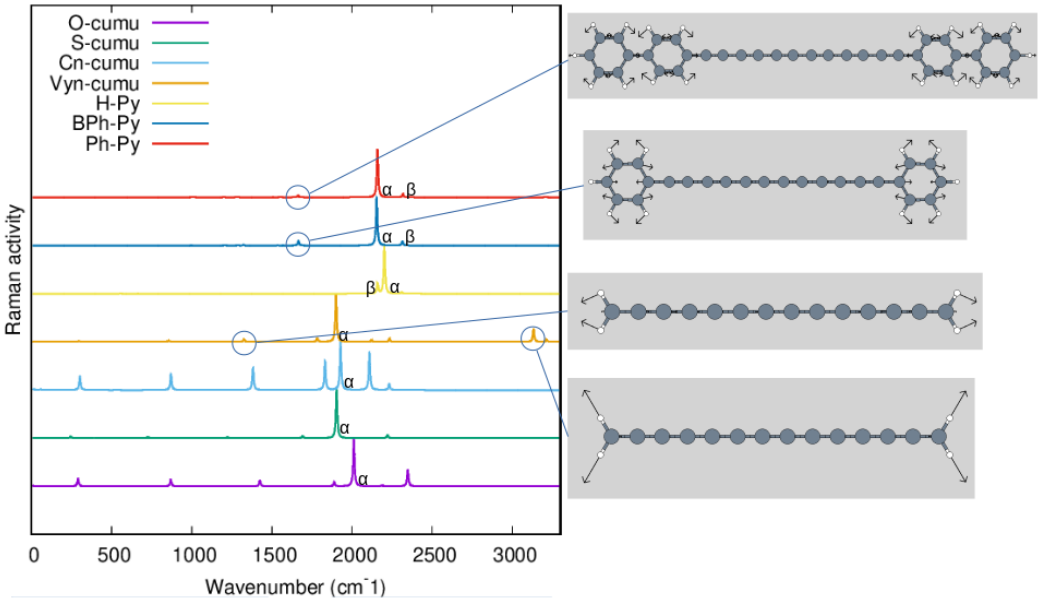

Figure 4.43: Calculated Raman spectra (normalized) of most relevant modes for each cumulene and polyynes

4.3.5 Identification of Raman activity between polyyinic chains (Ph, BPh and H)

In figure (4.44) we can see a comparison between the calculated Raman spectra for all the different polyynes studied in detail, in particular BPh-Py[n] (bis(diphenyl) polyyne), Ph-Py[n] (diphenyl polyyne) and H-Py[n].
As we can clearly see the BPh and Ph polyynes show an ECC line red shifted with respect with that of H-Py, this indicates an higher conjugation and therefore a lower energy gap as already found in (4.41).
We can see clearly the Raman activity yielded by the longitudinal modes is higher for phenyl conjugated structures 1274866$[\AA^4/amu]$ for BPh-Py[n] and 700671$[\AA^4/amu]$ for Ph-Py[n]) with respect of H-Py[n] are much more intense, this can be explained simply by looking at the value of the singular $\partial\alpha/\partial Q$, for diphenyl and bis(diphenyl) structures they are more shifted to positive values and yield values up to 60$[bohr^2 \cdot amu^{1/2}]$ for BPh-Py[n] and 45$[bohr^2 \cdot amu^{1/2}]$ for Ph-Py[n], whereas for hydrogen they are more limited ($< 20[bohr^2 \cdot amu^{1/2}]$) and especially the end chain CC contribution is close to 0 as we can see from figure (4.44).
Another consideration is the apparent superposition between BPh-Py and Ph-Py modes, where all the modes are in similar position, the phenyl mode as expected is almost in the same wavenumber (1666 cm^{-1} and 1663 cm^{-1}

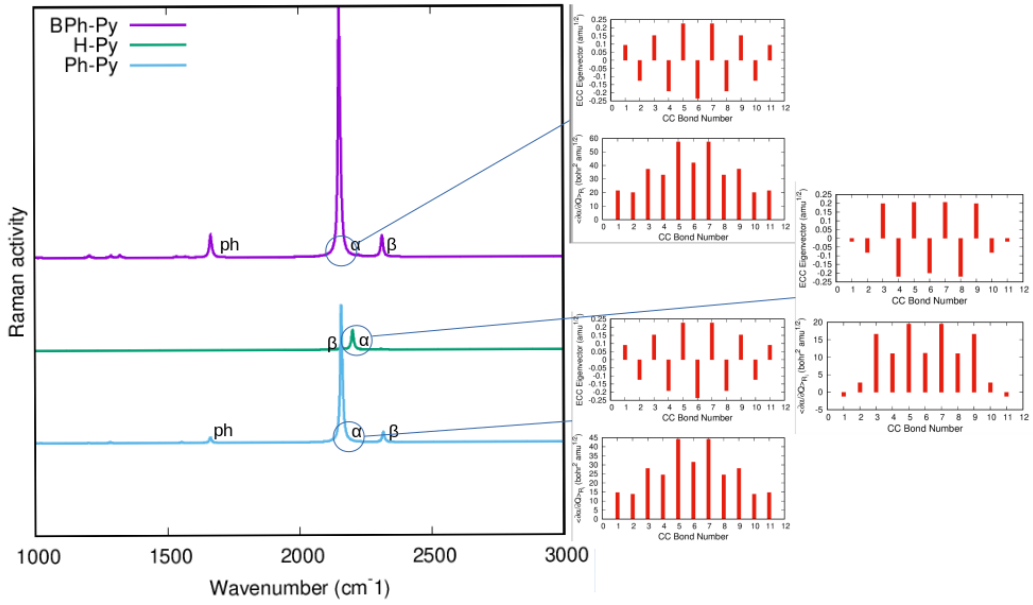

Figure 4.44: Calculated Raman spectra for the three polyyne molecules studied for 12 internal carbon atom in the wire

respectively), the α (2154 cm^{-1} and 2159 cm^{-1}) and the β (2315 cm^{-1} and 2318 cm^{-1}) are only slightly shifted, the presence of the phenyl mode is very clear and can be an indication of the presence of this family of compounds.

4.4 Final considerations of the overall structural and electronic values determined

By analyzing the different results we can group CAWs in three different categories.
This statement can be confusing, CAWs are divided in cumulenes and polyynes and are classified usually just by considering the BLA of the infinite carbyne. This definition based on BLA is misleading for small CAWs and we clarified in this chapter that their behaviour can't be classified based only on BLA or HOMO-LUMO ranges alone and this cannot determine a polyyne or cumulenic behaviour.
A better definition for the different types of CAWs can be defined by the shape of the $\partial\alpha/\partial R$ and on the overall relation between structural and electronic properties for a specific wire as can be seen in figure (4.38), this will lead us to the classification of 3 different structures (and not 2 as expected).

A *The cumulenic chains characterized by an almost constant* $\partial\alpha/\partial R$ such as O-cumu, C-cumu and S/Vyn-cumu odd chains.

These chains are also characterized by almost constant values for the BLA increasing the length of the chain: $\approx 0,003$ for O-cumu, $\approx 0,01$ for C-cumu, $\approx 0,002$ for S-cumu *odd* chains and $\approx 0,005$ for Vyn-cumu odd chains.
This more cumulenic character is also reflected in the energy gap, in fact for S-cumu odd chains the value for the energy gap is lower with respect to the S-cumu even chain gap, the trend is inverted by Vyn-cumu for the different position of its π orbitals.
This trend is also reflected in the Raman spectra where this structures don't have an effective ECC line and present a series of similar low intensity peaks, thus the identification of these chains Raman spectroscopy can be difficult.

B *The cumulenic chains characterized by an oscillating* $\partial\alpha/\partial R$ such as in S/Vyn-cumu even chains.

The trend for the BLA of these type of chains follow a monotonically decreasing behaviour, as for the polyynic (BPh-Py, Ph-Py and H-Py), with higher chain length the overall effect of the end groups of inducing an alternation of triple and single bonds will be lower, this effect is not

significant as in the case of the polyynes but can't be neglected.
The gap for these type of structures should be higher with respect to the odd chain counterpart, the quasi double bond of course yields an higher delocalization of π electrons.
The energy gap is monotonically decreasing with chain length due to the higher conjugation.
We have also an effect on the Raman spectrum, in fact we don't have peaks of similar intensity as for chains with total cumulenic character, but we have the presence of a non-negligible ECC line that can be compared in intensity of the one for H-Py.
These is an indication of the possibility of identify these structures through Raman spectroscopy.

C *The polyynic chains* characterized by an alternating positive and negative $\partial\alpha/\partial Q$ singular CC value.

The trend for both the energy gap and the BLA follow a monotonically decreasing behaviour as in the case of cumulenic chains with slight polyynic character.
The value of the Raman activity for the peaks show high values for the α and β lines, the singular $\partial\alpha/\partial Q$ yield the same sign since both the eigen vector and $\partial\alpha/\partial R$ are alternating between a positive and negative sign; this will generate an high value for the overall $\partial\alpha/\partial Q$ for the molecule.

Chapter 5

Prediction of the vibronic spectra for H-Py[n] and Ph-Py[n]

In this chapter the analysis of the computed vibronic spectra will be carried out both for hydrogen and diphenyl polyynes, these wires have been chosen for the presence of available experimental data.
Our objective will be to make a comparison of these data with our results.
The experimental data are partially made in our laboratory [6] (Ph-Py[2] to Ph-Py[10], H-Py[6] to H-Py[16]) and based on the work of Tabata [5] (H-Py[16] to H-Py[8]).

5.1 Methodology and calculation details

As a first step the ground state geometry determined by DFT calculations was used to compute the excited states and $g \rightarrow e$ transitions parameters.
From these data we were able to build up the Lorentian fitting for the UV-visible spectra.
The Lorentian fitting was constructed just by taking the values of the calculated wavelength, energy and oscillator strength for each dipole-allowed transition and considering the intensity of each peak as:

$$I_{ge} \propto |\mu_{ge}|^2 \propto f/E_{ge} \tag{5.1}$$

Since this simple Lorentian fitted spectrum was not enough to have a good comparison with experimental data we proceeded by optimizing each excited state that yielded a non-negligible oscillator strength for a dipole allowed transition from the ground state (f > 0.2).
After the determination of the optimized values for wavelength, energy of excited state, oscillator strength and electronic transition dipole moment, the Franck-Condon factors based on the UVFC program were calculated in order to determine the final vibronic spectra.
Calculations were done initially with PBE0 exchange-correlation functional (with cc-pVTZ basis set) and than also the calculation for B3LYP, HSE06 and CAM-B3LYP have been carried out to understand the role of the different exchange-correlation functionals on the computed vibronic spectra.
This discussion will be useful to have a deeper insight on the most reliable computational setup.

5.2 TDDFT predicted UV-visible spectrum and its comparison with the experimental data

In this section we will analyze in detail the calculated PBE0/cc-pVTZ vibronic spectrum comparing it with available experimental data both for H-Py[n] and Ph-Py[n] wires.

Hydrogen polyynes (H-Py[n])

Lorentian fitted spectrum The time dependant density functional PBE0/ cc-pVTZ excited states were computed for all chain lengths from the H-Py[4] to the H-Py[16] wire, this values are reported in table (5.1).
In this table are reported also the $\pi-$electron transitions that span the excited states, it should be noted that these transitions are only dipole-allowed transitions between parallel π orbitals ($\pi_x \rightarrow \pi_x$ or $\pi_y \rightarrow \pi_y$).
These data have been used to build a first-guess absorption lorentian fitted spectrum without vibronic coupling.
From table (5.1) and the Lorentian fitting on figure (5.1) we can determine some important observation.

1) *Vibronic contributions cannot be overlooked and a simple Lorentian fitting is not enough for an accurate interpretation of the absorption spectra*

As we can clearly observe from figure (5.1) the lorentian fitting of the computed TDDFT data just give information on the origin of each peak and its relative intensity since the vibronic coupling is not accounted.
It is therefore necessary for a more accurate analysis to compute the Franck-Condon factors, this will be explained in detail in the vibronic spectra paragraph.

2) *The calculated UV-visible bands with respect to the experimental results show a slightly lower wavelength for H-Py[6] and H-Py[8] and higher wavelengths for H-Py[14] and H-Py[16]*

This is related to the tendency of usual DFT function to overestimate the π electron conjugation for polyconjugated systems.
This effect is limited for short wires and instead become important for longer

Hydrogen polyynes				
N° C atoms	E_{ge} [eV]	λ_{ge} [nm]	f	HOMO→LUMO transitions
16	3,8892	318,79	7,1236	HL
	5,05	245,51	0,291	0.4 H(-2)L , 0.2 HL2
	5,5864	221,94	0,9072	0.4 H(-1)L1 , 0.3 HL2
14	4,213	294,29	6,3898	HL
	5,4928	225,72	0,2313	0.4 H(-2)L , 0.2 HL2
	6,1447	201,77	0,7351	0.4 H(-1)L1 , 0.3 HL2
12	4,6191	268,42	5,6107	HL
	6,0487	204,98	0,1737	0.4 H(-2)L , 0.2 HL2
	6,8632	180,65	0,5852	0.4 H(-1)L1 , 0.3 HL2
10	5,1363	241,39	4,7946	HL
	6,7556	183,53	0,1157	0.4 H(-2)L , 0.2 HL2
	7,8182	158,58	0,4531	0.4 H(-1)L1 , 0.3 HL2
8	5,8258	212,82	3,9268	HL
	7,6817	161,4	0,0646	0.4 H(-2)L , 0.2 HL2
	9,143	135,61	0,3433	0.4 H(-1)L1 , 0.3 HL2
6	6,7864	182,69	2,9891	HL
	11,0841	111,86	0,2602	0.4 H(-1)L1, 0.2 HL4
	11,4453	108,33	0,3856	0.6 HL5, 0.4 H(-1)L3
4	8,2635	150,04	1,9935	HL
	11,0728	111,97	0,2614	HL3

Table 5.1: 1st column represent the number of carbon atom present on the chain of the different H-Py[n], 2nd 3rd and 4th column represent respectively the ground → excited state (i) transition energy , wavelength and oscillator strength calculated PBE0/cc-pVTZ time dependent DFT, the last column represent the single electron HOMO-LUMO transitions that span the excited state (H(x)L(y) is defined as the transition HOMO(x)→ LUMO (y)), only the transition with **significant oscillator strength** are reported in this table and on the following

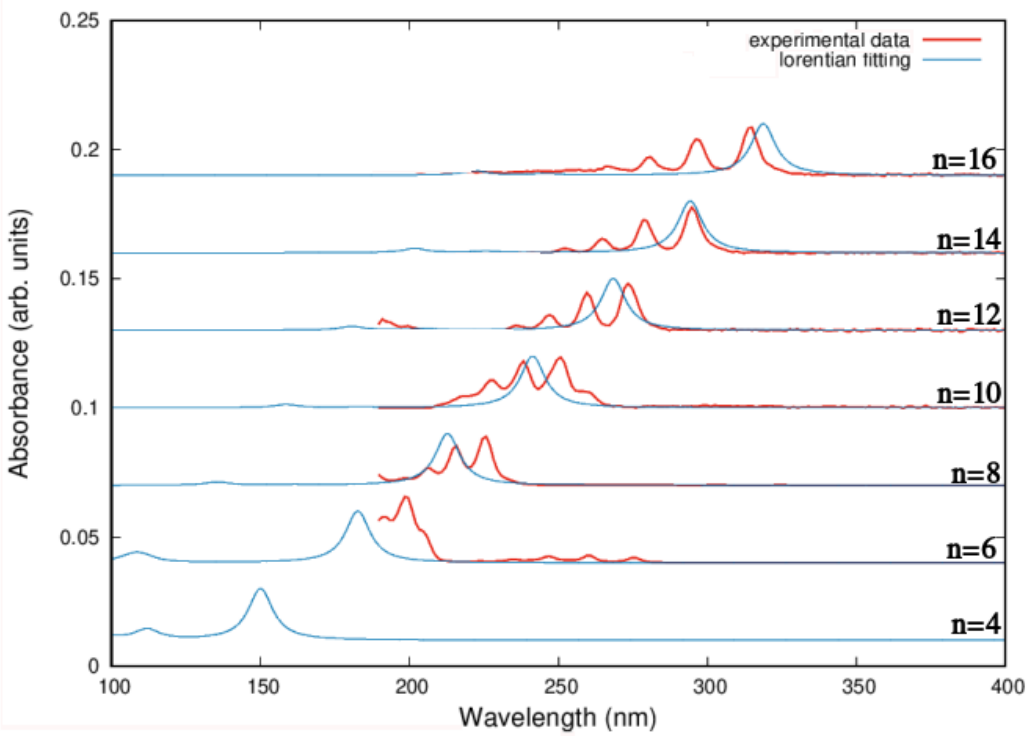

Figure 5.1: PBE0/cc-pVTZ lorentian fitting for H-Py[n] compared to experimental data obtained in our laboratory. A FWHM of 10 nm was chosen in order to have the best graphical representation

wires H-Py[16] and H-Py[14] where conjugation is higher, shifting the peaks to longer wavelengths.

3) *There are some low intensity peaks at high wavelengths in the experimental data but not showed in our computed spectra in the near-UV region*

These represents excited states directly spanned by the HOMO-LUMO excitation that are not dipole-allowed because they represent (or partially represent) the transition between perpendicular electronic transitions $\pi_{x,y} \rightarrow \pi_{y,x}$. These forbidden transition are usually relevant for the identification of short H-Py[4], H-Py[6] wires [56] since they represent the only peaks for H-Py above the 200 nm threshold, while the other peaks that falls in the far ultraviolet region (FUV) are not usually measured.
Experimental data report only the forbidden transition positions in these systems.
This peaks will be analyzed later in detail.

Vibronic spectra After the determination of the lorentian fitting, the time dependent DFT optimization for each relevant excited state was carried out. The new optimized values for energy, wavelength, oscillator strength and electronic transition dipole moment are reported in table (5.2).
Based on the optimized values for each excited state, FC factors were computed using UVFC program to determine the vibronic spectra.

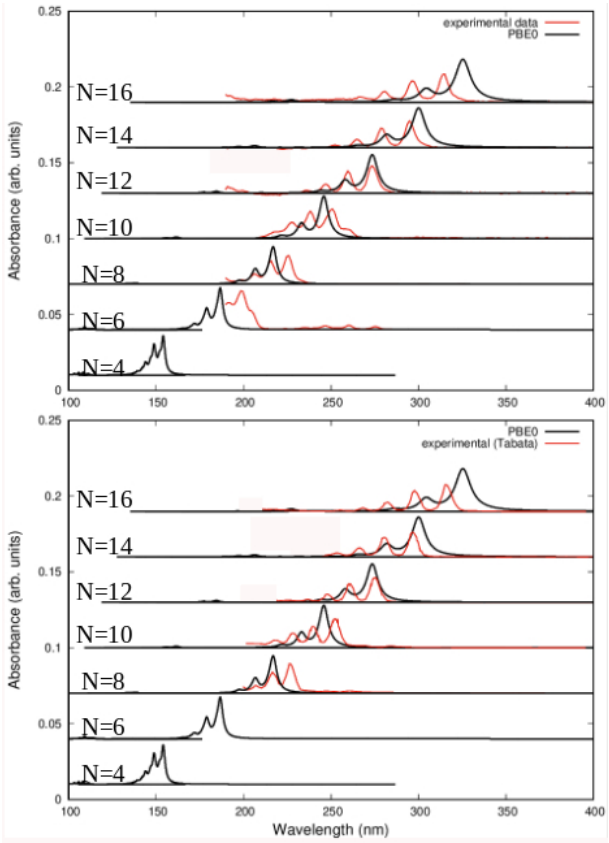

Figure 5.2: Calculated UV-vis spectra of hydrogen polyynes from H-Py[4] (bottom) to H-Py[16] (top) by PBE0/cc-pVTZ calculations and comparison with experimental data (made by Tabata [5] and in our laboratory [6])

A few considerations can be made over the vibronic spectra determined and represented in figure (5.2).

1) *The experimental peaks present vibronic bands which are broader with respect to the PBE0/cc-pVTZ peaks*

Hydrogen polyynes				
N° C atoms	E_{ge} [eV]	λ_{ge} [nm]	f	μ_{ge}
16	3,7367	331,8	7,5682	82,6687
	4,764	260,25	0,1623	1,3905
	5,3193	233,08	0,7975	6,1194
14	4,0555	305,72	6,7543	67,9806
	5,2001	238,43	0,1292	1,0142
	5,866	211,36	0,649	4,5158
12	4,4497	278,63	5,9041	54,1581
	5,7419	215,93	0,0964	0,6854
	6,5633	188,91	0,5235	3,2557
10	4,9492	250,51	5,0107	41,3237
	6,4198	193,13	0,0639	0,406
	7,4769	165,82	0,425	2,3203
8	5,605	221,2	4,0687	29,6294
	7,2796	170,32	0,0411	0,2307
	8,7048	142,43	0,3485	1,634
6	6,4986	190,79	3,0669	19,263
	10,4029	119,18	0,2849	1,1177
	11,2715	110	0,2894	1,0478
4	7,8213	158,52	1,998	10,4271
	10,675	116,14	0,2473	0,9457

Table 5.2: 1st column represent the number of carbon atom present on the chain of the different hydrogen polyynes, 2nd 3rd and 4th and 5th column represent the **optimized values** respectively the ground → excited state (i) transition energy , wavelength, oscillator strength and electronic transition dipole moment calculated by PBE0/cc-pVTZ time dependent DFT

We see that in the calculated vibronic spectra the $|g\rangle |0)_g \rightarrow |e\rangle |0)_e$ (corresponding to the origin of each peak) is in general much more intense than the other $|g\rangle |0)_g \rightarrow |e\rangle |N)_e$ ($N > 0$).
This different behaviour in principle can be related to the several approximations adopted, we know in fact that the normal modes of the excited state are just projection on the excited state geometry of the Hermite polynomial of the normal modes calculated by density functional analysis.
This limit affect the effective computation of the Franck-Condon factors.
Another important parameter affecting the FC factors is γ.
The γ parameter is related to the dimensionless displacement, B, that phisically represent the displacement of the geometry of the ground state with respect to the excited states for the vibronic transition (g→e), and in particular $\gamma = \frac{1}{2}B^2$.
With low γ the 0-0 transition will be more relevant with respect to the $0_g \rightarrow N_e$ peaks because the excited state geometry won't be significatively displaced with respect to the ground state.
The intensity of each individual $i \rightarrow f$ excitation (and therefore the modulation of each peak) is in fact strictly dependant on the vibrational coupling and therefore the γ parameters[1].
As we said before,

$$I_{if} \propto (\mu^0_{ge})^2 \prod_k^{TSmodes} S^2_{0,n_k} = (\mu^0_{ge})^2 \prod_k^{TSmodes} e^{-\gamma} \frac{\gamma^{n_k}}{n_k!} \tag{5.2}$$

Where S^2_{0,n_k} are the individual FC factors.

In table (5.3) we can see in detail that the number of important γ for each electronic transition in our molecules is limited, and it is always less than 6 for the H-Py[n] wires considered.
The important γ are evaluated based on both the value with respect of the highest value γ [$> 10, > 5\%$], and on its value [> 0.01]. In figure (5.3) the influence of the most relevant γ parameters are considered, we can see clearly that considering 4-5-6 most relevant gammas the overall shape of the peak almost doesn't change.
On this basis we can state that only few γ are necessary to compute the final vibronic spectra of H-Py[n] wires, and they didn't have any significant impact on the computed spectra.

[1]This was reported also on the introductive chapter

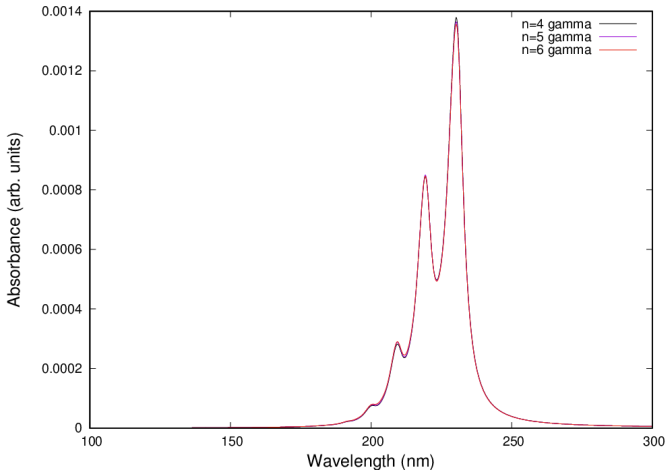

Figure 5.3: Analysis of the main peak for H-Py[10] with variation of the n° of γ considered

2) *Some of the peaks related to highly energetic dipole-allowed transition in the computed vibronic spectra in fig.(5.2) are not clearly visible since they yield low oscillator strength, we see them in fig.(5.4).*

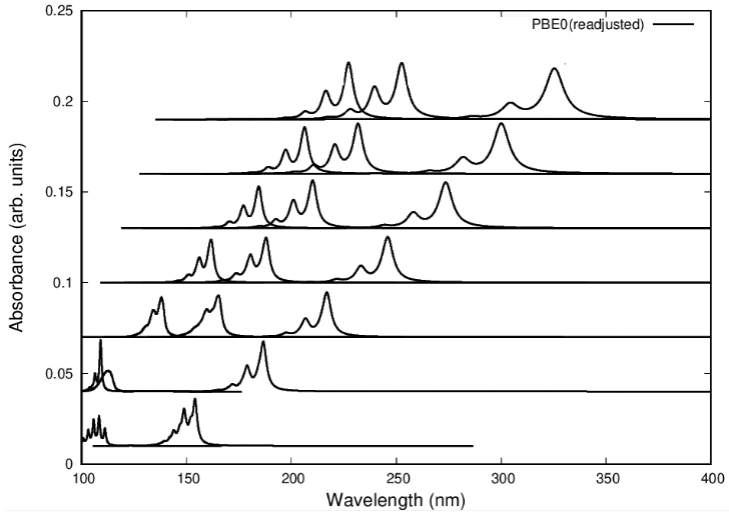

Figure 5.4: UV-visible spectra of hydrogen polyynes from H-Py[4] (bottom) to H-Py[16] (top), the high energetic (low wavelength) transitions are magnified in order to see the shift of each peak with chain length

Hydrogen polyynes						
N°C atoms	Peak pos [nm]	N° γ	N°[>10%]	N°[>5%]	N°[>0.01]	N° chosen
16	331,8	5	1	3	4	5
	260,25	8	3	3	4	5
	233,08	8	4	4	4	5
14	305,72	4	2	4	4	4
	174,01	7	3	4	5	7
	211,36	6	5	5	5	6
12	278,63	4	3	4	4	4
	215,93	6	3	4	4	4
	188,91	5	4	4	4	5
10	250,51	3	2	3	3	3
	193,13	6	4	4	5	6
	165,82	5	4	4	5	5
8	221,2	4	3	3	3	4
	170,32	5	4	4	4	5
	142,43	5	2	2	5	5
6	190,79	4	3	3	3	4
	119,18	4	2	2	4	4
	110	4	3	3	3	4
4	158,52	3	2	2	3	3
	116,14	3	3	3	3	3

Table 5.3: The table represent the n° of γ for each individual peak for which the FC factors and thus the distribution of the peak was calculated using the UVFC program. [> 10%] and [> 5%] correspond to the γ value corresponding to at least 10 and 5 percent of the highest γ value for that specific transition. The N° of chosen γ represent the number chosen for each individual calculation.The peak position is the transition wavelength calculated by optimized time dependant DFT calculations

.

Analysis of vibronic spectra In this paragraph we will analize the single electron transition that define the excited state relevant for our computed vibronic spectra.
This will be also related to the detailed analysis made by Wakabayashi et al. [18] [57] and Ding et al. [58], also experimental vibronic spectra for odd chains was available [59, 60] but we focused only on even wires.
As a general indication in fig. (5.5) we report the three main important transitions for these systems, generally used for the vibronic characterization of these wires.
The HOMO and LUMO level will be degenerate and divided into a π_x and π_y orbital as we can see from figure (5.6).
We observe the following:

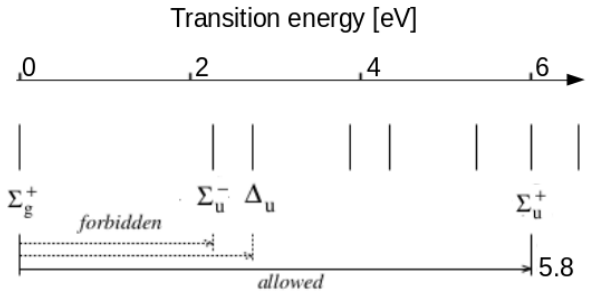

Figure 5.5: The different transitions for H-Py[6]

1) *The higher electronic transition dipole moment is carried as expected by the A $\Sigma_u^+ \longleftarrow$ X Σ_g^+ transition for all wires and is red shifting with chain length as expected [29]*

This transition is the one from the singlet ground state (Σ_g^+) to the first excited state and yields the highest wavelength and the lowest $E_e - E_g$ among the dipole-allowed transitions.
As expected it is the most favorable one and with the highest intensity peak.
The least energetic excited state for which we have a dipole allowed transition from the ground state is represented by the simmetry species Σ_u^+.
The excited state relative to this simmetry species is spanned by the excitation of same direction π orbitals (either $\pi_x \rightarrow \pi_x$ or $\pi_y \rightarrow \pi_y$) from the HOMO to the LUMO level.
The HOMO-LUMO transition will be $\pi_u \rightarrow \pi_g$ for H-Py[4n] or $\pi_g \rightarrow \pi_u$ in the case of H-Py[4n+2] wires.

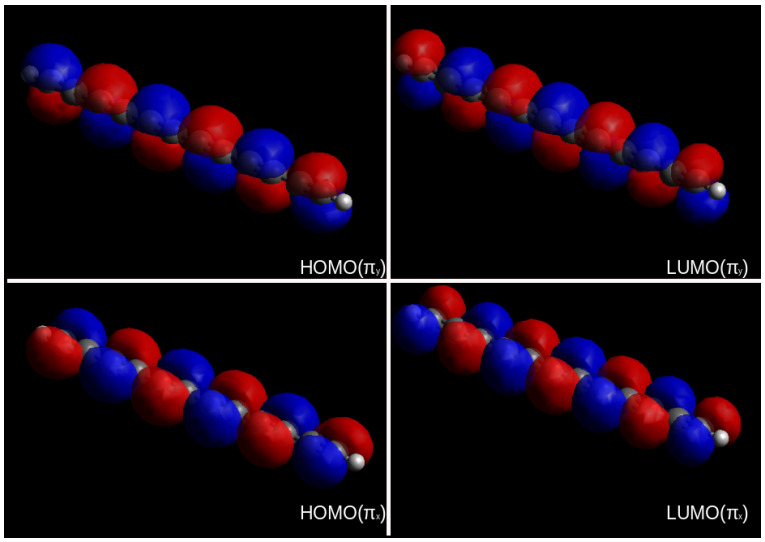

Figure 5.6: HOMO-LUMO π_x and π_y molecular orbitals for H-Py[12]

It is an allowed transition and is red shifting, with the values of 159-191-221-250-279-306-332 *nm* for H-Py[n] with n= 4,6,8,10,12,14,16 respectively, this is a totally expected behaviour due to the increase of the conjugation of the system.

2) *We report two other allowed transitions with much lower oscillator strength and wavelength with respect to the main peak in the case of H-Py[8] to H-Py[16], these peaks are also red shifting with chain length as we can see from figure (5.4).*

One of this transitions that we will call (A) is related to a combination of two single electron transition, the HOMO-2 → LUMO and the HOMO → LUMO+2.
The other (called B) is spanned by the combination of HOMO-1 → LUMO+1 and HOMO → LUMO+2.
These are generally low intensity dipole-allowed transitions.
In the case of H-Py[4] and H-Py[6] their oscillator strength become negligible with respect to other minor transitions (eg. the one spanned by the HOMO → LUMO +3 or HOMO → LUMO+5 orbitals) as we can see from table (5.2).
These peaks are all red shifting as we can see from the same table, yielding values of 170-193-216-238-260 nm for one peak, (for A), and 142-166-189-211-233 nm for the other(B), for H-Py[8] to H-Py[16].

3) *The peaks relative to the most relevant forbidden transitions* $\Delta_u \longleftarrow \Sigma_g^+$ *and* $\Sigma_u^- \longleftarrow \Sigma_g^+$ *are not showed in figure (5.2) or figure (5.4)*

This forbidden transition are very relevant since they are used for the identification of short length H-Py[n] since they are the only relevant peaks over the 200nm threshold [45] as we can see in figure (5.7).
We didn't computed the FC factors for these transitions because both of them yielded a negligible oscillator strenght.
The non optimized values for H-Py[4] calculated by TDDFT for these transitions were 4,8451 $E_{ge}[eV]$, 256 $\lambda_{ge}[nm]$ for the $\Sigma_u^- \longleftarrow \Sigma_g^+$ transition and 5,0544 $E_{ge}[eV]$, 245 $\lambda_{ge}[nm]$ for the $\Delta_u \longleftarrow \Sigma_g^+$ transition.
Instead for H-Py[6] they were 3,8172 $E_{ge}[eV]$, 325 $\lambda_{ge}[nm]$ for the $\Sigma_u^- \longleftarrow \Sigma_g^+$ transition and 3,9798 $E_{ge}[eV]$, 312 $\lambda_{ge}[nm]$ for the $\Delta_u \longleftarrow \Sigma_g^+$ transition.
The excited state relative to these simmetry species are both spanned by the HOMO-LUMO excitation and represent respectively the electronic transition between perpendicular π orbitals ($\pi_{x,y} \rightarrow \pi_{y,x}$) for the Σ_u^- simmetry species, and of both perpendicular and parallel π orbitals ($\pi_{x,y} \rightarrow \pi_{y,x}, \pi_{x,y} \rightarrow \pi_{x,y}$) for Δ_u.
The values of the electronic transition dipole moment for these transitions are related to the Herzberg-Teller expansion derivation since μ_{ge} will be 0, for forbidden transitions we have that the μ_{if} and thus the vibronic peak will be proportional to:

$$\mu_{if} = \sum_{\nu} a_\nu \langle \nu | \mu | f \rangle \tag{5.3}$$

Where ν is the wave function of a 'intermediate' vibronic state for which both $i \longrightarrow \nu$ and $\nu \longrightarrow f$ are allowed transitions(dipole or vibrationally allowed), thus the intensity of the unallowed $i \longrightarrow f$ transition will be borrowed from the allowed 'semi-transitions' to the intermediate level, we know in fact that a simmetry forbidden transition can become weakly allowed by state mixing caused by vibronic coupling.
The value of a_ν is given by:

$$a_\nu = \frac{\sum_i \left\langle \nu_{el} \left| \left(\frac{\partial H}{\partial Q_i} \right) \right|_0 \right| i_{el} \rangle \langle \nu_{vib} | Q_i | i_{vib} \rangle}{E_\nu - E_i} \tag{5.4}$$

The total wavefunction from this state mixing will be expressed as:

$$\Phi = \phi_i + \sum_{\nu} a_\nu \langle \nu | \mu | f \rangle \tag{5.5}$$

Note that the intermediate state is decomposed into the vibrational and electronic part $|\nu\rangle = |\nu_{vib}\rangle |\nu_{el}\rangle$, also the vibrational coupling with the normal mode is important for the intensity of forbidden transitions, the variation of the geometry of the molecule can modify slightly the initial and final simmetry, relaxing the selection rules for the specific transition
In particular the intensity of the forbidden ($\Delta_u \longleftarrow \Sigma_g^+$) transition from this completely simmetric ground state will be calculated in the Herzberg-Teller approximation as (seen by Ding et al. [58]:

$$I \propto \mu^2 \quad \mu \approx \sum_k \frac{< \Sigma_g^+ | e(x+y) | \Pi_u >< \Pi_u | \frac{\partial \mu}{\partial Q_k} | | \Delta_u >< \chi_{\nu''} | Q_k | \chi_{\nu'} >}{E(\Pi_u) - E(\Delta_u)} \tag{5.6}$$

This is the result of combining the eq. (5.3) and (5.4), $\chi_{\nu''}$ and $\chi_{\nu'}$ are respectively the vibrational wave functions for the electronic state Π_u and Δ_u and both ($\Pi_u \longleftarrow \Sigma_g^+$), ($\Delta_u \longleftarrow \Pi_u$) are allowed electronic transitions, this peaks are in high wavelength range and are not visible from our computational calculations, but are important since they are present in the experimental spectrum. We cannot observe these excited states on our computed vibronic spectra since the transition from the ground state to these simmetry species is forbidden (f=0), and the transition to these levels is only due to an intermediate transition (allowed or through vibronic coupling) from the ground state to the A, B Σ_u^+ or $\Pi_{u,g}$ orbital [18].

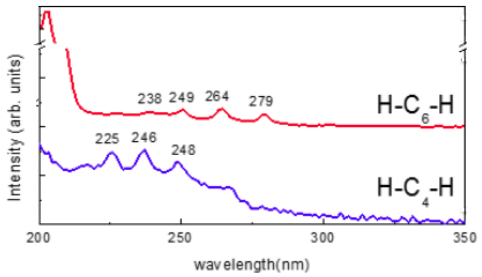

Figure 5.7: Experimentally determined position of the forbidden transition peaks for H-Py[4] and H-Py[6]

Diphenyl polyynes (Ph-Py[n])

Lorentian fitted spectrum In the case of phenyl-terminated polyynes the analysis is not simple, as we can see from table (5.5), since we have a large amount of transitions from the ground state.
The lorentian fitting was built up with the same consideration made on the H-Py[n] chains, and using the data calculated by PBE0/cc-pVTZ time dependant DFT reported in table (5.4).
Due to the high degree of vibronic coupling, the non-degeneracy of the HOMO($\pi_{x,y}$) and LUMO($\pi_{x,y}$) and the high amount of single particle transitions representing each $g \rightarrow e$ transition we will not give in detail the single particle representation of each state since it will be a too long and complex analysis to give a significant interpretation.

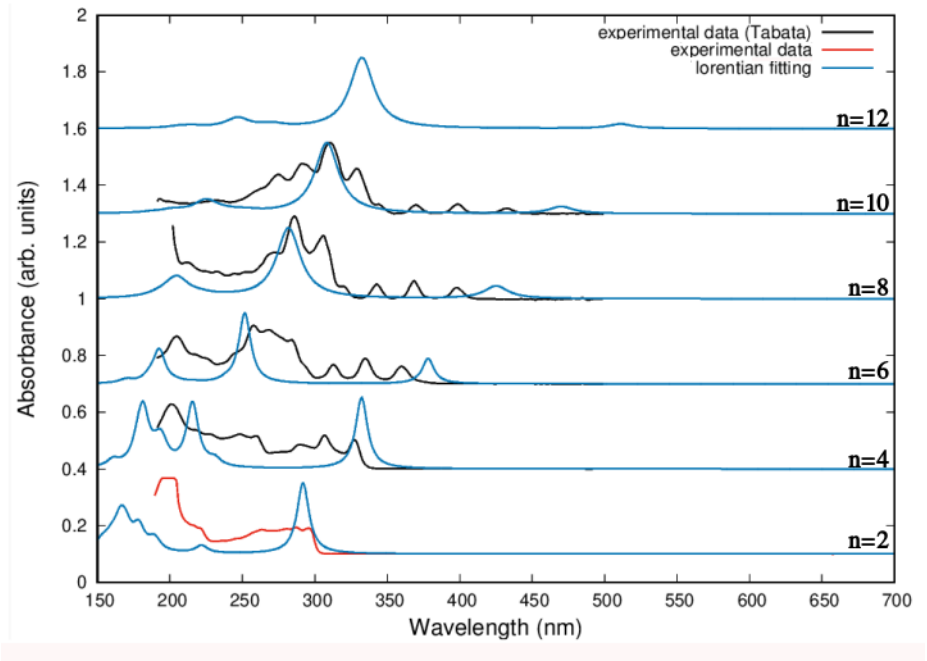

Figure 5.8: PBE0/cc-pVTZ determined lorentian fitting for Ph-Py[n] compared with experimental results both of Tabata and made in our laboratory, the FWHM was chosen arbitrarily for the best graphical representation

The following observations can be made based on the lorentian fitting of the time dependant DFT results reported in figure (5.8):

1) *As for H-Py[n] wires, the Lorentian fitting is not enough for a complete interpretation of the experimental spectrum*

As we can clearly observe from figure (5.8) the lorentian fitting of the computed TDDFT data just give information on the origin of each peak and its relative intensity while the vibronic coupling is not accounted and it is therefore necessary to compute the Franck-Condon factors.
That is what we did using the UVFC program that will be analyzed in the vibronic spectra paragraph.

2) *The peaks are red shifting with chain lenght as for H-Py[n] wires*

This effect again is related to an increase in the conjugation of the system with chain length.
The transition wavelength in fact increases from Ph-Py[2] to Ph-Py[12], with values of 331-388-463-543-623-699nm.

3) *There is an higher wavelength transition with respect to the most intense peak that is expecially relevant for lower chains (Ph-Py[2] and Ph-Py[4])*

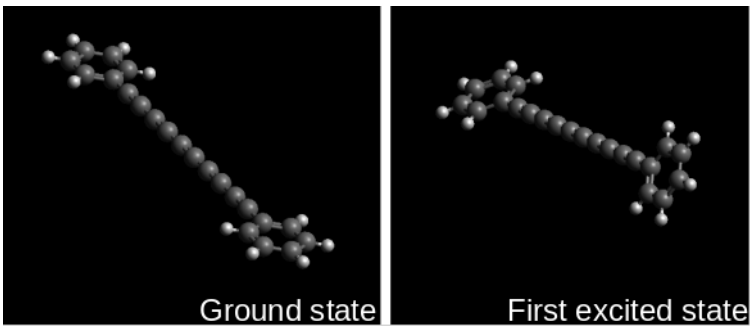

Figure 5.9: Ground state configuration (on the left), first excited state configuration, for which a dipole-allowed transition is possible from the ground state, representing the high wavelength transitions on the spectrum (on the right)

Diphenyl polyynes			
N° C atoms	$E_{ge}[eV]$	$\lambda_{ge}[nm]$	f
12	2,4257	511,12	0,2532
	3,7282	332,56	6,2418
	4,5791	270,76	0,3866
	5,0256	246,7	1,1364
10	2,6375	470,09	0,3439
	4,0211	308,34	5,3023
	5,5084	225,08	1,2745
8	2,9153	425,28	0,4865
	4,3978	281,92	4,1979
	6,0583	204,65	1,6439
6	3,2781	378,22	0,7006
	4,925	251,74	2,8952
	6,4342	192,7	1,7742
	6,6596	186,17	0,2682
4	3,7309	332,32	0,9353
	5,7499	215,63	1,2864
	6,3689	194,67	0,4029
	6,8242	181,68	1,195
	6,9582	178,18	0,3763
2	4,2474	291,91	0,9614
	5,5897	221,81	0,1522
	6,5424	189,51	0,2879
	6,9422	178,59	0,4812
	7,3222	169,33	0,4947
	7,487	165,6	0,6001
	7,7692	159,58	0,2314

Table 5.4: 1st column represent the number of carbon atom present on the chain of the different diphenyl polyynes, 2nd 3rd and 4th column represent respectively the ground → excited state (i) transition energy , wavelength and oscillator strength calculated PBE0/cc-pVTZ time dependant DFT

These peaks in the near-UV region are not related to dipole-forbidden transition as in the case of H-Py[n] but they are transition from the planar configuration of the ground state to a distorted configuration.
As shown in the excited state in figure (5.9) indeed the phenyl endgroups are slightly rotated one with respect to the other.
The calculated position of the peaks also in this case is significantly red shifted with respect to the experimental data, this is related to the overextimation of the conjugation and enhanced by the fact that this endgroups (phenyls) are highly π-conjugated systems composed by sp^2 carbon atoms.

Vibronic spectra After the determination of the spectra in figure (5.8), the time dependant DFT optimization for each relevant excited state was carried out and the vibronic spectra has been computed with the UVFC program.
The new optimized values for transition energy, wavelength, oscillator strength and electronic transition dipole moment are reported in table (5.5).

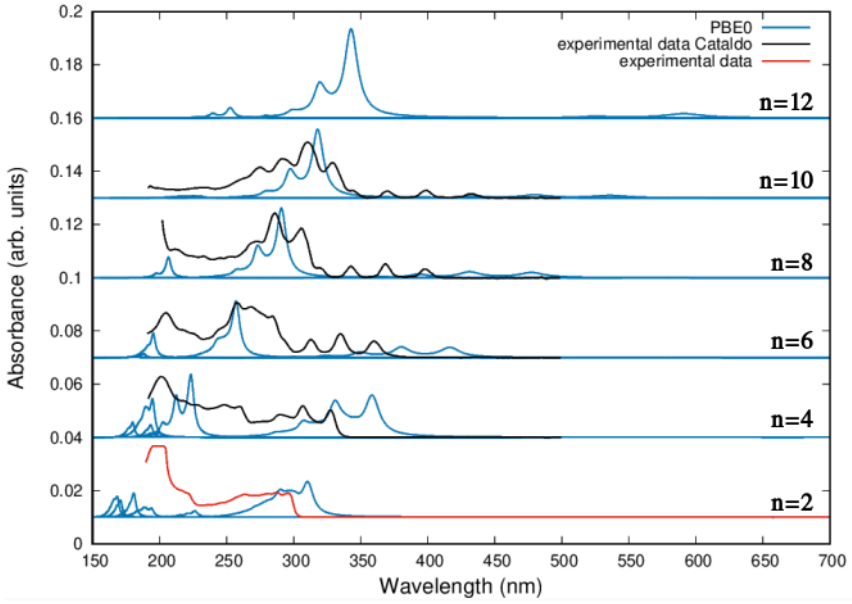

Figure 5.10: PBE0/cc-pVTZ calculated UV-vis spectra for diphenyl polyynes (Ph-Py[n])

Diphenyl polyynes				
N° C atoms	$E_{ge}[eV]$	$\lambda_{ge}[nm]$	f	μ_{ge}
12	1,7731	699,26	0,1604	3,6915
	3,5118	353,05	6,6497	77,2881
	4,2863	289,26	0,2857	2,7202
	4,7874	258,98	1,12	9,5489
10	1,9914	622,61	0,2291	4,6952
	3,7858	327,5	5,6615	61,0411
	5,2477	236,26	0,5559	4,3237
8	2,284	542,85	0,3473	6,2071
	4,1337	299,93	4,5356	44,7851
	5,9323	209	1,4973	10,3018
6	2,6805	462,53	0,5593	8,5167
	4,7129	263,07	3,0084	26,0544
	6,2618	198	1,6663	10,8619
	6,5126	190,38	0,2682	1,6811
4	3,1929	388,31	0,8731	11,1616
	5,3389	232,23	1,7536	13,4069
	6,0299	205,62	0,1417	0,9589
	6,1933	200,19	1,2963	8,543
	6,8183	181,84	0,3792	2,2702
2	3,748	330,8	1,002	10,9117
	5,3684	230,95	0,1538	1,1697
	6,1796	200,63	0,4702	3,1055
	6,7611	183,38	0,6693	4,0405
	7,1764	172,77	0,508	2,8895
	7,2428	171,18	0,7749	4,4001
	7,1249	0,4208	0,4208	2,4107

Table 5.5: 1st column represent the number of carbon atom present on the chain of the different diphenyl polyynes, 2nd 3rd and 4th and 5th column represent the **optimized values** respectively the ground → excited state (i) transition energy , wavelength, oscillator strength and electronic transition dipole moment calculated by PBE0/cc-pVTZ time dependent DFT

We can make several important observations of the UV-visible spectra reported in figure (5.10):

1) *As for H-Py[n] wires, the experimental peaks present vibronic bands which are broader with respect to the PBE0/cc-pVTZ peaks*

This is partially related to the same effect that we observed for H-Py[n] wires, due to the influence of the γ parameter.
The behaviour of the γ factors considered for the diphenyl polyynes is in fact different, since now many individual transitions present an high degree of vibrational coupling.
This is caused indeed by the presence of the phenyl groups, which are both electronically and vibronically coupled to the sp carbon chain.
The overall γ parameter are higher both in values and in number, as we can clearly see in table (5.6).
On this basis, it is evident that we have to consider a larger number of γ.
This is not possible due to the high computational costs, and the maximum number of relevant γ that we have been able to consider for each transition was 7 (with $\approx$1 day of calculation time).
A number of 8 γ would rise the calculation time up to $\approx$ 1 month using the same machine.

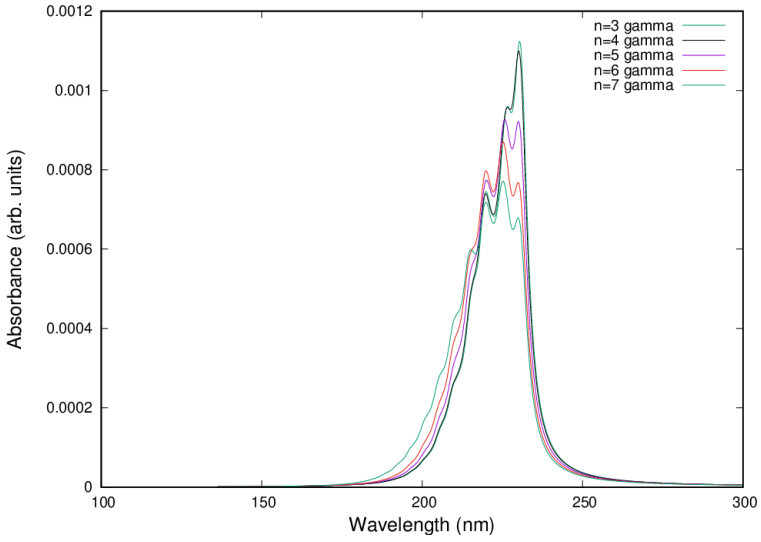

Figure 5.11: Analysis of a peak for Ph-Py[10] with variation of the n° of γ considered

As we can see from figure (5.11) the modulation of the individual peak with respect to the number of γ considered is significant.
Increasing the number of γ taken into account we will increase the vibrational coupling, therefore broadening the UV-visible spectra peaks and decreasing the relative intensity of the origin (the 0-0 transition).

2) *The broadening of each peak is significant due to the high vibronic coupling*

In figure (5.12) we have the comparison of the computed PBE0 vibronic spectra after the FC calculations to the lorentian fitting where we see clearly the broadening effect on each peak.

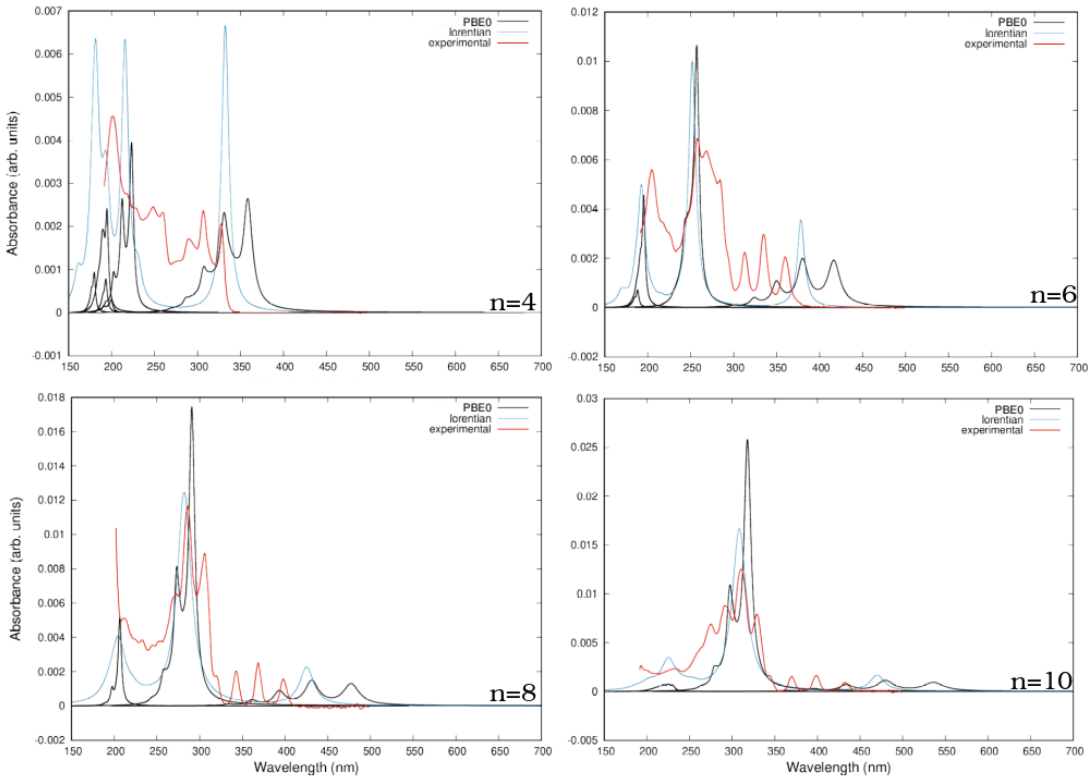

Figure 5.12: PBE0/cc-pVTZ calculated vibronic spectra for Ph-Py[n], n=4,6,8,10 compared with the lorentian fitted spectrum

Diphenyl polyynes						
N°C atoms	Peak pos [nm]	N° γ	N°[>10%]	N°[>5%]	N°[>0.01]	N° chosen
12	699,26	10	1	2	3	5
	353,05	11	2	3	5	5
	289,26	12	3	5	6	6
	258,98	11	2	4	7	6
10	622,61	10	1	1	4	4
	327,5	12	2	4	7	5
	236,26	16	9	9	12	7
8	542,85	9	1	1	4	4
	299,93	10	2	5	6	6
	209	11	3	4	8	5
6	462,53	9	1	1	8	5
	263,07	11	10	10	10	7
	198	12	8	8	8	7
	190,38	10	7	9	8	7
4	388,31	10	2	5	7	6
	232,23	10	3	5	8	6
	205,62	10	8	9	10	7
	200,19	10	6	8	9	7
	181,84	10	6	7	7	7
2	330,8	9	6	8	8	7
	230,95	9	6	7	7	7
	200,63	8	6	6	6	6
	183,38	9	5	5	6	6
	172,77	9	5	5	5	5
	171,18	10	5	7	8	7
	0,4208	8	4	4	8	6

Table 5.6: The table represent the n° of γ for each individual peak for which the FC factors and thus the distribution of the peak was calculated using the homemade UVFC program. [> 10%] and [> 5%] correspond to the γ value corresponding to at least 10 and 5 % of the highest γ value for that specific transition. The N° of chosen γ represent the number chosen for each individual calculation.The peak position is the transition wavelength calculated by optimized time dependent DFT calculations

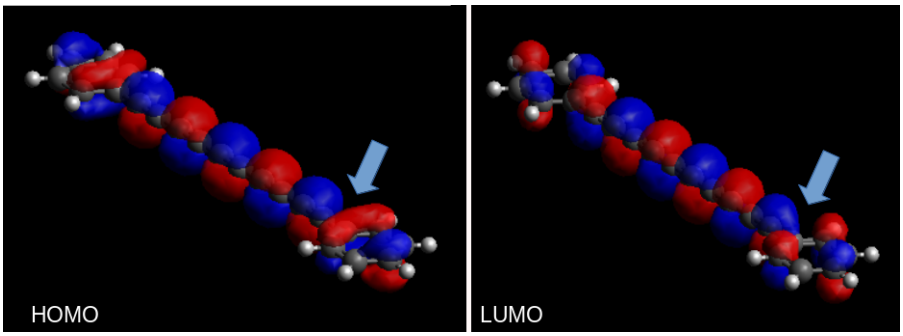

Figure 5.13: Shape of the HOMO and LUMO levels for a Ph-Py[10] wire

3) *The difference in wavelength between experimental and calculated spectra for the least energetic dipole-allowed transition seems to be almost constant and not depending with chain length*

The excited state that will be generated by this transition correspond, as we said before to a relative rotation between the phenyl groups from the planar configuration.
This excited state is mainly spanned by a single particle HOMO-LUMO quantum transition which causes also the electronic density to move from the phenyl endgroups to the central wire as observed in fig. (5.13).
This will generate a lower conjugation between π orbitals in the chain and on the phenyl groups, thus causing a distortion as seen in fig. (5.9).
Considering this, it is clear that this single particle transition is not relevantly affected by the length of the chain, since the most important effect is localized near the endgroups.

4) *The position of the other calculated peaks with respect to the experimental ones seems to yield a similar effect to the one reported for H-Py[n] wires*

In fact, if we analyze the position of these peaks, we can observe that for Ph-Py[6] and Ph-Py[4] all the peaks are shifted to lower wavelengths and for Ph-Py[8] and Ph[10] we have peaks almost in the same position. This is exactly the same effect that we observed for H-Py[n] wires.
Following this trend we will expect that for Ph-Py[12+] our PBE0 calculated spectra will present peaks slightly shifted to higher wavelengths, as observed for H-Py[n].

5.3 Functional dependence on the spectrum

In this section we analyze how the change of the exchange-correlation functionals (E_{xc}) can influence the calculated UV-vis spectra and the comparison with experimental data.
We selected mainly 2 other functionals, the CAM-B3LYP (even if present an hypsochromic shift [56] it is necessary to consider more accurately long range interactions [39] such as conjugation and vibronic coupling) and the HSE06 (that is known to better estimate the HOMO-LUMO gap [61, 62]).

Hydrogen polyynes (H-Py[n])

For the H-Py wires the analysis was mainly focused (aside from the PBE0 calculations seen before) to other hybrid functionals such as HSE06,B3LYP and CAM-B3LYP.
All the computation of the ground state, the excited states and the Franck-Condon parameters have been computed using these functionals together with cc-pVTZ basis set.
We can see that the values for the transition wavelength, oscillator strength and electric dipole transition moment do not change significantly for the B3LYP, HSE06 with respect to the calculation with the PBE0/cc-pVTZ basis set, with maximum difference of about 6 nm in the worst case.
The optimized values of the wavelength of the main dipole allowed transition and thus the position of the main $A\ \Sigma_u^+ \longleftarrow X\ \Sigma_g^+$ respectively for the PBE0, B3LYP and HSE06 is: for H-Py[16] (332-338-338nm), H-Py[14] (306-311-310nm), H-Py[12] (279-282-282nm), H-PY[10] (251-254-253nm), H-Py[8] (221-224-222nm),H-Py[6] (191-193-191nm) and for H-Py[4] (159-160-159nm).
Instead the values for the CAM-B3LYP are considerably different, with maximum difference of about 40nm.
Indeed it yields values of (300-280-260-237-212-185-155nm) from H-Py[16] to H-Py[4], with the deviation from the other values increasing with chain length.
The optimized values for the oscillator strength, that give information on the intensity of the main transition is also very different for CAM-B3LYP with respect to the others, for H-Py[16] (7,57-7,31-7,19 and 7,99), H-Py[14] (6,75-6,55-6,51 and 7,07), H-Py[12] (5,9-5,75-5,76 and 6,13), H-PY[10] (5,01-4,9-4,93 and 5,16), H-Py[8] (4,07-3,99-4,03nm and 4,17),H-Py[6] (3,07-3,02-3,06 and 3,13) and for H-Py[4] (2-1,97-2 and 2,04) respectively for the PBE0, B3LYP and HSE06 and CAM-B3LYP.
As we can see for longer chains the CAM-B3LYP main transition will be less intense: we know in fact that $I_{if} \propto \mu_{ge}^2$, with the values on the electric

B3LYP							
N°C atoms	$E_{ge}[eV]$	$\lambda_{ge}[nm]$	f	$E^*_{ge}[eV]$	$\lambda^*_{ge}[nm]$	f*	μ^*_{ge}
16	3,7892	327,2	6,8773	3,6653	338,26	7,3079	81,3802
14	4,1162	301,21	6,1931	3,9862	311,03	6,5503	67,0715
12	4,524	274,06	5,4651	4,3824	282,91	5,7496	53,5506
10	5,0466	245,68	4,6803	4,8834	253,89	4,8982	40,9408
8	5,739	216,04	3,8479	5,541	223,76	3,9909	29,3986
6	6,7008	185,03	2,9364	6,4336	192,71	3,0165	19,1379
4	8,1854	151,47	1,9673	7,7578	159,83	1,9705	10,3674
HSE06							
N°C atoms	$E_{ge}[eV]$	$\lambda_{ge}[nm]$	f	$E^*_{ge}[eV]$	$\lambda^*_{ge}[nm]$	f*	μ^*_{ge}
16	3,78	328	6,7648	3,6644	338,35	7,1886	80,0718
14	4,1188	301,02	6,1502	3,994	310,42	6,5084	66,5131
12	4,5389	273,16	5,4695	4,3991	281,84	5,7582	53,4277
10	5,0741	244,35	4,7122	4,9091	252,56	4,9337	41,0213
8	5,7797	214,52	3,889	5,5746	222,41	4,0363	29,5542
6	6,7553	183,54	2,9753	6,4784	191,38	3,0552	19,2494
4	8,2479	150,32	1,9911	7,8103	158,74	1,9956	10,4293
			:				
CAM-B3LYP							
N°C atoms	$E_{ge}[eV]$	$\lambda_{ge}[nm]$	f	$E^*_{ge}[eV]$	$\lambda^*_{ge}[nm]$	f*	μ^*_{ge}
16	4,4844	276,48	7,6779	4,1365	299,74	7,985	69,8762
14	4,7576	260,6	6,7955	4,4186	280,6	7,0652	65,2651
12	5,1093	242,66	5,8996	4,7756	259,62	6,1258	52,3577
10	5,5705	222,57	4,9854	5,2366	236,76	5,1609	40,2265
8	6,1989	200,01	4,0437	5,8515	211,88	4,1662	29,061
6	7,0881	174,92	3,0576	6,7006	185,03	3,1256	19,0395
4	8,4732	146,33	2,0306	7,9737	155,49	2,0384	10,4344

Table 5.7: 1st column represent the number of carbon atom present on the chain of the different H-Py[n] , 2nd 3rd and 4th column represent respectively the ground $\rightarrow$ excited state (i) transition energy , wavelength and oscillator strength *only of the most significant peak* [A $\Sigma_u^+ \longleftarrow \Sigma_g^+$] for each type of functional , 5th 6th, 7th, 8th represent respectively the optimized values for the transition energy , wavelength, oscillator strength and transition dipole moment of each transition

transition dipole moment which are generally lower.
Since the main parameter for each transition is very different for CAM-B3LYP we will expect that also the Franck-Condon factors the situation will be different from PBE0, as analized in detail in the following paragraph.

Vibronic spectra computed with CAM-B3LYP As we can see from figure (5.14) the CAM-B3LYP exchange correlation functional better fit the trend of the peaks for increasing chain length (that can be correlated to a better estimation of the vibronic coupling in our system).
Still the position of each peak is not computed correctly, but this blue shift effect, caused by an high HF exchange contribution of the overall exchange-correlation functional - $> 40\%$, was expected [56].
We observe on figure (5.15) that by applying a rigid translation of the spectrum of about 20nm the trend better fits the experimental data.
This translation has been calculated as a difference between the origin (TDDFT calculated with CAM-B3LYP functional) of the main peak for wire of intermediate length (H-Py[8]) and the origin determined by experimental results.

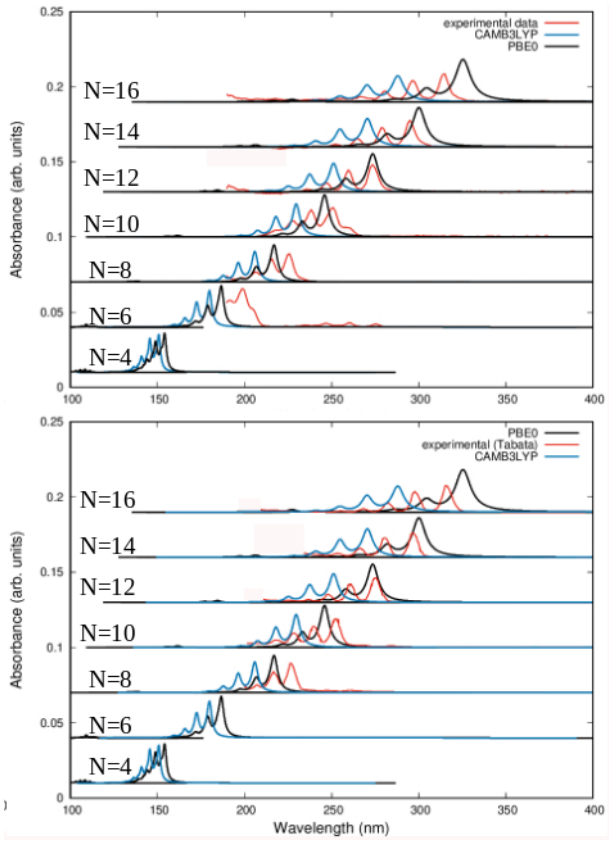

Figure 5.14: CAM-B3LYP/cc-pVTZ vibronic spectra after Franck-Condon compared with experimental data made in our laboratory(top) and Tabata's (bottom)

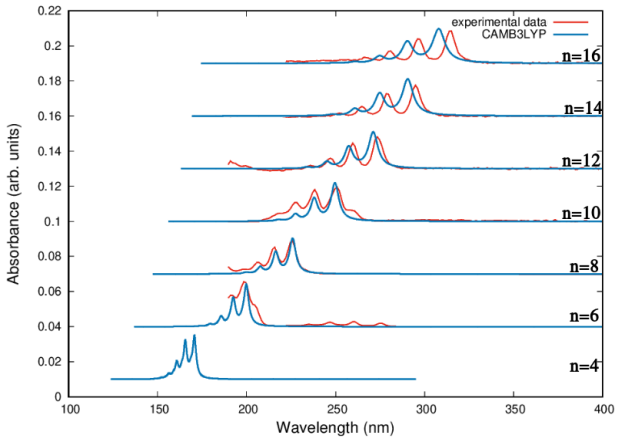

Figure 5.15: CAM-B3LYP/cc-pVTZ vibronic spectra rigidly shifted by 20 nm compared with experimental data made in our laboratory

.

Vibronic spectra computed with HSE06 The HSE06 (HSEH1PBE) has been since it is know from other works to better estimate the HOMO-LUMO gap [61, 62].
In our case it showed high similarity to PBE0 functional, both for the oscillator strength and wavelength for each transition.
In this functional the difference is mainly related with the overextimation of the conjugation for long wires (for H-Py[14] and H-Py[16]), that is even worse than for the PBE0, while we have a better extimation of the conjugation in shorter wires (H-Py[6] and H-Py[4]).
We note that the HSE06 yield the same correlation part of the functional (PBE), also used for PBE0 and only the exchange part is changed. A significant difference between these two functionals is not expected.

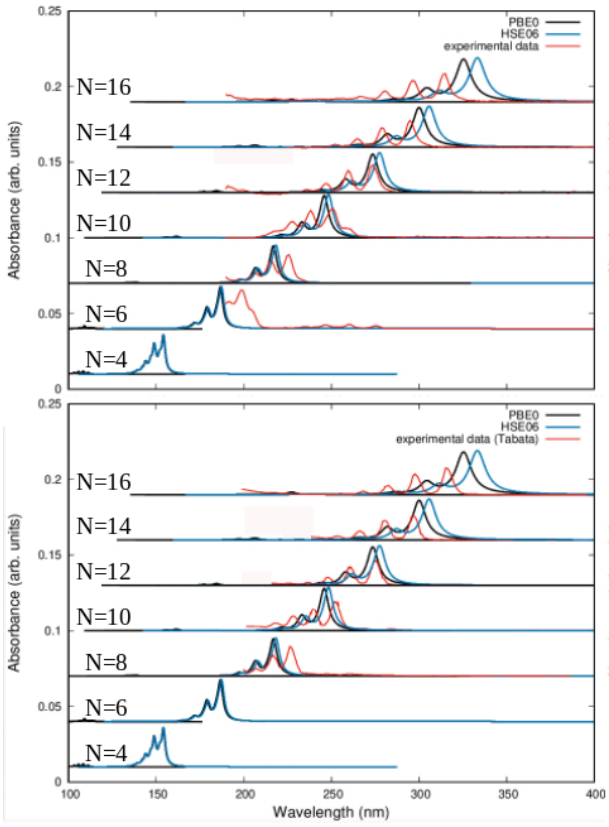

Figure 5.16: HSE06/cc-pVTZ vibronic spectra compared with experimental data made in our laboratory(left) and Tabata's (right)

Diphenyl polyynes (Ph-Py[n])

In this section we will study the difference on the computed UV-visible spectra using the HSE06 and the CAM-B3LYP as for H-Py[n].
In the previous discussion we found that the CAM-B3LYP was the one with significant differences to the PBE0 functional and with the best fit on the modulation of the UV-visible peaks.
In table (5.3) the values of transition energy, wavelength, oscillator strength and electronic transition dipole moment are reported both for HSE06 and CAM-B3LYP time dependent DFT simulations.

CAM-B3LYP						
$E_{ge}[eV]$	$\lambda_{ge}[nm]$	f	$E^*_{ge}[eV]$	$\lambda^*_{ge}[nm]$	f^*	μ^*_{ge}
3,0662	404,36	0,2404	2,094	592,08	0,139	2,7097
4,5036	275,3	5,4357	4,1506	298,72	5,7818	56,8591
5,7221	216,68	1,3741	-	-	-	-
6,6868	185,42	0,5629	6,3803	194,32	0,6316	0,6316
HSE06						
$E_{ge}[eV]$	$\lambda_{ge}[nm]$	f	$E^*_{ge}[eV]$	$\lambda^*_{ge}[nm]$	f^*	μ^*_{ge}
2,5632	483,7	0,3741	1,9736	628,22	0,2521	5,2148
3,9239	315,97	4,9398	3,7146	333,77	5,3506	58,7943
4,8816	253,98	0,5134	4,589	270,18	0,3839	3,4146
5,4286	228,39	1,0576	5,0693	244,58	0,132	1,0625

Table 5.8: 1st 2nd and 3rd column represent respectively the ground → excited state (i) transition energy , wavelength and oscillator strength *only of the most significant peaks* for **Ph-Py[10]** , 4th 5th, 6th, 7th represent respectively the optimized values for the transition energy , wavelength, oscillator strength and transition dipole moment of each transition

Vibronic spectra computed with CAM-B3LYP As we have seen for H-Py[n] wires the CAM-B3LYP functional better fits the relative intensity of each peak with respect to the origin and the trends for increasing length of the chain. As we can see from figure (5.17) and table (5.3) this is also true for Ph-Py[n] wires. The hypsochromic shift found also for H-Py[n] CAM-B3LYP vibronic spectra, related to the HF exact exchange, was expected.
The position highest wavelength peak (the one related to the HOMO-LUMO transition) correlates better with experimental data, even if its intensity seems to yield lower values.
The relative peak intensity of the highest intensity transition is better fitted in this case, with the intensity of the origin signicantly reduced with respect to the PBE0 calculations.
Due to the high number of excited states and high vibrational coupling the state localized at $\approx 220[nm]$ was not computed.

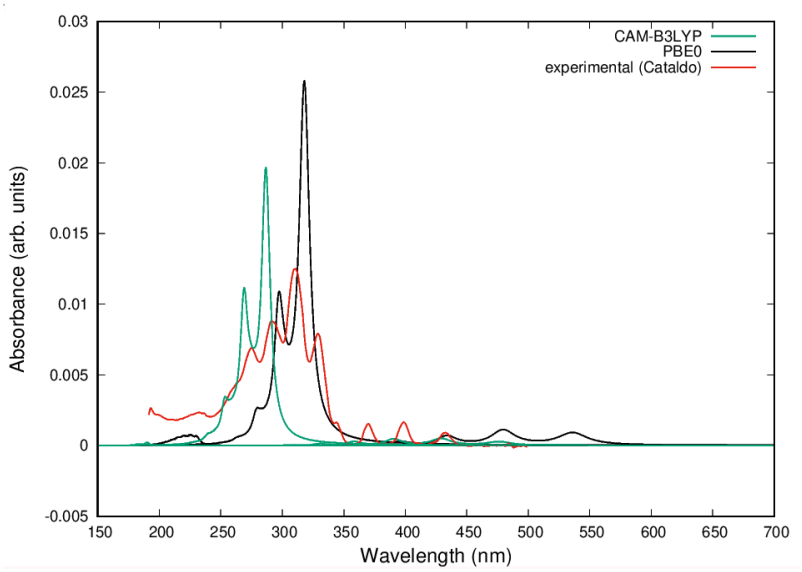

Figure 5.17: CAM-B3LYP/cc-pVTZ vibronic spectrum for Ph-Py[10] compared to the previous PBE0/cc-pVTZ calculations

Vibronic spectra computed with HSE06 As we have seen for H-Py[n] wires, the HSE06 functional doesn't change the overall shape of the curves and also in this case generate only a slight shift to higher wavelengths of all the calculated peaks with respect to PBE0, this effect was also observed for H-Py[n] wires.

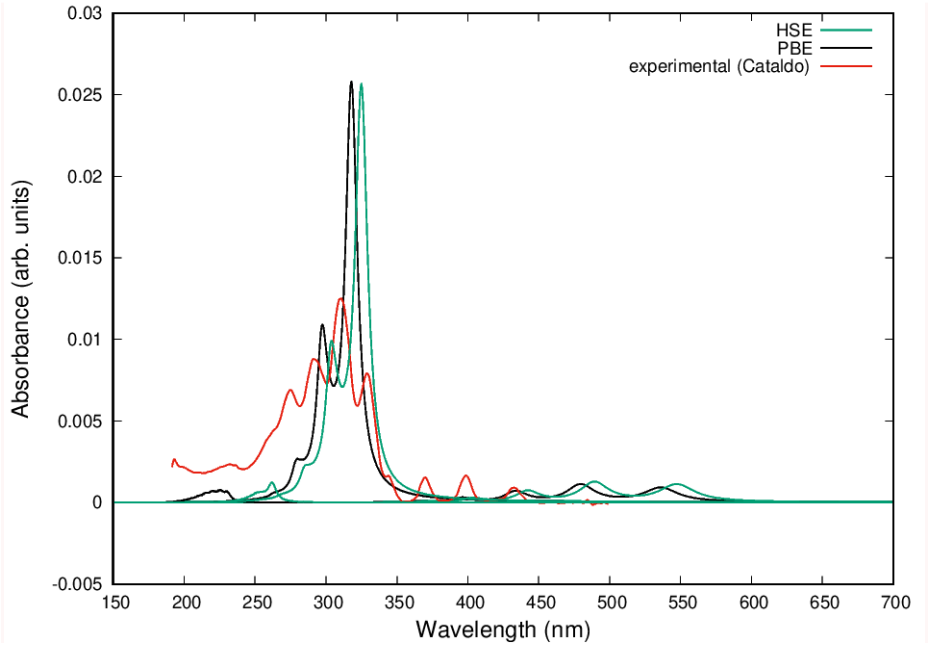

Figure 5.18: HSE06/cc-pVTZ vibronic spectrum for Ph-Py[10] compared to the previous PBE0/cc-pVTZ calculations

5.4 Discussion on the vibronic transitions and UV-visible spectra determined

In this chapter I have shown how we have been able to compute the vibronic spectra both for H-Py[n] and Ph-Py[n] polyynes, comparing the trends and the overall shape of the spectrum with available experimental data.
Several observation can be made on the results that we achieved in this chapter:

- We were able to compute the vibronic spectra based on DFT and UVFC calculations both for H-Py[n] and Ph-Py[n] wires
- We demonstrated that a simple analysis based on the Lorentian fitted spectrum with no vibronic contribution was not enough to give an interpretation of experimental data, vibronic effects need to be taken into account and computed properly
- We obtained a very good aggreement with experimental data, especially for H-Py[n] wires and we have been able to give an interpretation on the trends observed in the measured spectrum
- We were able to analyze the role of the different exchange-correlation functionals on the predition of the vibronic spectra. In particular, we verified that the CAM-B3LYP better fitted the overall distribution on the relative intensity of each peak, showing a proper assessment of the vibrational coupling
- The comparison allowed us to assess also several differences from the vibronic spectrum to the experimental data, which motivate further works and investigation on this topic.
  The first difference is related to the trends observed in the spectra with increasing conjugation, for all Ph-Py[n] wires and for H-Py[n] with $n > 6$. This discrepancy is due to an overextimation of the conjugation effect of the DFT method adopted, which needs further development and investigation.
  The second difference is related to the relative intensity distribution of the band with respect to its origin calculated by time dependent DFT, this was limited in the case of PBE0 and HSE06 exchange-correlation functionals.
  This effect can be due to differences in geometry from the actual and

the calculated excited state, again related to the accuracy of E_{xc} functionals used for TDDFT simulations.
For Ph-Py[n] in general the problem is further related to the fact that the vibrational coupling in these systems is more complex than for H-Py[n] and require high computational costs to carry out more accurately the evaluation of the FC factors, as we underlined on the analysis on the γ parameter for these structures.
The third difference is that the presence of dipole-forbidden transition (used in other works for the identification of short H-Py[n] wires) have not been taken into account in any of the vibronic spectra here computed.
This is related to the fact that our calculation focused only on dipole-allowed transition with oscillator strength significantly different from 0.

Chapter 6

Conclusions

This thesis work has been focused on the computational analysis of important properties of short length CAWs considering the effect of chain length and endgroups, and comparing them with spectroscopic results.
At first we determined structural and optoelectronic properties for 2 different types of cumulenes (S-cumu[n], O-cumu[n]) to find their relation to the Raman spectra that we were able to compute. This method is known to be reliable and was used in other works.
The definition of CAWs based on the correlation with the infinite carbyne was shown to be limited and the polarizability derivatives over the single CC bonds in the chain instead was found to be a powerful tool to distinguish the finite length chains into three main categories (instead of 2).
The structural and electronic properties were analyzed in detail for several CAWs, the HOMO-LUMO gap and BLA in particular showed an overall decreasing pattern with chain length as expected from the higher conjugation, cumulenes instead showed an almost constant BLA with chain length.
The Raman activity and position of each LO mode for both S-cumu[n] and O-cumu[n] was analyzed in detail, this showed a consistently different behaviour between odd and even wires.
Then we focused on the development of an effective method to compute the vibronic spectra through the analysis of the Franck-Condon factors, built up to have a comparison with experimental results and also to determine the effectiveness of a possible analysis of this type.
Our method was composed by several steps, at first the ground state geometry was determined through DFT calculations, than under TDDFT the excited state geometry and the information relative to each excited state and corresponding transition was computed.
With this informations a first preliminary spectra was determined, just with the built up of lorentian functions based on the position and intensity found

in this first calculation.
Than, to compute the vibronic spectra the FC factors were calculated using an homemade UVFC software.
This method in general proved to be effective and in good aggreement with experimental data.
The peak analysis of the highest wavelength transitions was carried out in detail, highlighting the dependence between the shift of charge in the wire and the intensity and position of each peak.
The assessment of the vibronic coupling of each peak was affected mainly by the selection of the hybrid functional. CAM-B3LYP proved to be the best on fitting the peaks and on analyzing the situation with increasing chain length , set aside the hypsochromic shift effect well known from the literature. A second effect was related to technical details such as the γ parameter, which proved to limit the capability of computing the Franck-Condon factors of highly vibronic coupled systems such as Ph-Py[n] wires.
In general the properties determined through DFT analysis were shown to be deeply correlated to both the Raman and UV-VIS spectra computed.
The computational methods proved to be fundamental, not only for a correct interpretation of experimental spectroscopic results of sp hybridized carbon wires, but also for the analysis of their properties.
These important results allows a deeper understanding of the behaviour of CAWs, both for the effect caused by different chain lengths and endgroups and the effect of the interaction with external fields (through the spectroscopic results determined).

6.1 Appendix

In this appendix are reported all the DFT calculated PBE0/cc-pVTZ values for HOMO-LUMO gap, bond length and bond length alternation for all the wires studied on the comparison section.
In particular the values for Vyn-cumu[n] in table (6.3), for Cn-cumu[n] in table (6.4), for BPh-Py[n] in table (6.2), for Ph-Py[n] in table (6.1) and for H-Py[n] in table (6.5).

Diphenyl polyynes					
Bond length values					
	N=4	N=6	N=8	N=10	N=12
ϕ-C_1	1,41560	1,41420	1,41350	1,41310	1,41280
C_1-C_2	1,21270	1,21460	1,21540	1,21570	1,21600
C_2-C_3	1,35530	1,34850	1,34600	1,34470	1,34410
C_3-C_4	1,21270	1,21870	1,22120	1,22220	1,22280
C_4-C_5		1,34850	1,34070	1,33780	1,33640
C_5-C_6		1,21460	1,22120	1,22390	1,22520
C_6-C_7			1,34600	1,33780	1,33470
C_7-C_8			1,21540	1,22220	1,22520
C_8-C_9				1,34480	1,33640
C_9-C_10				1,21570	1,22280
C_10-C_11					1,34410
C_11-C_12					1,21600
C_n-ϕ	1,41560	1,41420	1,41350	1,41310	1,41280
Energy (Hartree)					
HOMO	-0,22656	-0,22555	-0,22502	-0,22476	-0,22468
LUMO	-0,06629	-0,07822	-0,08839	-0,09695	-0,10410
GAP	0,16027	0,14733	0,13663	0,12781	0,12058
Energy (eV)					
HOMO	-6,16501	-6,13753	-6,12311	-6,11603	-6,11386
LUMO	-1,80384	-2,12848	-2,40522	-2,63815	-2,83271
GAP	4,36117	4,00906	3,71789	3,47789	3,28115
Bond length alternation					
BLA(i)	0,14260	0,13390	0,13060	0,12900	0,12810
	0,14260	0,12980	0,12480	0,12250	0,12130
		0,12980	0,11950	0,11560	0,11360
		0,13390	0,11950	0,11390	0,11120
			0,12480	0,11390	0,10950
			0,13060	0,11560	0,10950
				0,12260	0,11120
				0,12910	0,11360
					0,12130
					0,12810
BLA	0,14260	0,13185	0,12497	0,12028	0,11674

Table 6.1: Important values for Ph-Py[n] chains with n=4,6,8,10,12. ϕ represent the phenyl end group.

Bis(diphenyl) polyyne					
Bond length values					
	N=4	N=6	N=8	N=10	N=12
C_1-C_2	1,21329	1,21512	1,21590	1,21630	1,21651
C_2-C_3	1,35463	1,34793	1,34544	1,34420	1,34352
C_3-C_4	1,21329	1,21913	1,22153	1,22260	1,22310
C_4-C_5		1,34793	1,34032	1,33750	1,33608
C_5-C_6		1,21512	1,22153	1,22420	1,22540
C_6-C_7			1,34545	1,33750	1,33444
C_7-C_8			1,21590	1,22260	1,22540
C_8-C_9				1,34420	1,33608
C_9-C_{10}				1,21630	1,22310
C_{10}-C_{11}					1,34352
C_{11}-C_{12}					1,21651
Energy (Hartree)					
HOMO	-0,21815	-0,21853	-0,21903	-0,22155	-0,22180
LUMO	-0,07050	-0,08199	-0,09019	-0,09587	-0,10270
GAP	0,14765	0,13654	0,12884	0,12568	0,11910
Energy (eV)					
HOMO	-5,93617	-5,94651	-5,96011	-6,02869	-6,03549
LUMO	-1,91840	-2,23106	-2,45420	-2,60876	-2,79461
GAP	4,01776	3,71544	3,50592	3,41993	3,24088
Bond length alternation					
BLAi	0,14134	0,13282	0,12954	0,12790	0,12700
	0,14134	0,12880	0,12391	0,12160	0,12041
		0,12880	0,11879	0,11490	0,11298
		0,13281	0,11879	0,11330	0,11068
			0,12392	0,11330	0,10904
			0,12955	0,11490	0,10904
				0,12160	0,11068
				0,12790	0,11298
					0,12042
					0,12700
BLA media	0,14134	0,13081	0,12408	0,11943	0,11602

Table 6.2: Important values for BPh-Py[n] chains with n=4,6,8,10,12. ϕ represent a phenyl endgroup

Vinyl cumulene

Bond length values									
	N=4	N=5	N=6	N=7	N=8	N=9	N=10	N=11	N=12
C_1-C_2	1,2659	1,2699	1,2668	1,2691	1,2672	1,2687	1,2673	1,2684	1,2675
C_2-C_3	1,2831	1,2759	1,2814	1,2777	1,2809	1,2786	1,2807	1,2791	1,2806
C_3-C_4	1,2659	1,2760	1,2680	1,2731	1,2690	1,2721	1,2694	1,2715	1,2695
C_4-C_5		1,2699	1,2814	1,2731	1,2792	1,2748	1,2785	1,2756	1,2783
C_5-C_6			1,2668	1,2777	1,2690	1,2748	1,2701	1,2736	1,2704
C_6-C_7				1,2691	1,2810	1,2721	1,2785	1,2737	1,2778
C_7-C_8					1,2672	1,2786	1,2693	1,2756	1,2704
C_8-C_9						1,2687	1,2808	1,2715	1,2783
C_9-C_{10}							1,2673	1,2791	1,2695
C_{10}-C_{11}								1,2684	1,2806
C_{11}-C_{12}									1,2674
Energy (Hartree)									
HOMO	-0,2454	-0,2425	-0,2365	-0,2344	-0,2305	-0,2290	-0,2262	-0,2250	-0,2230
LUMO	-0,0889	-0,0820	-0,1075	-0,1017	-0,1201	-0,1151	-0,1291	-0,1248	-0,1361
GAP	0,1564	0,1605	0,1290	0,1327	0,1105	0,1139	0,0971	0,1002	0,0869
Energy (eV)									
HOMO	-6,6771	-6,5564	-6,4358	-6,3545	-6,2733	-6,2149	-6,1566	-6,1124	-6,0681
LUMO	-2,4199	-2,6731	-2,9263	-3,0969	-3,2675	-3,3909	-3,5143	-3,6089	-3,7035
GAP	4,2572	3,8833	3,5094	3,2576	3,0058	2,8240	2,6422	2,5034	2,3647
Bond length alternation									
BLA(i)	0,0171	0,0060	0,0146	0,0085	0,0137	0,0098	0,0134	0,0106	0,0132
	0,0171	0,0000	0,0134	0,0045	0,0119	0,0065	0,0113	0,0075	0,0111
		0,0060	0,0134	0,0000	0,0102	0,0027	0,0090	0,0041	0,0088
			0,0146	0,0045	0,0102	0,0000	0,0084	0,0020	0,0079
				0,0085	0,0120	0,0027	0,0085	0,0000	0,0074
					0,0138	0,0065	0,0092	0,0019	0,0074
						0,0098	0,0115	0,0041	0,0078
							0,0135	0,0075	0,0087
								0,0106	0,0111
									0,0132
	0,0171	0,0040	0,0140	0,0052	0,0120	0,0054	0,0106	0,0054	0,0097

Table 6.3: Important values for Vyn-cumu[n] with n=4,..,12.

Carbon cumulenes									
Bond length									
	N=4	N=5	N=6	N=7	N=8	N=9	N=10	N=11	N=12
C_1-C_2	1,2830	1,2836	1,2848	1,2860	1,2860	1,2876	1,2871	1,2888	1,2879
C_2-C_3	1,2716	1,2688	1,2702	1,2669	1,2691	1,2660	1,2683	1,2653	1,2677
C_3-C_4	1,2830	1,2688	1,2761	1,2728	1,2762	1,2752	1,2767	1,2768	1,2773
C_4-C_5		1,2836	1,2702	1,2728	1,2705	1,2707	1,2705	1,2696	1,2702
C_5-C_6			1,2848	1,2669	1,2762	1,2707	1,2755	1,2730	1,2755
C_6-C_7				1,2860	1,2691	1,2752	1,2705	1,2730	1,2711
C_7-C_8					1,2860	1,2660	1,2767	1,2696	1,2755
C_8-C_9						1,2876	1,2683	1,2768	1,2702
C_9-C_{10}							1,2871	1,2653	1,2773
C_{10}-C_{11}								1,2888	1,2677
C_{11}-C_{12}									1,2879
Energy (Hartree)									
HOMO	-0,3088	-0,3160	-0,2922	-0,2980	-0,2807	-0,2853	-0,2722	-0,2757	-0,2656
LUMO	-0,1299	-0,1855	-0,1454	-0,1893	-0,1553	-0,1916	-0,1623	-0,1932	-0,1673
GAP	0,1788	0,1305	0,1468	0,1088	0,1254	0,0936	0,1099	0,0825	0,0984
Energy (eV)									
HOMO	-8,4021	-8,1767	-7,9514	-7,7950	-7,6385	-7,5229	-7,4072	-7,3177	-7,2282
LUMO	-3,5361	-3,7465	-3,9568	-4,0910	-4,2251	-4,3203	-4,4156	-4,4835	-4,5514
GAP	4,8659	4,4303	3,9946	3,7040	3,4134	3,2025	2,9916	2,8342	2,6768
Bond length alternation									
BLA(i)	0,0114	0,0148	0,0145	0,0190	0,0169	0,0216	0,0187	0,0234	0,0202
	0,0114	0,0000	0,0059	0,0059	0,0070	0,0092	0,0084	0,0114	0,0096
		0,0148	0,0059	0,0000	0,0057	0,0044	0,0062	0,0072	0,0070
			0,0145	0,0059	0,0057	0,0000	0,0051	0,0035	0,0053
				0,0190	0,0070	0,0044	0,0051	0,00000	0,0045
					0,0169	0,0092	0,0062	0,0035	0,0045
						0,0216	0,0084	0,0072	0,0053
							0,0187	0,0114	0,0070
								0,0234	0,0096
									0,0202
BLA	0,0114	0,0098	0,0102	0,0100	0,0099	0,0101	0,0096	0,0101	0,0093

Table 6.4: Important values for carbon cumulenes for each of the Cn-cumu[n] chains with n=4,5,6,7,8,9,10,11,12

Hydrogen polyyne					
Bond length values					
	N=4	N=6	N=8	N=10	N=12
H-C_1	1,06360	1,06360	1,06380	1,06350	1,06350
C_1-C_2	1,20410	1,20640	1,20730	1,20760	1,20780
C_2-C_3	1,36400	1,35510	1,35240	1,35100	1,35040
C_3-C_4	1,20410	1,21400	1,21750	1,21880	1,21930
C_4-C_5		1,35510	1,34410	1,34090	1,33930
C_5-C_6		1,20640	1,21760	1,22140	1,22290
C_6-C_7			1,35240	1,34090	1,33700
C_7-C_8			1,20730	1,21880	1,22290
C_8-C_9				1,35100	1,33930
C_9-C_{10}				1,20760	1,21930
C_{10}-C_{11}					1,35040
C_{11}-C_{12}					1,20780
C_n-H	1,06360	1,06360	1,06380	1,06360	1,06350
Energy (Hartree)					
HOMO	-0,28192	-0,26786	-0,25923	-0,25344	-0,24931
LUMO	-0,02920	-0,06345	-0,08412	-0,09795	-0,10785
GAP	0,25272	0,20441	0,17511	0,15549	0,14146
Energy (eV)					
HOMO	-7,67144	-7,28885	-7,05401	-6,89646	-6,78407
LUMO	-0,79457	-1,72656	-2,28902	-2,66536	-2,93475
GAP	6,87687	5,56228	4,76499	4,23110	3,84932
Bond length alternation					
BLA (i)	0,15990	0,14870	0,14510	0,14340	0,14260
	0,15990	0,14110	0,13490	0,13220	0,13110
		0,14110	0,12660	0,12210	0,12000
		0,14870	0,12650	0,11950	0,11640
			0,13480	0,11950	0,11410
			0,14510	0,12210	0,11410
				0,13220	0,11640
				0,14340	0,12000
					0,13110
					0,14260
BLA	0,15990	0,14490	0,13550	0,12930	0,12484

Table 6.5: Important values for H-Py[n] with n=4,6,8,10,12.

Bibliography

[1] Carlo S Casari and Alberto Milani. Carbyne: from the elusive allotrope to stable carbon atom wires. *MRS Communications*, pages 1–13, 2018.

[2] Carlo S Casari, Matteo Tommasini, Rik R Tykwinski, and Alberto Milani. Carbon-atom wires: 1-d systems with tunable properties. *Nanoscale*, 8(8):4414–4435, 2016.

[3] Niko Pavlicek, Przemyslaw Gawel, Daniel R Kohn, Zsolt Majzik, Yaoyao Xiong, Gerhard Meyer, Harry L Anderson, and Leo Gross. Polyyne formation via skeletal rearrangement induced by atomic manipulation. *Nature chemistry*, 10(8):853–858, 2018.

[4] Haiyan Wang, Jan Szczepanski, Philip Brucat, and Martin Vala. Infrared spectra and dissociation pathways of the linear carbon–sulfur clusters cns and scns (n$\leq$ 29): Theoretical calculations. *International journal of quantum chemistry*, 102(5):795–805, 2005.

[5] Hiroshi Tabata, Minoru Fujii, Shinji Hayashi, Tatsuya Doi, and Tomonari Wakabayashi. Raman and surface-enhanced raman scattering of a series of size-separated polyynes. *Carbon*, 44(15):3168–3176, 2006.

[6] A. Milani, A. Lucotti, V. Russo, M. Tommasini, F. Cataldo, A. Li Bassi, and C. S. Casari. Charge transfer and vibrational structure of sp-hybridized carbon atomic wires probed by surface enhanced raman spectroscopy. *The Journal of Physical Chemistry C*, 115(26):12836–12843, 2011.

[7] Vasilii I. Artyukhov, Mingjie Liu, and Boris I. Yakobson. Mechanically induced metal–insulator transition in carbyne. *Nano Letters*, 14(8):4224–4229, 2014.

[8] Alberto Milani, Matteo Tommasini, Valentino Barbieri, Andrea Lucotti, Valeria Russo, Franco Cataldo, and Carlo S Casari. Semiconductor-to-metal transition in carbon-atom wires driven by sp2 conjugated end

groups. *The Journal of Physical Chemistry C*, 121(19):10562–10570, 2017.

[9] Francesco Innocenti, Alberto Milani, and Chiara Castiglioni. Can raman spectroscopy detect cumulenic structures of linear carbon chains? *Journal of Raman Spectroscopy*, 41(2):226–236, 2010.

[10] HW Kroto. Jr heath. sc o'brien, rf curl and re smalley. *Astrophys. J*, 314:352, 1987.

[11] Andre Konstantin Geim. Graphene: status and prospects. *science*, 324(5934):1530–1534, 2009.

[12] Lei Shi, Philip Rohringer, Kazu Suenaga, Yoshiko Niimi, Jani Kotakoski, Jannik C Meyer, Herwig Peterlik, Marius Wanko, Seymur Cahangirov, Angel Rubio, et al. Confined linear carbon chains as a route to bulk carbyne. *Nature materials*, 15(6):634, 2016.

[13] Wesley A Chalifoux and Rik R Tykwinski. Synthesis of polyynes to model the sp-carbon allotrope carbyne. *Nature chemistry*, 2(11):967–971, 2010.

[14] Mingchao Wang and Shangchao Lin. Ballistic thermal transport in carbyne and cumulene with micron-scale spectral acoustic phonon mean free path. *Scientific reports*, 5:18122, 2015.

[15] Ying Zhu, Hongcun Bai, and Yuanhe Huang. Electronic property modulation of one-dimensional extended graphdiyne nanowires from a first-principle crystal orbital view. *ChemistryOpen*, 5(1):78–87, 2016.

[16] Pavel B Sorokin, Hoonkyung Lee, Lyubov Yu Antipina, Abhishek K Singh, and Boris I Yakobson. Calcium-decorated carbyne networks as hydrogen storage media. *Nano letters*, 11(7):2660–2665, 2011.

[17] Shujiang Yang and Miklos Kertesz. Linear c n clusters: Are they acetylenic or cumulenic? *The Journal of Physical Chemistry A*, 112(1):146–151, 2008.

[18] Tomonari Wakabayashi, Yoriko Wada, Naoya Iwahara, and Tohru Sato. Vibronic bands in the homo-lumo excitation of linear polyyne molecules. *Journal of Physics: Conference Series*, 428(1):012004, 2013.

[19] Mingjie Liu, Vasilii I. Artyukhov, Hoonkyung Lee, Fangbo Xu, and Boris I. Yakobson. Carbyne from first principles: Chain of c atoms, a nanorod or a nanorope. *ACS Nano*, 7(11):10075–10082, 2013.

[20] Walter J Lafferty, Arthur G Maki, and Earle K Plyler. High-resolution infrared determination of the structure of carbon suboxide. *The Journal of Chemical Physics*, 40(1):224–229, 1964.

[21] Hai-Yan Wang, Xin Lu, Rong-Bin Huang, and Lan-Sun Zheng. Theoretical studies of xcnx (x= o, s, se; n= 1–8): structures, spectroscopic properties, and dissociation energies. *Journal of Molecular Structure: THEOCHEM*, 593(1-3):187–197, 2002.

[22] Formation of hydrogen-capped polyynes by laser ablation of c60 particles suspended in solution. *Carbon*, 41(11):2141 – 2148, 2003.

[23] Yu P Kudryavtsev, RB Heimann, and SE Evsyukov. Carbynes: advances in the field of linear carbon chain compounds. *Journal of materials science*, 31(21):5557–5571, 1996.

[24] Peter Siemsen, Robert C Livingston, and François Diederich. Acetylenic coupling: a powerful tool in molecular construction. *Angewandte Chemie International Edition*, 39(15):2632–2657, 2000.

[25] Haiyan Wang, Jan Szczepanski, Andrew Cooke, Philip Brucat, and Martin Vala. Vibrational absorption spectra of cns (n= 2, 6) and cns2 (n= 7, 9, 11, 13, 15) linear carbon–sulfur clusters. *International journal of quantum chemistry*, 102(5):806–819, 2005.

[26] Franco Cataldo, Ornella Ursini, Alberto Milani, and Carlo S Casari. One-pot synthesis and characterization of polyynes end-capped by biphenyl groups (α, ω-biphenylpolyynes). *Carbon*, 126:232–240, 2018.

[27] Tomonari Wakabayashi, Aik-Loong Ong, Dmitry Strelnikov, and Wolfgang Krätschmer. Flashing carbon on cold surfaces. *The Journal of Physical Chemistry B*, 108(12):3686–3690, 2004.

[28] Curt Wentrup, Peter Kambouris, Richard A Evans, David Owen, Graham Macfarlane, Josselin Chuche, Jean Claude Pommelet, Abdelhamid Ben Cheikh, Michel Plisnier, and Robert Flammang. 2, 5-dithiacyclopentylideneketene and ethenedithione, s: C: C: S, generated by flash vacuum pyrolysis. *Journal of the American Chemical Society*, 113(8):3130–3135, 1991.

[29] Raman and sers investigation of isolated sp carbon chains. *Chemical Physics Letters*, 417(1):78 – 82, 2006.

[30] Sara Eisler, Aaron D. Slepkov, Erin Elliott, Thanh Luu, Robert McDonald, Frank A. Hegmann, and Rik R. Tykwinski. Polyynes as a model for carbyne: synthesis, physical properties, and nonlinear optical response. *Journal of the American Chemical Society*, 127(8):2666–2676, 2005.

[31] Rudolf Ernst Peierls and Rudolf Sir Peierls. *Quantum theory of solids*. Oxford University Press, 1955.

[32] Neil W Ashcroft and N David Mermin. Solid state physics (saunders college, philadelphia, 1976). *Google Scholar*, page 461, 2010.

[33] Masatoshi Ohishi. Search for complex organic molecules in space. *Journal of Physics: Conference Series*, 728(5):052002, 2016.

[34] Gilberto Casillas, Alvaro Mayoral, Mingjie Liu, Arturo Ponce, Vasilii I Artyukhov, Boris I Yakobson, and Miguel Jose-Yacaman. New insights into the properties and interactions of carbon chains as revealed by hrtem and dft analysis. *Carbon*, 66:436–441, 2014.

[35] Fanghao Hu, Chen Zeng, Rong Long, Yupeng Miao, Lu Wei, Qizhi Xu, and Wei Min. Supermultiplexed optical imaging and barcoding with engineered polyynes. *Nature methods*, 15(3):194, 2018.

[36] HH Kuhn, AD Child, TA Skotheim, RL Elsenbaumer, and JR Reynolds. Handbook of conducting polymers. *TA Skotheim, RL Elsenbaumer and JR Raynolds, Eds*, page 993, 1998.

[37] Tom Ziegler. Approximate density functional theory as a practical tool in molecular energetics and dynamics. *Chemical Reviews*, 91(5):651–667, 1991.

[38] Axel D Becke. Density-functional thermochemistry. iii. the role of exact exchange. *The Journal of chemical physics*, 98(7):5648–5652, 1993.

[39] Takeshi Yanai, David P Tew, and Nicholas C Handy. A new hybrid exchange–correlation functional using the coulomb-attenuating method (cam-b3lyp). *Chemical Physics Letters*, 393(1-3):51–57, 2004.

[40] Johanna I Fuks, Lionel Lacombe, Søren EB Nielsen, and Neepa T Maitra. Exploring non-adiabatic approximations to the exchange–correlation functional of tddft. *Physical Chemistry Chemical Physics*, 20(41):26145–26160, 2018.

[41] Ernest R Davidson. Comment on "comment on dunning's correlation-consistent basis sets". *Chemical physics letters*, 260(3-4):514–518, 1996.

[42] M. J. Frisch and G. et al. Gaussian˜16 Revision B.01, 2016. Gaussian Inc. Wallingford CT.

[43] Hanwell et al. Avogadro: an advanced semantic chemical editor, visualization, and analysis platform. *Journal of Cheminformatics*, 4(1):17, Aug 2012.

[44] G. Schaftenaar and J.H. Noordik. Molden: a pre- and post-processing program for molecular and electronic structures*. *Journal of Computer-Aided Molecular Design*, 14(2):123–134, Feb 2000.

[45] Robert van Leeuwen. Causality and symmetry in time-dependent density-functional theory. *Phys. Rev. Lett.*, 80:1280–1283, Feb 1998.

[46] Peter W Atkins and Ronald S Friedman. *Molecular quantum mechanics*. Oxford university press, 2011.

[47] Johannes Gierschner, Hans-Georg Mack, Larry Lüer, and Dieter Oelkrug. Fluorescence and absorption spectra of oligophenylenevinylenes: Vibronic coupling, band shapes, and solvatochromism. *The Journal of chemical physics*, 116(19):8596–8609, 2002.

[48] W Siebrand. Radiationless transitions in polyatomic molecules. i. calculation of franck—condon factors. *The Journal of Chemical Physics*, 46(2):440–447, 1967.

[49] Fabrizia Negri and Marek Z Zgierski. The vibronic structure of the s 0↔ s 1 and s 0↔ s 2 transitions in simple oligomers of thiophene. *The Journal of chemical physics*, 100(4):2571–2587, 1994.

[50] Anna R Mantini, Mario P Marzocchi, and Giulietta Smulevich. Raman excitation profiles and second-derivative absorption spectra of β-carotene. *The Journal of chemical physics*, 91(1):85–91, 1989.

[51] ZG Soos and D Mukhopadhyay. Vibronic analysis of overlapping resonances and the third-harmonic-generation spectrum of β-carotene. *The Journal of chemical physics*, 101(7):5515–5522, 1994.

[52] Stoyan Karabunarliev, Martin Baumgarten, Eric R Bittner, and Klaus Müllen. Rigorous franck–condon absorption and emission spectra of conjugated oligomers from quantum chemistry. *The Journal of Chemical Physics*, 113(24):11372–11381, 2000.

[53] Matteo Tommasini, Daniele Fazzi, Alberto Milani, Mirella Del Zoppo, Chiara Castiglioni, and Giuseppe Zerbi. Intramolecular vibrational force fields for linear carbon chains through an adaptative linear scaling scheme. *The Journal of Physical Chemistry A*, 111(45):11645–11651, 2007.

[54] Shujiang Yang, Miklos Kertesz, Viktor Zólyomi, and Jenő Kürti. Application of a novel linear/exponential hybrid force field scaling scheme to the longitudinal raman active mode of polyyne. *The Journal of Physical Chemistry A*, 111(12):2434–2441, 2007.

[55] Thomas Gibtner, Frank Hampel, Jean-Paul Gisselbrecht, and Andreas Hirsch. End-cap stabilized oligoynes: Model compounds for the linear sp carbon allotrope carbyne. *Chemistry – A European Journal*, 8(2):408–432.

[56] Iffat H. Nayyar, Artëm E. Masunov, and Sergei Tretiak. Comparison of td-dft methods for the calculation of two-photon absorption spectra of oligophenylvinylenes. *The Journal of Physical Chemistry C*, 117(35):18170–18189, 2013.

[57] Tomonari Wakabayashi, Hiroyuki Nagayama, Kota Daigoku, Yosuke Kiyooka, and Kenro Hashimoto. Laser induced emission spectra of polyyne molecules c2nh2 (n=5–8). *Chemical Physics Letters*, 446(1):65 – 70, 2007.

[58] H. Ding, T. W. Schmidt, T. Pino, F. Güthe, and J. P. Maier. Towards bulk behaviour of long hydrogenated carbon chains? *Phys. Chem. Chem. Phys.*, 5:4772–4775, 2003.

[59] H. Ding, T. W. Schmidt, T. Pino, A. E. Boguslavskiy, F. Güthe, and J. P. Maier. Gas phase electronic spectra of the linear carbon chains hc2n+1h (n=3–6,9). *The Journal of Chemical Physics*, 119(2):814–819, 2003.

[60] Andreas Mavrandonakis, Max Mühlhäuser, George E. Froudakis, and Sigrid D. Peyerimhoff. The electronic spectrum of linear pentadiynylidene in comparison with isomeric ethynylcyclopropenylidene. *Phys. Chem. Chem. Phys.*, 4:3318–3321, 2002.

[61] Jochen Heyd and Gustavo E Scuseria. Efficient hybrid density functional calculations in solids: Assessment of the heyd–scuseria–ernzerhof screened coulomb hybrid functional. *The Journal of chemical physics*, 121(3):1187–1192, 2004.

[62] Juan E. Peralta, Jochen Heyd, Gustavo E. Scuseria, and Richard L. Martin. Spin-orbit splittings and energy band gaps calculated with the heyd-scuseria-ernzerhof screened hybrid functional. *Phys. Rev. B*, 74:073101, Aug 2006.